An enzymology and structural biology approach towards elucidation of *E. coli* fatty acid biosynthesis and its application to the production of bio-renewables

by

Aaron M. Marcella

A dissertation submitted to the graduate faculty

in partial fulfillment for the degree of

DOCTOR OF PHILOSOPHY

Major: Biochemistry

Program of Study Committee:
Adam W. Barb, Major Professor
Richard Honzatko
Mark Hargrove
Basil Nikolau
Zengyi Shao

The student author and the program of study committee are solely responsible for the content of this dissertation. The Graduate College will ensure this dissertation is globally accessible and will not permit alterations after a degree is conferred.

Iowa State University

Ames, Iowa

2017

DEDICATION

I would like to dedicate this work to my grandpa, Terence Twomey. My grandpa has always been an example of what compassion, love, hard work, and dedication truly are.

TABLE OF CONTENTS

Page

ACKNOWLEDGMENTS vi

ABSTRACT……..... vii

CHAPTER 1 INTRODUCTION: FATTY ACID BIOSYNTHESIS 1

CHAPTER 2 PREPARATION OF HOLO- AND MALONYL-
[ACYL-CARRIER-PROTEIN] IN A MANNER SUITABLE
FOR ANALOG DEVELOPMEN……18

Introduction……..19

Materials and methods…….....22

Expression and identification of a stable complex…….....27

Separation of ACP and holo-ACP synthase…….30

Conversion to malonyl-ACP…….....33

Enzymatic analysis of malonyl-ACP……35

Conclusion…….....36

Works cited……..38

CHAPTER 3 A RAPID FLUOROMETRIC ASSAY FOR THE
S-MALONYLTRANSACYLASE FABD AND OTHER
SULFHYDRYL UTILIZING ENZYMES……...40

Introduction……41

Materials and methods…….....45

Results and discussion…… …….....52

Works cited……60

CHAPTER 4 THE R117A VARIANT OF THE ESCHERICHIA COLI MALONYL-COENZYME A:HOLO-(ACYL CARRIER PROTEIN) TRANSACYLASE FABD SYNTHESIZES NOVEL ACYL-(ACYL CARRIER PROTEINS)……..62

Introduction……64

Materials and methods…….....67

Initial analyses…….....69

Specific activities of FabD and FabD R117A……..……71

K_M and k_{cat} comparisons ……..…….....74

FabD-catalyzed decarboxylation of malonyl-ACP……..77

Discussion…….....79

Supplemental information……..…….....83

Works cited……87

CHAPTER 5 STRUCTURE, HIGH AFFINITY AND NEGATIVE COOPERATIVITY OF THE ESCHERICIA COLI HOLO-(ACYL CARRIER PROTEIN):HOLO-(ACYL CARRIER PROTEIN) SYNTHASE COMPLEX……..90

Introduction……..91

Materials and methods…….....94

Holo-ACPP binding by ACPS…….....101

X-ray crystallography of ACPS……..103

X-ray crystallography of the holo-ACPP:ACPS complex …….....105

Identifying the ACPS binding interface of holo-ACPP.…….....108

NMR measurement of holo-ACPP orientation in the complex…….....109

Discussion…….....111

Supplemental information……..……116

Works cited……122

ACKNOWLEDGMENTS

I would like to thank my wife, Elise Marcella, for all of her support through my time as a graduate student in pursuit of my PhD. My son Finnick has been pretty awesome as well in the few months he's been around during my time as a student, always greeting me with a smile at the end of the day.

My parents, Steve and Kathy Marcella have always been supportive of my goals and I appreciate all of the guidance they've given me through my life, especially these past four years.

I would like to thank my PI, Adam Barb for continuous support through all the highs and lows of my graduate study. Your optimism and unbridled joy for science that you brought to lab every single day is truly inspirational. I would also like to thank my committee members, Richard Honzatko, Mark Hargrove, Basil Nikolau, and Zengyi Shao, for their guidance and support throughout the course of this research, especially Dr. Honzatko for all of his help with X-ray crystallography and life lessons.

ABSTRACT

Prokaryotic fatty acid biosynthesis is an important process to study due to its necessity for cell survival and production of highly reduced carbon chains. A characterization of several proteins involved in *E. coli* fatty acid biosynthesis is presented. This work provides a method for generating large amounts of pure malonyl acyl-carrier-protein using both the wild type malonyl-CoA:holo-ACP transacylase (FabD) and a variant studied further in our lab. This preparation overcomes the phenomena of a 50:50 mixture of malonyl and acetyl-ACP in the reaction and is crucial for the efficacy of future assays involving malonyl-ACP. A new assay has been developed to measure activity of the FabD enzyme using a fluorescent probe and can be scaled from a rapid to high throughput assay using 96 well plates. FabD variants were studied with the above assay and kinetic constants were determined for several different CoA substrates with enhanced chemical functionality. The structure of holo-ACP synthase in apo and acyl-carrier-protein bound forms was investigated in depth using a combination of X-ray crystallography, NMR spectroscopy, and isothermal titration calorimetry. This work is a comprehensive study of the enzymes involved in the first steps of fatty acid biosynthesis using several biochemical and biophysical techniques.

CHAPTER 1: INTRODUCTION TO FATTY ACID BIOSYNTHESIS

Type I and Type II FAS:

Fatty acid biosynthesis is essential for the growth and development of all organisms from the simplest single celled prokaryotes to humans [1,2,3]. The two main classes of fatty acid synthase (FAS), Type I and Type II generate highly reduced carbon chain end products, but do so using either a single polypeptide mega-enzyme or a system made up of many individual enzymes, respectively [4]. Type I FAS is found in mammals and yeast and is made up of a single polypeptide with all of the enzymatic activities necessary to generate fatty acids localized onto a single scaffold. The shared single polypeptide structure of these two enzymes is met with a very different quaternary structure. Human FAS consists of a homodimer with two 250 kDa subunits, while yeast FAS is a 2.6 MDa dodecamer. The yeast FAS has a $\alpha_6\beta_6$ organization where one α and β component combined contain the eight activities necessary for fatty acid biosynthesis yielding six complete biosynthetic replicates in yeast [5]. Each of these Type I FAS systems have a tethered acyl-carrier protein (ACP) capable of reaching all of the different active site centers on the molecule [4,5,6]. This localization of all active sites onto one polypeptide could be a more efficient process of generating fatty acids, at the expense of synthesizing a very complex molecular machine. It should be noted, however, that replacing the yeast FAS with all of the components of *E. coli* FAS rescues this pathway and allows for growth of the organism [7]. The ability to replace Type I FAS with Type II suggests fatty acid synthesis necessity outweighs the manner in which they are

synthesized. This was a big step to breaking down the single polypeptide into its component parts and allowing for simplified engineering of each enzyme [7].

The groundwork into defining the Type II prokaryotic FAS began with the basic isolation and characterization of several enzymes from *Escherichia coli* [8,9,10,11,12]. The condensation reaction was particularly exciting being the first catalyzed by a biological system to be discovered [12]. This research set the stage for a more complete characterization of these enzymes and their respective activities and over the next 20-30 years these enzymes were studied in great detail [13,14,15,16]. The driving force for studying prokaryotic FAS was the promise of potential inhibitors of the pathway and novel antibiotics. The dissociated enzyme system is attractive to researchers as it provides unique motifs not found in the mammalian system [2]. Adverse effects of drugs targeting Type II FAS may be alleviated by the lacking structural relationship to Type I FAS. Drugs made to specifically target Type II FAS could be specific to that pathway and have few side effects in the human system. This key difference is what drives the research into not only understanding how the two systems work, but how one type can be exploited without having an effect on the other.

Microbes and mammals have been discussed, but the plant FAS system resembles the Type II system [17]. This may be unexpected as higher order organisms like mammals use a Type I system, what is even more surprising is that unlike mammals and microbes that synthesize fatty acids in the cytoplasm or cytosol, plants make their fatty acids in an organelle (plastid)[17,18]. These fatty acids that are synthesized then need to be transported out of the plastid into the

cytoplasm to be activated into glycerophospholipids at the ER for making cell membranes [17]. This covers the most critical organisms and their methodology for synthesizing fatty acids, but it should be noted mitochondria also maintain their own FAS machinery and it resembles the Type II system [19]. Mitochondrial FAS functions with an entire suite of enzymes and its own soluble ACP as opposed to the tethered ACP of mammalian and yeast FAS. There is clear diversity in the ways each organism makes their fatty acids, and this is also evident in the types of fatty acids made and the use of these fatty acids.

Fatty Acid use and incorporation:

Fatty acids are utilized for the formation of cellular membranes, bacterial defense material (lipopolysaccharides), long term energy storage, and other purposes like plant waxes [18,20]. The first fundamental difference observed is the distribution of chain lengths and branching of the fatty acids. Plants have distinct distributions of fatty acids, an example is rapeseed has >50% C20-C22 whereas maize, soybean, and safflower all have >50 % C18:2 and no C20-C22 [21,22]. These defining characteristics are exploited every day in the food industry for cooking oils as well as in the use of biodiesel [22,23]. These distinct distributions set the stage for metabolic engineering around a suitable starting point of fatty acid content. Bacteria have distinct ranges of fatty acid content and the biggest difference can be observed when comparing thermophilic to non-thermophilic bacteria. In one study it was shown that a thermophilic bacterium had an increased amount of short/medium chain (C12-C15) when compared to non-thermophilic that had a more traditional range of C16-C18[24]. The

thermophilic bacteria also have a greatly increased percentage of iso-branched fatty acids and little to no unsaturated fatty acids which aid in membrane stability and rigidity at high temperatures where the unsaturated fatty acids will be found in more temperate bacteria. *E. coli* generate mostly C16-C18 fatty acids, but interestingly show a marked decrease in C18 when growth is shifted from 30 °C to 45 °C. This decrease in longer chain fatty acids in E. coli at increased temperatures and in thermophiles is believed to help with membrane stability at increased temperatures and maintaining a liquid crystalline state [25,26].

Fatty acid incorporation into membranes is possibly their most obvious and important use. Fatty acids are linked to a central glycerol molecule with the final product being a glycerophospholipid which is packaged into the phospholipid bilayer. These membranes are essential for life and help in determining a major branch point in evolution [27]. Early membrane synthesizing proteins can be found that used the limited fatty acids available to create the membranes and one from archaea was studied in detail [28]. The glycerophospholipids are necessary for creating the phospholipid bilayer separating two aqueous compartments and their contents from each other. In eukaryotes this separation is important as compartmentalization is critical to the efficacy of the organism. There are many membrane bound organelles each with their own biological role and they function best when separated. This separation provides a diffusion barrier as well as a more defined shape that can be necessary for certain organelles [29]. In prokaryotes these membranes are mostly for energy potential, but also provide a cellular defense mechanism. The

trans-membrane protein ATPase relies on a proton gradient to function in generating large amounts of ATP and without a membrane the formation of this gradient would not be feasible [30,31]. These fatty acids can also be used to make triacylglycerol molecules whose importance varies across the various forms of life, but is an excellent form of energy storage [32,33].

Fats in the form of triacylglycerols, wax esters, polyhydroxyalkanoates (bacteria only) are an important long term storage form of energy as they contain highly reduced carbon chains and can provide large amounts of energy to the cell when needed (**Figure 1-1**). In bacteria these fatty acids are broken down in the cytosol by the process of beta oxidation which yields one acetyl-CoA molecule for every 2 carbons in the fatty acid chain.

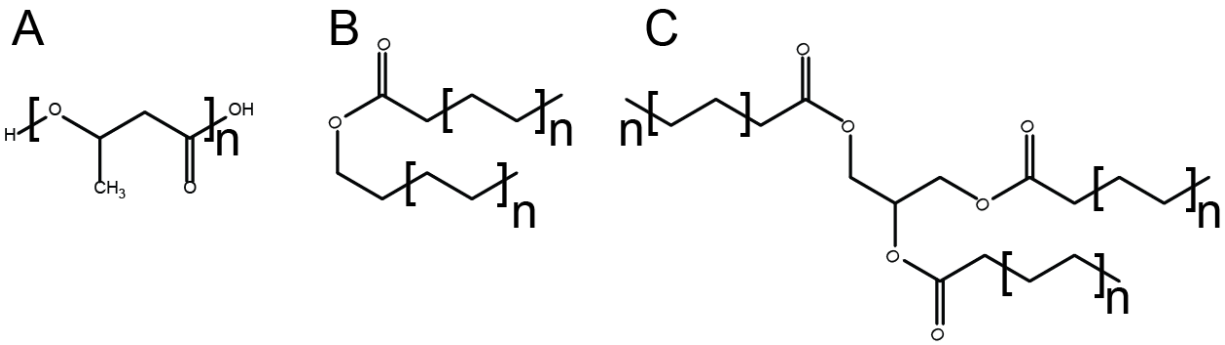

Figure 1-1. The three most common forms of reduced carbon chain energy storage for many organisms **A.** Polyhydroxyalkanoates. **B.** fatty acid wax esters **C.** triacylglycerol

Beta oxidation provides cells with reducing factors and acetyl-CoA which all play an important role in driving central metabolism. The energy production from the oxidation of a C16 fatty acid provides 2.4 times more ATP than the complete breakdown of glucose by weight [34]. This shows the immense amount of energy stored in the fatty acids and why they make such a good storage form. When

fatty acids are packaged into triacylglycerols they are stored in a nearly anhydrous form allowing them to pack their total energy even more densely than proteins or sugars (glycogen) which are hydrated [32].

Lipopolysaccharides (LPS) are a fatty acid containing antigenic molecule. LPS plays a critical role in the antigenic mode of a bacterial capsule and gives gram negative bacteria their infectiousness. The first subunit of LPS is lipid A which consists of a lipid containing portion with six fatty acid chains connected to a disaccharide sugar, usually β(1→6)-linked D-glucosamine [35]. There is then a core oligosaccharide and an O-polysaccharide that are linked to the lipid A which can also have antigenic properties. The lipid A component of LPS is highly conserved among gram negative bacteria [20,35]. Lipid A anchors the LPS to the outer membrane, presenting the polysaccharides which act as a protective barrier and can also have some immune activating properties [35,36]. Fatty acids play a crucial role in the life of many organisms and function in numerous ways, this is evidenced by the great diversity evidenced above for these many incorporations of fatty acids. The enzymes involved in the early stages of transacylation and condensation are of interest in this work and will be detailed below.

Enzymes of Interest:

Holo-ACP Synthase (ACPS) is the first enzyme of interest in this dissertation as it primes the acyl carrier protein (ACP) with the phosphopantetheine moiety from Coenzyme A as shown in **Figure 1-2**. The ACPS enzyme has been expressed and purified from several organisms and in

all cases relies on a divalent cation such as magnesium for functionality [37,38,39,40,41]. This enzyme catalyzes a hydrolysis reaction where the coenzyme A molecule is cleaved at the phosphodiester bond leaving 3',5' adenosine diphosphate and phosphopantheine. After the hydrolysis, the hydroxyl group of serine 36 on ACP can perform a nucleophilic attack on the phosphopantethiene completing the catalytic cycle.

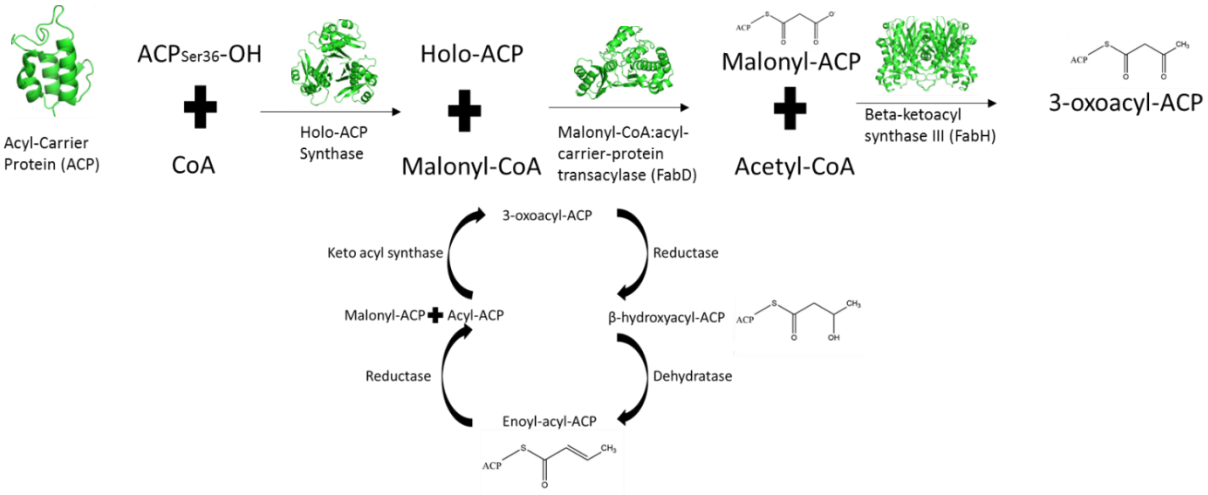

Figure 1-2 *E. coli* fatty acid biosynthesis pathway high-lighting the key reactions with enzymes and substrates shown as crystal structure cartoon diagrams.

At this point holo-ACP is ready for the next modification which primes it for the iterative condensation reactions. Holo-ACP is a soluble cytosolic protein in bacteria and plants, but in mammals and yeast it is tethered to the single polypeptide FAS and can access each active site pocket on the mega enzyme.

There was debate within the literature about the oligomerization of the enzyme and its dependence on whether or not the organism was gram positive or negative [38]. For *E. coli* and *Mycoplasma pneumoniae* it was believed that it

formed a dimeric structure while in other organisms such as *Bacillis subtillis* it formed a trimeric structure [39,40]. This observation was even more intriguing as the crystal structure of the trimeric enzyme suggested that the only way to form three active sites was to have this axially symmetric trimer where residues from neighboring chains could provide substrate stabilization and catalytic function [40]. Work presented in this dissertation sheds some light on the interpretation of the data previously collected and provides solution and crystal data to definitely show oligomerization state of the *E. coli* holo-ACP Synthase.

The next step in the pathway is the transfer of a malonate moiety from malonyl-CoA to holo-ACP catalyzed by the malonyl-CoA:ACP transacylase (FabD) enzyme. This is a critical reaction as malonyl-ACP is the key intermediate in growing the fatty acid chain two carbon units at a time. The reaction starts with the transfer of malonate from malonyl-CoA to the active site nucleophile Ser92 on *E. coli* FabD. Following this transfer and the release of CoA, the phosphopantetheine on holo-ACP will enter the active site and the free thiol on holo-ACP is modified with the malonate group. At this point malonyl-ACP will serve as the condensing substrate for all subsequent rounds of condensation in fatty acid biosynthesis and this makes it a critical intermediate in fatty acid biosynthesis and FabD an essential enzyme [42]. FabD has been crystallized many times from many different organisms leading to significant knowledge about substrate binding and active site chemistry [41,43,44,45,46,47,48,49]. These numerous structural studies show the highly conserved fold and organization of the enzyme active site. There is a distinct catalytic dyad

consisting of the active site nucleophile (ser92) and the catalytic base his201. These two residues are critical to enzyme function[50], but there are several other amino acid side chains pointing into the active site that are involved in substrate stabilization and pocket formation. These amino acids are arginine 117, glutamine 11, and glutamine 250. Glutamine 11 functions to stabilize the malonate-enzyme intermediate while also hydrogen bonding with arginine 117 which stabilizes the distal carboxylate of the malonate moiety through a salt bridge and is consequently stabilized itself by glutamine 250 and another hydrogen bond[48]. While the aforementioned residues act to stabilize the active site there are also conserved residues that form non covalent stabilizing interactions with the adenine nucleotide portion of malonyl-CoA.

The β-ketoacyl synthase III (FabH) enzyme functions next in the fatty acid biosynthesis pathway. This enzyme performs an ordered ping pong reaction in the same way that the FabD enzyme does, but uses cysteine as its active site nucleophile instead of serine [13,51]. Similarly to FabD, FabH first binds its CoA substrate (acetyl-CoA) and transfers the acetate moiety from acetyl-CoA to the cysteine 112 in the active site. This reaction is facilitated by the active site base histidine 244 which activates the cysteine by absconding its proton [52]. The FabH-acetate intermediate is stabilized by the formation of an oxyanion hole consisting of backbone amides on cysteine 112 and glycine 306 [52]. Following acetate transfer the malonyl modified phosphopantetheine of malonyl-ACP enters the active site, the terminal carboxylate is decarboxylated, and the resulting carbanion can perform nucleophilic attack on the carbonyl carbon of the

acetate-enzyme intermediate. This concludes the catalytic event and leaves the final acetoacetyl-ACP product. This reaction is also catalyzed by KASI and KASII enzymes where the priming substrate is an acyl-ACP and not acetyl-CoA, but still utilize malonyl-ACP as the condensing unit [53]. One of the interesting characteristics of FabH is that unlike the KASI and KASII enzymes it functions with a CoA and ACP based substrate where the former enzymes utilize two ACP based substrates. This would suggest alternative substrate recognition on the surface of the proteins in the context of similar active site chemistry and substrate binding.

There are three enzymes that work to fully reduce the second keto group on acetoacetyl-CoA to an alkane. They are the reductase (FabG), a dehydratase, and a final enoyl-ACP reductase. FabG uses NADPH to reduce the keto group to an alcohol [54]. The NADPH utilization has made the FabG enzyme useful for linked enzyme assays coupling condensing or transacylase enzymes to the NADPH dependent FabG reaction [55]. After the keto group is reduced to an alcohol the alcohol is removed by the dehydratase enzyme (FabZ) [56,57]. This dehydration leaves a 2-enoyl product which must be reduced a final time to yield the fully saturated acyl chain that can be further elongated by more condensation reactions. This final reduction reaction is catalyzed by the enoyl-ACP reductase enzyme (FabI) which can act on numerous acyl chain length substrates [58]. The FabI chemistry is extremely interesting, first NADH or NADPH donates a proton to the distal side of the double bond leaving a carbanion on what was the proximal side of the double bond, then this carbanion can abstract a proton from

a tyrosine active site residue [59]. The tyrosine hydroxyl has a pka of ~10 making it a potential proton donor in the context of an enzyme active site. At this point the fully reduced acyl chain is prepared for iterative condensations, reductions and dehydrations.

There has been significant effort into metabolic engineering of plants, yeast, and bacteria to select for the overproduction of fatty acids or molecules from the fatty acid pathway [60,61]. Large volume growth of organisms and their many metabolites that can be applied to everyday petrochemical supplements makes them a focus of study. To this point there have been very few engineering attempts involving the enzymes studied in this work and others involved in fatty acid biosynthesis with the exception of thioesterases from various organisms with altered substrate specificity [62]. The KASIII enzyme has been mutated to allow for increased acyl-CoA substrate plasticity by mutations at residue 87 [61]. These mutations of a phenylalanine to either tryptophan or threonine allowed for increased formation of polyhydroxyalkanoates in bacteria [63]. Overexpression of FabH leads to the accumulation of shorter chain fatty acids [13,61], a promising step in purifying useable fatty acids and allowing for the conversion by esterification or decarboxylation. The FabD enzyme has not been studied using mutagenesis for engineering, but has been overexpressed in E. coli and the resulting fatty acid pool analyzed. These studies showed that overexpression of the FabD enzyme increases the total amount of fatty acids in the cell [64]. This type of study lends merit to the motivation of mutating FabD to accept non canonical substrates and using that enzyme in an organism. The limited

mutagenesis and basic functional studies necessitates the structural and functional characterization of these enzymes with an overall focus on downstream metabolic engineering, regulatory effects, and potential inhibitor design.

Fatty acid biosynthesis is critical to the proliferation of all forms of life, but its products are also of interest due to their application to biorenewable resources [65,66,67]. Highly reduced carbon chains provide products or intermediates that resemble important molecules derived from fossil fuel sources. Short to medium chain fatty acids would provide drop in replacements for fuels while long chain fatty acids can be used to supplement oils and lubricants. Biorenewable sources of diacids such as adipic acid can be implemented into nylon production [68]. This dissertation will discuss our efforts to analyze the structure and function of enzymes and enzyme variants that have enhanced substrate recognition capabilities. We also investigated the structure of these enzymes and determined how substrate recognition can be manipulated to allow for less stringent substrate specificity.

Works Cited

1. Wakil SJ, Stoops JK, Joshi VC (1983) Fatty acid synthesis and its regulation. Annu Rev Biochem 52: 537-579.

2. Campbell JW, Cronan JE, Jr. (2001) Bacterial fatty acid biosynthesis: targets for antibacterial drug discovery. Annu Rev Microbiol 55: 305-332.
3. White SW, Zheng J, Zhang YM, Rock (2005) The structural biology of type II fatty acid biosynthesis. Annu Rev Biochem 74: 791-831.
4. Smith S, Witkowski A, Joshi AK (2003) Structural and functional organization of the animal fatty acid synthase. Prog Lipid Res 42: 289-317.
5. Lomakin IB, Xiong Y, Steitz TA (2007) The crystal structure of yeast fatty acid synthase, a cellular machine with eight active sites working together. Cell 129: 319-332.
6. Maier T, Leibundgut M, Ban N (2008) The crystal structure of a mammalian fatty acid synthase. Science 321: 1315-1322.
7. Fernandez-Moya R, Leber C, Cardenas J, Da Silva NA (2015) Functional replacement of the Saccharomyces cerevisiae fatty acid synthase with a bacterial type II system allows flexible product profiles. Biotechnol Bioeng 112: 2618-2623.
8. Alberts AW, Majerus PW, Talamo B, Vagelos PR (1964) Acyl-Carrier Protein. Ii. Intermediary Reactions of Fatty Acid Synthesis. Biochemistry 3: 1563-1571.
9. Alberts AW, Goldman P, Vagelos PR (1963) The condensation reaction of fatty acid synthesis. I. Separation and properties of the enzymes. J Biol Chem 238: 557-565.
10. Goldman P, Alberts AW, Vagelos PR (1963) The Condensation Reaction of Fatty Acid Synthesis.Iii. Identification of the Protein-Bound Product of the Reaction and Its Conversion to Long Chain Fatty Acids. J Biol Chem 238: 3579-3583.
11. Goldman P, Alberts AW, Vagelos PR (1963) The condensation reaction of fatty acid biosynthesis. II. Requirement of the enzymes of the condensation reaction for fatty acid synthesis. J Biol Chem 238: 1255-1261.
12. Brady RO (1958) The Enzymatic Synthesis of Fatty Acids by Aldol Condensation. Proc Natl Acad Sci U S A 44: 993-998.
13. Tsay JT, Oh W, Larson TJ, Jackowski S, Rock CO (1992) Isolation and characterization of the beta-ketoacyl-acyl carrier protein synthase III gene (fabH) from Escherichia coli K-12. J Biol Chem 267: 6807-6814.
14. Ruch FE, Vagelos PR (1973) The isolation and general properties of Escherichia coli malonyl coenzyme A-acyl carrier protein transacylase. J Biol Chem 248: 8086-8094.
15. Heath RJ, Rock CO (1996) Regulation of fatty acid elongation and initiation by acyl-acyl carrier protein in Escherichia coli. J Biol Chem 271: 1833-1836.
16. Ruch FE, Vagelos PR (1973) Characterization of a malonyl-enzyme intermediate and identification of the malonyl binding site in malonyl coenzyme A-acyl carrier protein transacylase of Escherichia coli. J Biol Chem 248: 8095-8106.
17. Ohlrogge JB, Jaworski JG (1997) Regulation of Fatty Acid Synthesis. Annu Rev Plant Physiol Plant Mol Biol 48: 109-136.

18. Harwood JL (1996) Recent advances in the biosynthesis of plant fatty acids. Biochim Biophys Acta 1301: 7-56.
19. Hiltunen JK, Schonauer MS, Autio KJ, Mittelmeier TM, Kastaniotis AJ, et al. (2009) Mitochondrial fatty acid synthesis type II: more than just fatty acids. J Biol Chem 284: 9011-9015.
20. Raetz CR, Whitfield C (2002) Lipopolysaccharide endotoxins. Annu Rev Biochem 71: 635-700.
21. Sheppard AJ, Iverson JL, Weihrauch JL (1978) Fatty Acids and Glycerides, Compostion of Selected Dietary Fats, Oils, Margarines, and Butter. Handbook of Lipid Research 1: 341-379.
22. El Boulifi N, Aracil J, Martinez M (2010) Lipase-catalyzed synthesis of isosorbide monoricinoleate: process optimization by response surface methodology. Bioresour Technol 101: 8520-8525.
23. Perera MA, Qin W, Yandeau-Nelson M, Fan L, Dixon P, et al. (2010) Biological origins of normal-chain hydrocarbons: a pathway model based on cuticular wax analyses of maize silks. Plant J 64: 618-632.
24. Chan M, Himes RH, Akagi JM (1971) Fatty acid composition of thermophilic, mesophilic, and psychrophilic clostridia. J Bacteriol 106: 876-881.
25. Mejia R, Gomez-Eichelmann MC, Fernandez MS (1999) Fatty acid profile of Escherichia coli during the heat-shock response. Biochem Mol Biol Int 47: 835-844.
26. Koga Y (2012) Thermal adaptation of the archaeal and bacterial lipid membranes. Archaea 2012: 789652.
27. Lombard J, Lopez-Garcia P, Moreira D (2012) The early evolution of lipid membranes and the three domains of life. Nat Rev Microbiol 10: 507-515.
28. Soderberg T, Chen A, Poulter CD (2001) Geranylgeranylglyceryl phosphate synthase. Characterization of the recombinant enzyme from Methanobacterium thermoautotrophicum. Biochemistry 40: 14847-14854.
29. Heald R, Cohen-Fix O (2014) Morphology and function of membrane-bound organelles. Curr Opin Cell Biol 26: 79-86.
30. Gogarten JP, Kibak H, Dittrich P, Taiz L, Bowman EJ, et al. (1989) Evolution of the vacuolar H+-ATPase: implications for the origin of eukaryotes. Proc Natl Acad Sci U S A 86: 6661-6665.
31. Cingolani G, Duncan TM (2011) Structure of the ATP synthase catalytic complex (F(1)) from Escherichia coli in an autoinhibited conformation. Nat Struct Mol Biol 18: 701-707.
32. Berg J, Tymoczko J, Stryer L (2002) Biochemistry. Section 22.1.
33. Alvarez HM, Steinbuchel A (2002) Triacylglycerols in prokaryotic microorganisms. Appl Microbiol Biotechnol 60: 367-376.
34. Darvey IG (1998) How does the ratio of ATP yield from the complete oxidation of

palmitic acid to that of glucose compare with the relative energy

contents of fat and carbohydrate? Biochemical Education 26: 22-23.

35. Lerouge I, Vanderleyden J (2002) O-antigen structural variation: mechanisms and possible roles in animal/plant-microbe interactions. FEMS Microbiol Rev 26: 17-47.
36. Zhang GH, Wu RD, Zheng HY, Zhang XL, Zhang MX, et al. (2015) Lipopolysaccharide Increases Immune Activation and Alters T Cell Homeostasis in SHIVB'WHU Chronically Infected Chinese Rhesus Macaque. J Immunol Res 2015: 202738.
37. Gehring AM, Lambalot RH, Vogel KW, Drueckhammer DG, Walsh CT (1997) Ability of Streptomyces spp. acyl carrier proteins and coenzyme A analogs to serve as substrates in vitro for E. coli holo-ACP synthase. Chem Biol 4: 17-24.
38. Lambalot RH, Walsh CT (1995) Cloning, overproduction, and characterization of the Escherichia coli holo-acyl carrier protein synthase. J Biol Chem 270: 24658-24661.
39. McAllister KA, Peery RB, Zhao G (2006) Acyl carrier protein synthases from gram-negative, gram-positive, and atypical bacterial species: Biochemical and structural properties and physiological implications. J Bacteriol 188: 4737-4748.
40. Parris KD, Lin L, Tam A, Mathew R, Hixon J, et al. (2000) Crystal structures of substrate binding to Bacillus subtilis holo-(acyl carrier protein) synthase reveal a novel trimeric arrangement of molecules resulting in three active sites. Structure 8: 883-895.
41. Bunkoczi G, Pasta S, Joshi A, Wu X, Kavanagh KL, et al. (2007) Mechanism and substrate recognition of human holo ACP synthase. Chem Biol 14: 1243-1253.
42. Takiff HE, Baker T, Copeland T, Chen SM, Court DL (1992) Locating essential Escherichia coli genes by using mini-Tn10 transposons: the pdxJ operon. J Bacteriol 174: 1544-1553.
43. Liu Y, Feng Y, Wang Y, Li X, Cao X, et al. (2015) Structural and biochemical characterization of MCAT from photosynthetic microorganism Synechocystis sp. PCC 6803 reveal its stepwise catalytic mechanism. Biochem Biophys Res Commun 457: 398-403.
44. Hong SK, Kim KH, Park JK, Jeong KW, Kim Y, et al. (2010) New design platform for malonyl-CoA-acyl carrier protein transacylase. FEBS Lett 584: 1240-1244.
45. Hong SK, Kim KH, Kim EE (2010) Cloning, purification, crystallization and preliminary X-ray crystallographic analysis of MCAT from Staphylococcus aureus. Acta Crystallogr Sect F Struct Biol Cryst Commun 66: 20-22.
46. Baugh L, Gallagher LA, Patrapuvich R, Clifton MC, Gardberg AS, et al. (2013) Combining functional and structural genomics to sample the essential Burkholderia structome. PLoS One 8: e53851.
47. Ghadbane H, Brown AK, Kremer L, Besra GS, Futterer K (2007) Structure of Mycobacterium tuberculosis mtFabD, a malonyl-CoA:acyl carrier protein transacylase (MCAT). Acta Crystallogr Sect F Struct Biol Cryst Commun 63: 831-835.

48. Oefner C, Schulz H, D'Arcy A, Dale GE (2006) Mapping the active site of Escherichia coli malonyl-CoA-acyl carrier protein transacylase (FabD) by protein crystallography. Acta Crystallogr D Biol Crystallogr 62: 613-618.
49. Serre L, Verbree EC, Dauter Z, Stuitje AR, Derewenda ZS (1995) The Escherichia coli malonyl-CoA:acyl carrier protein transacylase at 1.5-A resolution. Crystal structure of a fatty acid synthase component. J Biol Chem 270: 12961-12964.
50. Dreier J, Li Q, Khosla C (2001) Malonyl-CoA:ACP transacylase from Streptomyces coelicolor has two alternative catalytically active nucleophiles. Biochemistry 40: 12407-12411.
51. Jackowski S, Rock CO (1987) Acetoacetyl-acyl carrier protein synthase, a potential regulator of fatty acid biosynthesis in bacteria. J Biol Chem 262: 7927-7931.
52. Davies C, Heath RJ, White SW, Rock CO (2000) The 1.8 A crystal structure and active-site architecture of beta-ketoacyl-acyl carrier protein synthase III (FabH) from escherichia coli. Structure 8: 185-195.
53. Borgaro JG, Chang A, Machutta CA, Zhang X, Tonge PJ (2011) Substrate recognition by beta-ketoacyl-ACP synthases. Biochemistry 50: 10678-10686.
54. Toomey RE, Wakil SJ (1966) Studies on the mechanism of fatty acid synthesis. XV. Preparation and general properties of beta-ketoacyl acyl carrier protein reductase from Escherichia coli. Biochim Biophys Acta 116: 189-197.
55. Ploux O, Masamune S, Walsh CT (1988) The NADPH-linked acetoacetyl-CoA reductase from Zoogloea ramigera. Characterization and mechanistic studies of the cloned enzyme over-produced in Escherichia coli. Eur J Biochem 174: 177-182.
56. Brown A, Affleck V, Kroon J, Slabas A (2009) Proof of function of a putative 3-hydroxyacyl-acyl carrier protein dehydratase from higher plants by mass spectrometry of product formation. FEBS Lett 583: 363-368.
57. Sharma SK, Kapoor M, Ramya TN, Kumar S, Kumar G, et al. (2003) Identification, characterization, and inhibition of Plasmodium falciparum beta-hydroxyacyl-acyl carrier protein dehydratase (FabZ). J Biol Chem 278: 45661-45671.
58. Vick JE, Clomburg JM, Blankschien MD, Chou A, Kim S, et al. (2015) Escherichia coli enoyl-acyl carrier protein reductase (FabI) supports efficient operation of a functional reversal of beta-oxidation cycle. Appl Environ Microbiol 81: 1406-1416.
59. Massengo-Tiasse RP, Cronan JE (2009) Diversity in enoyl-acyl carrier protein reductases. Cell Mol Life Sci 66: 1507-1517.
60. Clomburg JM, Gonzalez R (2010) Biofuel production in Escherichia coli: the role of metabolic engineering and synthetic biology. Appl Microbiol Biotechnol 86: 419-434.
61. Handke P, Lynch SA, Gill RT (2011) Application and engineering of fatty acid biosynthesis in Escherichia coli for advanced fuels and chemicals. Metab Eng 13: 28-37.

62. Lennen RM, Pfleger BF (2012) Engineering Escherichia coli to synthesize free fatty acids. Trends Biotechnol 30: 659-667.
63. Nomura CT, Tanaka T, Gan Z, Kuwabara K, Abe H, et al. (2004) Effective enhancement of short-chain-length-medium-chain-length polyhydroxyalkanoate copolymer production by coexpression of genetically engineered 3-ketoacyl-acyl-carrier-protein synthase III (fabH) and polyhydroxyalkanoate synthesis genes. Biomacromolecules 5: 1457-1464.
64. Zhang X, Agrawal A, San KY (2012) Improving fatty acid production in Escherichia coli through the overexpression of malonyl coA-acyl carrier protein transacylase. Biotechnol Prog 28: 60-65.
65. Nikolau BJ, Perera MA, Brachova L, Shanks B (2008) Platform biochemicals for a biorenewable chemical industry. Plant J 54: 536-545.
66. Tan Z, Yoon JM, Nielsen DR, Shanks JV, Jarboe LR (2016) Membrane engineering via trans unsaturated fatty acids production improves Escherichia coli robustness and production of biorenewables. Metab Eng 35: 105-113.
67. Gronenberg LS, Marcheschi RJ, Liao JC (2013) Next generation biofuel engineering in prokaryotes. Curr Opin Chem Biol 17: 462-471.
68. Vardon DR, Rorrer NA, Salvachua D, Settle AE, Johnson CW, et al. (2016) cis,cis-Muconic acid: separation and catalysis to bio-adipic acid for nylon-6,6 polymerization. Green Chemistry 18: 3397-3413.

CHAPTER 2. PREPARATION OF HOLO- AND MALONYL-[ACYL-CARRIER-PROTEIN] IN A MANNER SUITABLE FOR ANALOG DEVELOPMENT

Aaron M. Marcella, Fuyuan Jing, Adam W. Barb

Roy J. Carver Department of Biochemistry, Biophysics and Molecular Biology

Iowa State University, Ames, IA 50011

A paper in **Protein Expression and Purification**

Highlights:

1. We demonstrate the lab-scale production of holo-ACP and malonyl-ACP to high titers

2. The ACP and ACP synthase polypeptides form a discrete oligomer

3. The beta-ketoacyl synthase FabH efficiently utilizes our malonyl-ACP preparation

4. We describe a fluorescence-based assay to monitor FabH activity

Abstract

The fatty acid biosynthetic pathway generates highly reduced carbon based molecules. For this reason fatty acid synthesis a target of pathway engineering to produce novel specialty or commodity chemicals using renewable techniques to supplant molecules currently derived from petroleum. Malonyl-[acyl carrier protein] (malonyl-ACP) is a key metabolite in the fatty acid pathway and donates two carbon units to the growing fatty acid chain during each step of biosynthesis. Attempts to test engineered fatty acid biosynthesis enzymes in vitro will require malonyl-ACP or malonyl-ACP analogs. Malonyl-ACP is challenging to prepare due to the instability of the carboxylate leaving group and the multiple steps of post-translational modification required to activate ACP. Here we report the expression and purification of holo- and malonyl-ACP from *Escherichia coli* with high yields (>15 mg per L of expression). The malonyl-ACP is efficiently recognized by the *E. coli* keto-acylsynthase enzyme, FabH. A FabH assay using malonyl-ACP and a coumarin-based fluorescent reagent is described that provides a high throughput alternative to reported radioactive assays.

Introduction

The promise of biorenewable chemicals for the chemical industry extends beyond replacing the petroleum source of contemporary chemical precursors and reaches towards developing new molecules with alternative functionalization and structure [1]. To achieve this goal, enzymes, biosynthetic pathways, and

microorganisms must be engineered to synthesize alternative substrates. One fundamental barrier to progress is preparing appropriate substrates, many of which are protein-bound intermediates and thus challenging synthetic targets.

Fatty acid biosynthesis (FAS) is one pathway targeted for engineering [2]. Prokaryotic fatty acid biosynthesis employs a dissociated multi-polypeptide system that allows for the targeting of individual enzymes, unlike eukaryotic FAS which uses a fused system [3]. The products of the pathway are long chain hydrocarbons that have significant commercial value. The *Escherichia coli* FAS machinery can be manipulated into producing free fatty acids [4]. It has also been demonstrated that varying fatty acid chain length can be selected for in *E. coli* variants [5]. Alternative, shorter compounds can be produced by truncating the pathway and will serve as novel starting points to prepare a wide range of compounds. It is widely believed that the pathways may be engineered for the production of custom molecules [6-8]

E. coli β-keto-acylsynthase III (FabH) catalyzes the Claisen-condensation of malonyl-ACP and acetyl-coenzyme A (acetyl-CoA) as the priming step of fatty acid biosynthesis (Figure 2-1) [9]. This reaction yields the four carbon acetoacetyl-ACP product which serves as the substrate for two NADH/NADPH-dependent reduction steps, generating butyryl-ACP that can be extended in a malonyl-ACP dependent reaction by the keto-acylsynthase I or II enzymes [10]. In vitro examination of this system requires high titers of malonyl-ACP.

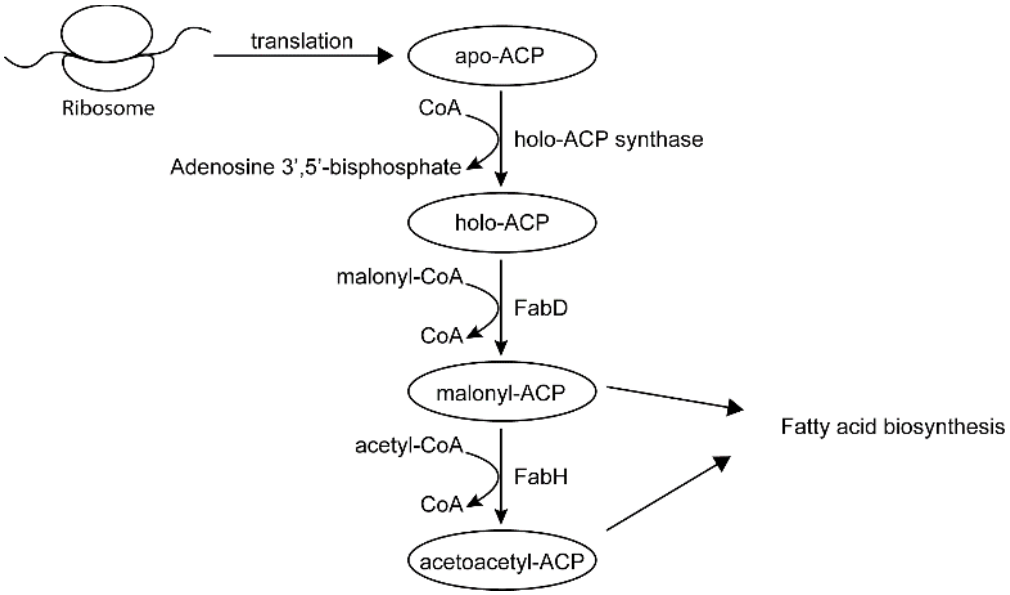

Figure 2-1. An excerpt from the fatty acid biosynthesis pathway highlights the steps of ACP modification. ACP and its various modified forms are highlighted. The enzymes that catalyze these reactions are indicated in ***bold***.

Malonyl-ACP is challenging to prepare for multiple reasons, the first of which is that holo-ACP is required as a substrate (Fig 2-1) [11]. Holo-ACP is formed by the transfer of phosphopantetheine from CoA to serine 36 of apo-ACP, the unmodified polypeptide [12, 13]. This reaction can be performed on the benchtop or *in vivo* with overexpression of the holo-ACP synthase gene [11]. Malonyl-ACP is then formed by the transfer of the malonyl moiety from malonyl-CoA to holo-ACP and is catalyzed by the malonly-CoA:ACP transacylase, FabD [14, 15]. Once prepared, malonyl-ACP spontaneously decarboxylates to form acetyl-ACP.

We developed a strategy to prepare holo-ACP by coexpressing apo-ACP and holo-ACP synthase in *E. coli* with a pETDueT^{TM} (EMD Millipore) vector. This system allows for a simplified expression system that provides post-translational modification in situ. Because malonyl-ACP is labile, we developed a strategy to

modify holo-ACP in vitro. The combination of improved expression techniques and a high-throughput fluorescence based assay will allow for facile modification of the ACP or malonyl-CoA donor to probe engineered enzymes in vitro.

Materials and Methods

Materials- All materials were purchased from Sigma-Aldrich unless noted otherwise. All buffers were made with double distilled water.

Expression and purification of holo-ACP- Holo-ACP was expressed in *E. coli* BL21* DE3 cells harboring a pETDuet™-vector (EMD-Millipore) containing the apo-ACP and holo-ACP synthase genes under control of individual T7 promoters. Apo-ACP was cloned into *BamHI* and *EcoRI* of the first multiple cloning site (MCS) while holo-ACP synthase was inserted into the *NdeI* and *XhoI* restriction sites in the second MCS of the pETDuet™ vector. The holo-ACP expression cassette is designed to include a 6xHis tag at the N-terminus and the holo-ACP synthase cassette includes no modifications. *E. coli* cells were transformed with the protein expression vector and grown to mid log phase (OD_{600}=0.5) at 37 °C in a shaking incubator (Thermo Scientific MaxQ 4000) and induced with 0.5 mM Isopropyl β-D-1-thiogalactopyranoside (IPTG). At the moment of induction, temperature was reduced to 18 °C. After 16-18 hours cells were pelleted and resuspended in 25 mL lysis buffer (20 mM Tris(hydroxymethyl)aminomethane (TRIS), 500 mM sodium chloride, 1 mM 2-mercaptoethanol pH=8.1). The cell suspension was then passed through an Emulsiflex C5 homogenizer (Avestin) five times at 15000 psi. Cell debris was

removed from the lysate by centrifugation at 14000 rpm for 1 h in a Fisher Scientific Sorvall Legend XTR centrifuge operating at 4 °C. The clarified lysate (CL) was applied to a 5 mL nickel-NTA column (Qiagen) pre-equilibrated with lysis buffer. The flow through (FT) was collected and set aside on ice. The column was washed with 25 mL of the base buffer 20 mM TRIS, 500 mM sodium chloride, 1 mM 2-mercaptoethanol, pH 8.1 (W1), then washed again with 25 mL of the base buffer plus 30 mM imidazole (W2), followed by 25 mL of the base buffer plus 50 mM imidazole (W3). Protein was eluted in three 5 mL fractions with a buffer consisting of the base buffer plus 100 mM imidazole, followed by three 5 mL fractions with the base buffer plus 250 mM imidazole. Fractions were analyzed by SDS-PAGE by loading 2.5 µl of each elution and wash fraction onto a 20% SDS PAGE gel.

Fractions containing holo-ACP were pooled and diluted to a final salt concentration of 50 mM and loaded onto a 2.6 cm diameter column containing 150 mL Q-Sepharose Fast Flow resin (GE healthcare). A two buffer system was employed to wash and run the column. Buffer A consisted of 25 mM 3-morpholinopropane-1-sulfonic acid (MOPS), 1 mM 2-mercaptoethanol, pH 7.1. Buffer B was buffer A plus 1M potassium chloride, pH 7.1. All buffers were made with a filter sterilized stock of MOPS buffer. The Q-column was loaded at a flow rate of 2 mL/min and then washed at the same flow rate with 50 mL of Buffer A, followed by elution with a 200 mL linear gradient from 200-600 mM potassium chloride by adjusting the ratio of A/B. The column was then washed with 25 mL

Buffer B, then 200 mL Buffer A. Fractions (8 mL) were collected and analyzed by SDS-PAGE.

Determining the amount of free thiol on holo-ACP- Purified holo-ACP (~10 mg) was concentrated to 500 µL using a 3 kDa MWCO Amicon centrifugal filter unit and then passed over a 5 mL G25 column equilibrated with 20 mM Tris-HCl, 100 mM NaCl, pH 7.5 to remove DTT. Fractions containing ACP were pooled and the volume reduced to 1 mL.

An aliquot of the ACP sample (50 µL) was added to a 950 µl solution containing 100 mM Tris-HCL and 200 µM 5,5'-dithiobis-(2-nitrobenzoic acid) (DTNB), pH 7.5. After a 30 min incubation at RT, absorbency at 412 nM was measured using a quartz cuvette and a Varian, Inc. Cary® 50 UV-Vis spectrophotometer. A similar reaction with 50 µL of the G25 equilibration buffer added to the 950 µL reaction mix listed above served as a blank for the A_{412} measurements. Each reaction was performed in triplicate. Similar assays were performed on control reactions that included the loading of only DTT on the G25 column. These results indicated that DTT and ACP eluted in resolved, non-overlapping peaks and DTT did not contaminate the ACP fractions.

Another aliquot was analyzed by ^{1}H NMR. The NMR sample (600 µL) consisted of 229.87 µL ACP, 5% D_2O, 200 µM DSS, 25 mM MOPS, 100 mM NaCl, 1 mM DTT, pH 7.0. The signals from five resolved methyl peaks upfield of the bulk protein signal were integrated and compared to the internal DSS standard to determine protein concentration using an 18.8T Bruker instrument equipped with an AvanceIII console and a 5 mm cryoprobe.

Expression and Purification of FabD and FabH: The genes encoding FabH and FabD were inserted into the pET29a and pET28b expression vectors (EMD Millipore) respectively. The constructs were unmodified and contained no tags. The expression was conducted as described above for holo-ACP. The FabH clarified lysate was applied to the 150 mL Q-Sepharose column and washed with 50 mL of a 100 mM sodium phosphate, 1 mM 2-mercaptoethanol, pH 7.0 buffer, followed by a linear gradient from 0-500 mM potassium chloride using same buffer, supplemented with 1 M potassium chloride. The column was then washed with 25 mL of the 1M potassium chloride buffer followed by 200 mL of the phosphate buffer with no potassium chloride. Fractions containing FabH as determined by SDS-PAGE were concentrated to ~5 mL using a 10kDa-cutoff Amicon filter (EMD) and applied to a 600 mm Superdex 200 column with a diameter of 26 mm (GE Healthcare). The S200 Column was run at a flow rate of 0.5 mL/min. Buffer used was 100 mM sodium phosphate and 1 mM dithiothreitol. The fractions containing FabH were concentrated and stored in 50% glycerol. The procedure for purifying FabD was the same as FabH, but the Q-column buffers consisted of 25 mM MOPS in place of sodium phosphate. The S200 buffer for FabD contained 25 mM MOPS, 100 mM sodium chloride, and 1 mM dithiothreitol.

Malonyl-ACP Preparation: Malonyl-ACP was prepared in a reaction containing 90 μM holo-ACP, 2.25 mM malonyl-CoA, 6 μM FabD, 25 mM MOPS, 100 mM sodium chloride, and 1 mM dithiothreitol, pH 7.1 in a final volume of 4 ml and incubated for 16-20 hours at 0 °C. Complete conversion to malonyl-ACP was

verified by MALDI-TOF MS using a Voyager-DE Pro MALDI-TOF instrument (Applied Biosystems). The spotting conditions were as follows: protein was diluted to ~10 μg/μL in DI water, this was then mixed 1 μL:1 μL in alpha-Cyano-4-hydroxycinnamic acid (ACH), and one μL was spotted on a JBI 100 well MALDI plate. Following conversion, malonyl-ACP was adsorbed onto a 1 ml nickel-NTA column (Qiagen). Reaction components were removed by extensively washing the column with a buffer containing 25 mM MOPS, 500 mM sodium chloride, 1 mM dithiothreitol, pH 7.1. Malonyl-ACP was eluted with the same buffer containing 25 mM MOPS, 500 mM sodium chloride, 1 mM dithiothreitol, and 30, 50 or 250 mM imidazole. Fractions containing malonyl-ACP were concentrated and exchanged into a buffer containing 25 mM MOPS, 100 mM sodium chloride, pH 7.1 using a 3 kDa-cutoff centrifugal filter device as described above. Protein was then diluted with glycerol to a final concentration of 10-25% (v/v) and 500 μM malonyl-ACP and stored at -80 °C.

FabH Activity Assays: A fluorometric assay was adapted [16] to monitor the appearance of CoA via a reaction of a fluorescent reagent 7-diethylamino-3-(4-maleimidophenyl)-4-methylcoumarin (CPM) with the newly formed CoA thiol. The FabH assay was conducted with 50 μM acetyl-CoA, 50 μM malonyl-ACP (or malonyl-CoA), 100 mM phosphate buffer, pH 7.0, at 30 °C in a volume of 100 μl. FabH concentrations ranged from 0.5-5 μM for the reactions with malonyl-CoA and 1-25 nM for the reactions with malonyl-ACP. Six 10 μl aliquots were removed from the reaction at various times and quenched with 190 μl of 10 μM CPM in 100% DMSO solution. Fluorescence was measured with excitation at 384 nm

and emission at 470 nm using a Cary Eclipse fluorimeter. The fluorimeter was calibrated using a standard curve of CoA in the quench solution.

Size exclusion chromatography of holo-ACP- Fractions containing holo-ACP from the Q-column were concentrated to 2-5 mL using a 3 kDa molecular weight cutoff centrifugal filter device (EMD Millipore) and loaded onto a 475 mm Superdex 75 (S75; GE Healthcare) column with a diameter of 26 mm. The column was washed with 25 mM MOPS, 100 mM sodium chloride, and 1 mM dithiothreitol. The column was run with a flow rate of 0.5 mL / min using the same buffer and 3.5 ml fractions were collected. SDS PAGE was used to analyze the fractions. Fractions containing holo-ACP were concentrated to <1 mL and diluted with glycerol to a final concentration of 25% (v/v) and stored at -80 °C.

Results and Discussion

Expression and identification of a stable complex

We developed a method that permits simultaneous expression of the ACP polypeptide and holo-ACP synthase enzyme in *E. coli* to facilitate recovery of holo-ACP. The ability to prepare ACP with a high percentage in the holo- form eliminates the need to separate holo-ACP and apo-ACP for downstream analysis. Furthermore, this coexpression method saves an additional step of CoA-dependent apo-ACP conversion in vitro.

ACP from the *E. coli* cell lysate was purified using an immobilized metal ion affinity column as shown in Figure 2-2.

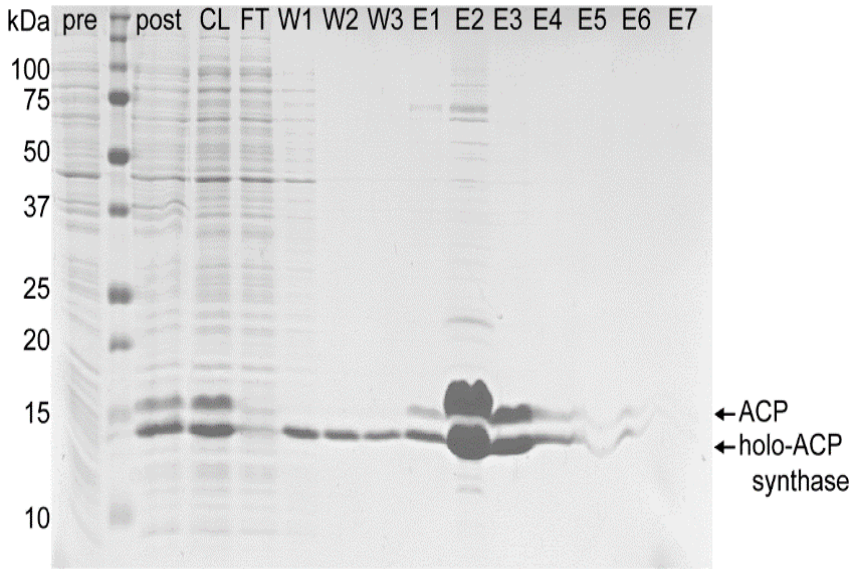

Figure 2-2. Purification of a holo-ACP:holo-ACP synthase complex using immobilized metal ion affinity chromatography."Pre" and "post" refers to samples of bacteria harvested at the time of IPTG addition or at the end of the culture, respectively. "CL" refers to the lysate following centrifugation, and "FT" is the lysate following passage over the column. Washes "W" and elutions "E" are as described.

ACP eluted at the same position as the coexpressed holo-ACP-synthase. MALDI-TOF MS analysis revealed that a high percentage of the ACP pool was modified with a phosphopantetheine moiety.

The ACP and holo-ACP synthase proteins were not separated by a S-75 size exclusion column. Although a very small amount of ACP eluted as a monomer from a gel-filtration column, the predominate pool of ACP eluted much

earlier and at the same time as the holo-ACP synthase as shown in Figure 2-3.

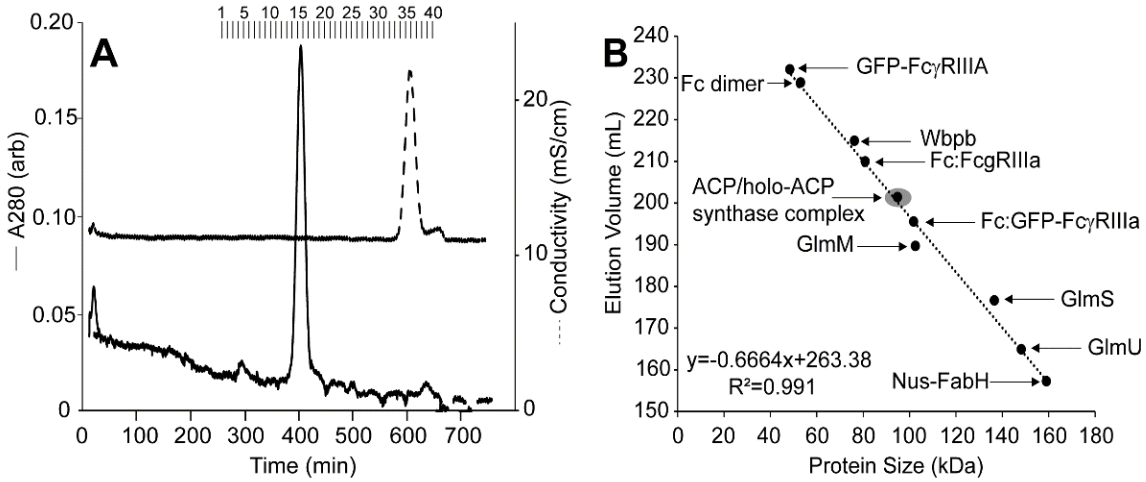

Figure 2-3. Size exclusion chromatography of the ACP:holo-ACP synthase complex. (A) Profiles of absorbency at 280 nm (*solid* line) and conductivity (*dashed* line) are shown from the purification using a Superdex S200 column. **(B)** Calibration curve for the S200 column using proteins of known mass.

ACP and holo-ACP synthase appeared to form a multimer that was stable and eluted in a single, sharp peak at a volume of 200 mL that corresponds to a molecular weight of 95.1 kDa (Figure 2-3) [17, 18]. This is a surprise because the masses of holo-ACP and holo-ACP synthase are 10.6 kDa and 13.9 kDa, respectively, though the *E. coli* holo-ACP synthase purifies as a homodimer [19]. It appears, based on the SDS-PAGE analysis that ACP and holo-ACP synthase elute with 1:1 stoichiometry. The molecular weights, stoichiometry, and dimer model for one partner suggest formation of a 4:4 heterooctamer with a theoretical molecular mass of 97.4 kDa. This predicted mass is only 2.5% greater than the observed mass of the ACP:holo-ACP synthase complex. Because estimates of molecular weight using gel filtration chromatography are sensitive to the shape of

the analyte, it is formally possible that the complex may also be either a 1:1 heterodimer, 2:2 heterotetramer or 3:3 heterohexamer.

The formation of a discrete multimeric complex is likely important for holo-ACP synthase function. It is important to note that the abundance of apo, holo, and acetyl-ACP in the complex is similar to the abundance of these forms in the free ACP that eluted much later from the column (data not shown). This is not surprising as *E. coli* holo-ACP synthase can utilize both CoA and acetyl-CoA with comparable efficiencies [19].

Separation of ACP and holo-ACP synthase

Initial attempts to disrupt the ACP-holo-ACP synthase complex with a size exclusion chromatography step at neutral, high or low pH, increased salt concentration, or metal ion affinity chromatography following incubation with 6M urea were largely unsuccessful.

Anion exchange chromatography was utilized, in lieu of the size exclusion chromatography step, to achieve the separation following a linear salt gradient as shown in Figure 2-4.

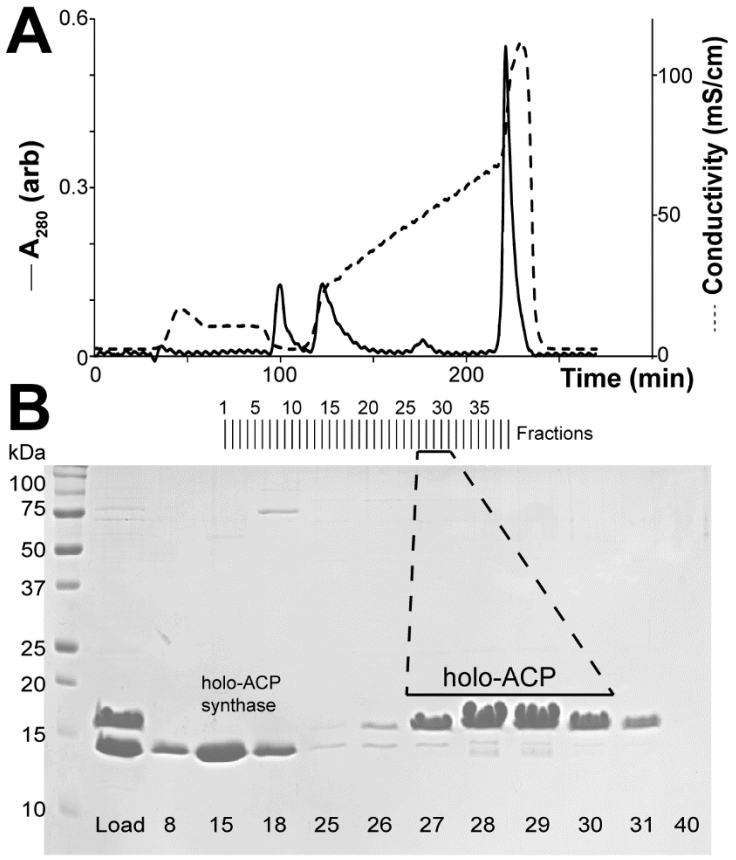

Figure 2-4. ACP is efficiently separated from holo-ACP synthase using anion exchange chromatography. (A) Profiles of absorbency at 280 nm (*solid* line) and conductivity (*dashed* line) are shown from purification using an anion exchange column. **(B)** SDS PAGE analysis of the fractions using a 20% acrylamide gel. Fraction numbers corresponding to the column purification are indicated.

The fractions containing holo-ACP synthase (8-18) contained only holo-ACP synthase and no ACP as shown in Figure 2-5. Fractions 27-31 and contained 15 mg of holo and acetyl-ACP (Table 1), but not holo-ACP synthase and are analyzed in Figure 2-6A. A portion of the holo-ACP pool shows the characteristic shift of 177 mass units, indicating the presence of His6-tag gluconoylation [20, 21].

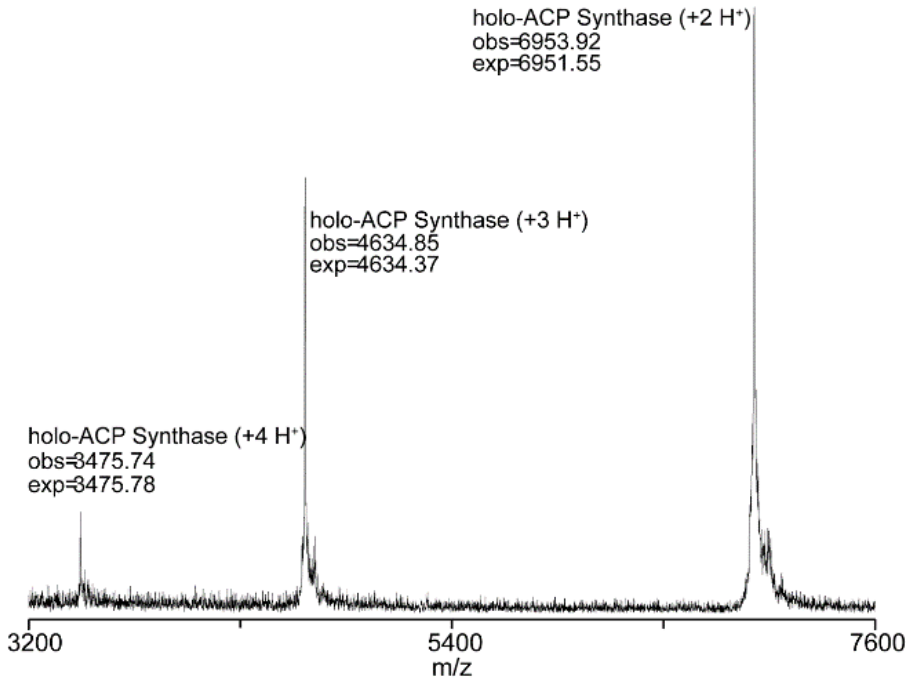

Figure 2-5. Analysis of holo-ACP synthase by mass spectrometry.
A MALDI-TOF spectrum of the holo-ACP-synthase following anion exchange purification. Three peaks shown for the synthase correspond to the $+2H^+$, $+3H^+$ and $+4H^+$ forms.

We pursued a chemical method to measure the degree of phosphopantetheine modification in the holo-ACP preparation using natural features of apo and holo-ACP because the MALDI-MS based method does not provide an accurate quantification. Phosphopantetheinylation catalyzed by the holo-ACP synthase introduces a free thiol to holo-ACP that is not present in apo-ACP which also contains no cysteine residues. Thus, a measurement of the free thiol content in a holo-ACP prep using the thiol-reactive reagent DTNB divided by the protein concentration as measured with NMR is expected to provide the percentage of phosphopantetheinylation that is accessible to further modification by FabD, the malonyl-CoA:ACP transferase. We determined that a sample containing 1.000 ± 0.083 molar equivalents of ACP polypeptide reacted with

0.800 ± 0.029 molar equivalents of DTNB. This result indicates that 80.0 ± 5.8% of the ACP pool contains a free thiol.

Conversion to malonyl-ACP

Malonyl-ACP is formed in a malonyl-CoA dependent reaction catalyzed by the malonyl-CoA:ACP transacylase FabD. Purified *E. coli* FabD efficiently converted holo-ACP to malonyl-ACP as shown in Figure 2-6B.

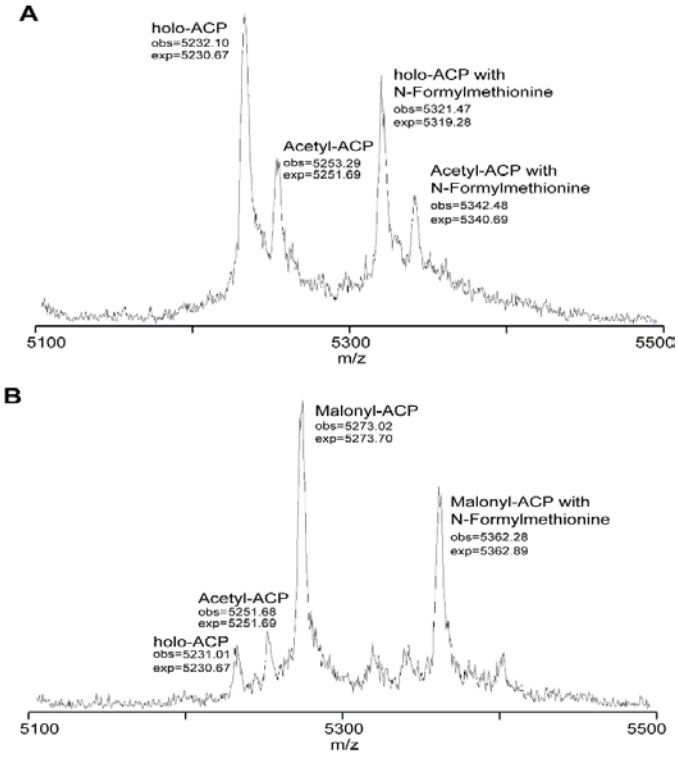

Figure 2-6. FabD efficiently converts holo-ACP to malonyl-ACP.(A) MALDI-TOF analysis of ACP fractions after anion exchange chromatography.**(B)** A MALDI-TOF spectrum following the FabD-catalyzed conversion of holo-ACP to malonyl-ACP. The ($+2H^+$) ions are shown in each panel.

This reaction was performed at 0°C to prevent spontaneous decarboxylation, which occurs rapidly at higher temperatures. Previous techniques to monitor malonyl-ACP involve conformational sensitive gel electrophoresis [10]. This

method provided insufficient resolution of holo and malonyl-ACP in our laboratory, so we optimized an existing MALDI-TOF method for high sensitivity detection [22].

It is curious to note that the levels of acetyl-ACP decrease during the reaction. *E. coli* FabD failed to catalyze a reaction with either acetyl-ACP or acetyl-CoA, suggesting a minor component in the reaction was responsible for depleting the acetyl-ACP pool. This unexpected side reaction was repeatable, and beneficial as it removed a contaminant to the malonyl-ACP preparation and occurred in a CoA dependent-manner. The acetyltransferase activity was removed from the ACP preparation by size exclusion chromatography using a Superdex 75 column (Figure 2-7).

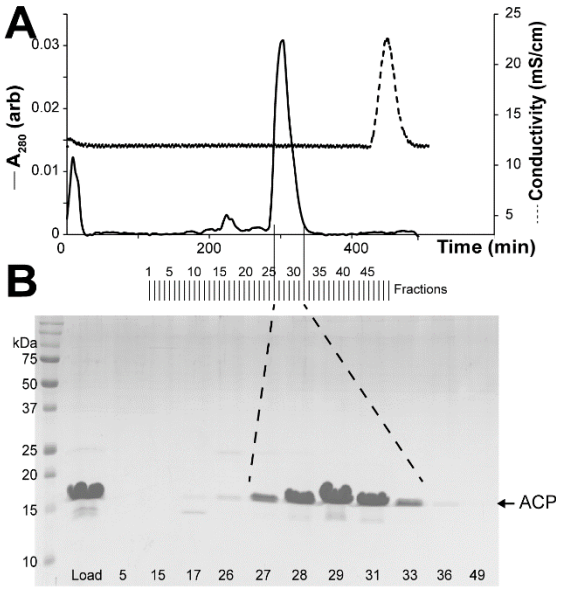

Figure 2-7. ACP elutes in a single peak from a Superdex75 size exclusion column. (A) Profiles of absorbency at 280 nm (*solid* line) and conductivity (*dashed* line) are shown. **(B)** SDS PAGE analysis of the S75 fractions using a 20% acrylamide gel. Fraction numbers corresponding to the column purification are indicated.

Following conversion to malonyl-ACP, reaction components are removed with a final metal affinity chromatography step using a 1 mL nickel column. Malonyl-ACP elutes in the 250 mM imidazole fractions. In total, 15 mg of malonyl-ACP was recovered from 1 L of *E. coli* expression (Table 2-1).

Table 2-1. Purification and preparation of malonyl-ACP from a 1 L *E. coli* expression.

Stage	total protein (mg)
Clarified Lysate	206
Nickel Column	62
Q Column	15

Enzymatic analysis of malonyl-ACP

Malonyl-ACP is a viable substrate for the enzyme FabH as shown by a fluorometric assay that traps the product CoA using the fluorescent coumarin-based reagent, CPM (Figure 2-8) [16]. Furthermore, the initial reaction velocity increased linearly with respect to FabH concentration (Fig 2-8B). The assay used is an alternative to the reported radioactivity-based assays and we observed a FabH reaction rate of specific activity of 1 µmole CoA mg^{-1} FabH min^{-1}. Radioactive assays for FabH monitoring [2-^{14}C] malonyl-ACP production have shown a specific activity of 3 µmoles CoA mg^{-1} FabH min^{-1} [9].

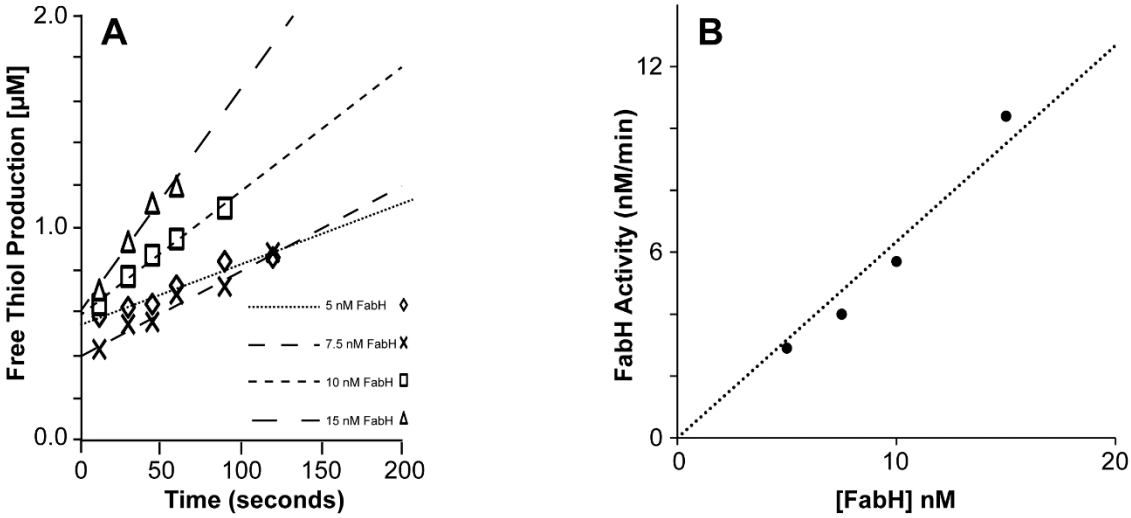

Figure 2-8. FabH efficiently utilizes malonyl-ACP. (A) The accumulation of CoA is plotted for various reactions with FabH, acetyl-CoA, and malonyl-ACP. Only early portions of the reaction are shown. **(B)** The rate of CoA formation increases linearly (*dotted* line) with FabH concentration using acetyl-CoA and malonyl-ACP as substrates. The result shown is representative of multiple, independent experiments.

Conclusion

Here we demonstrate a complete strategy for holo- and malonyl-ACP production and characterization. Through co-expression with a modifying enzyme, holo-ACP was prepared with a single protein expression step followed by a rapid two-step column purification. High yields of malonyl-ACP were prepared following a single in vitro enzymatic conversion. The utility of these reagents to probe the enzymes of fatty acid biosynthesis was also presented and the fluorescent method reported serves as a viable alternative to radioactive assays. This expression and purification strategy is amenable to modifications, particularly with respect to alterations at the malonyl moiety because the FabD-catalyzed CoA-ACP thiol exchange is the final step in the process. This work provides new and accessible

tools to probe fatty acid biosynthesis and substrates for enzymes designed as green catalysts for the renewable production of commodity or specialty chemicals.

Acknowledgements

We thank Prof. Basil Nikolau, Dr. Bruce Fulton, Dr. Ganesh P. Subedi and Dr. Uzma I. Zakai at ISU for their assistance with this project. This material is based upon work supported by the National Science Foundation under Award No. EEC-0813570, by funds from the Roy J. Carver Department of Biochemistry, Biophysics & Molecular Biology, the Center for Metabolic Biology, and the Laurence H. Baker Center for Bioinformatics & Biological Statistics at Iowa State University. Any opinions, findings, and conclusions or recommendations expressed in this material are those of the author(s) and do not necessarily reflect the views of the National Science Foundation.

Works Cited

[1] B.J. Nikolau, M.A. Perera, L. Brachova, B. Shanks, Platform biochemicals for a biorenewable chemical industry. Plant J 54 (2008) 536-545.

[2] J.W. Campbell, J.E. Cronan, Jr., Bacterial fatty acid biosynthesis: targets for antibacterial drug discovery. Annu Rev Microbiol 55 (2001) 305-332.

[3] S.J. Wakil, J.K. Stoops, V.C. Joshi, Fatty acid synthesis and its regulation. Annu Rev Biochem 52 (1983) 537-579.

[4] P. Xu, Q. Gu, W. Wang, L. Wong, A.G. Bower, C.H. Collins, M.A. Koffas, Modular optimization of multi-gene pathways for fatty acids production in E. coli. Nat Commun 4 (2013) 1409.

[5] H. Wu, K.Y. San, Engineering Escherichia coli for odd straight medium chain free fatty acid production. Appl Microbiol Biotechnol 98 (2014) 8145-8154.

[6] J.L. Blatti, J. Michaud, M.D. Burkart, Engineering fatty acid biosynthesis in microalgae for sustainable biodiesel. Curr Opin Chem Biol 17 (2013) 496-505.

[7] T.P. Howard, S. Middelhaufe, K. Moore, C. Edner, D.M. Kolak, G.N. Taylor, D.A. Parker, R. Lee, N. Smirnoff, S.J. Aves, J. Love, Synthesis of customized petroleum-replica fuel molecules by targeted modification of free fatty acid pools in Escherichia coli. Proc Natl Acad Sci U S A 110 (2013) 7636-7641.

[8] C. Khosla, J.D. Keasling, Metabolic engineering for drug discovery and development. Nat Rev Drug Discov 2 (2003) 1019-1025.

[9] R.J. Heath, C.O. Rock, Inhibition of beta-ketoacyl-acyl carrier protein synthase III (FabH) by acyl-acyl carrier protein in Escherichia coli. J Biol Chem 271 (1996) 10996-11000.

[10] R.J. Heath, C.O. Rock, Enoyl-acyl carrier protein reductase (fabI) plays a determinant role in completing cycles of fatty acid elongation in Escherichia coli. J Biol Chem 270 (1995) 26538-26542.

[11] Y. Liu, Y. Feng, Y. Wang, X. Li, X. Cao, S. Xue, Structural and biochemical characterization of MCAT from photosynthetic microorganism Synechocystis sp. PCC 6803 reveal its stepwise catalytic mechanism. Biochem Biophys Res Commun (2015).

[12] J. Elovson, P.R. Vagelos, Acyl carrier protein. X. Acyl carrier protein synthetase. J Biol Chem 243 (1968) 3603-3611.

[13] R.S. Flugel, Y. Hwangbo, R.H. Lambalot, J.E. Cronan, Jr., C.T. Walsh, Holo-(acyl carrier protein) synthase and phosphopantetheinyl transfer in Escherichia coli. J Biol Chem 275 (2000) 959-968.

[14] F.E. Ruch, P.R. Vagelos, Characterization of a malonyl-enzyme intermediate and identification of the malonyl binding site in malonyl coenzyme A-acyl carrier protein transacylase of Escherichia coli. J Biol Chem 248 (1973) 8095-8106.

[15] C. Oefner, H. Schulz, A. D'Arcy, G.E. Dale, Mapping the active site of Escherichia coli malonyl-CoA-acyl carrier protein transacylase (FabD) by protein crystallography. Acta Crystallogr D Biol Crystallogr 62 (2006) 613-618.

[16] C.C. Chung, K. Ohwaki, J.E. Schneeweis, E. Stec, J.P. Varnerin, P.N. Goudreau, A. Chang, J. Cassaday, L. Yang, T. Yamakawa, O. Kornienko, P. Hodder, J. Inglese, M. Ferrer, B. Strulovici, J. Kusunoki, M.R. Tota, T. Takagi,

A fluorescence-based thiol quantification assay for ultra-high-throughput screening for inhibitors of coenzyme A production. Assay Drug Dev Technol 6 (2008) 361-374.

[17] A.W. Barb, Intramolecular N-Glycan/Polypeptide Interactions Observed at Multiple N-Glycan Remodeling Steps through [(13)C,(15)N]-N-Acetylglucosamine Labeling of Immunoglobulin G1. Biochemistry 54 (2015) 313-322.

[18] G.P. Subedi, Q.M. Hanson, A.W. Barb, Restricted motion of the conserved immunoglobulin G1 N-glycan is essential for efficient FcgammaRIIIa binding. Structure 22 (2014) 1478-1488.

[19] K.A. McAllister, R.B. Peery, G. Zhao, Acyl carrier protein synthases from gram-negative, gram-positive, and atypical bacterial species: Biochemical and structural properties and physiological implications. J Bacteriol 188 (2006) 4737-4748.

[20] K.F. Geoghegan, H.B. Dixon, P.J. Rosner, L.R. Hoth, A.J. Lanzetti, K.A. Borzilleri, E.S. Marr, L.H. Pezzullo, L.B. Martin, P.K. LeMotte, A.S. McColl, A.V. Kamath, J.G. Stroh, Spontaneous alpha-N-6-phosphogluconoylation of a "His tag" in Escherichia coli: the cause of extra mass of 258 or 178 Da in fusion proteins. Anal Biochem 267 (1999) 169-184.

[21] J.C. Aon, R.J. Caimi, A.H. Taylor, Q. Lu, F. Oluboyede, J. Dally, M.D. Kessler, J.J. Kerrigan, T.S. Lewis, L.A. Wysocki, P.S. Patel, Suppressing posttranslational gluconoylation of heterologous proteins by metabolic engineering of Escherichia coli. Appl Environ Microbiol 74 (2008) 950-958.

[22] S. Lin, J.E. Cronan, The BioC O-methyltransferase catalyzes methyl esterification of malonyl-acyl carrier protein, an essential step in biotin synthesis. J Biol Chem 287 (2012) 37010-37020.

CHAPTER 3: A RAPID FLUOROMETRIC ASSAY FOR THE S-MALONYLTRANSACYLASE FABD AND OTHER SULFHYDRYL UTILIZING ENZYMES

Aaron M. Marcella, Adam W. Barb

Roy J. Carver Department of Biochemistry, Biophysics and Molecular Biology
2437 Pammel Drive
Molecular Biology Building, rm 4210
Iowa State University, Ames, IA 50011
A paper in the Journal of Biological Methods

Running Title:

Fluorometric assay for fatty acid biosynthesis

Abbreviations:
Fatty acid synthase (FAS), ketoacyl synthase III (FabH), malonyl-Coenzyme A transacylase (FabD), coenzyme A (CoA-SH), acyl carrier protein (ACP), 3-morpholinopropane-1-sulfonic acid (MOPS), ethylenediaminetetraacetic acid (EDTA), 2-mercaptoethanol (BME), dithiothreitol (DTT), trichloroacetic acid (TCA), 7-diethylamino-3-(4-maleimidophenyl)-4-methylcoumarin (CPM), Luria-Bertani (LB)

Abstract

The development of biorenewable chemicals will support green chemistry initiatives and supplement the catalog of starting materials available to the chemical industry. Bacterial fatty acid biosynthesis is being pursued as a source of protein catalysts to synthesize novel reduced carbon molecules in fermentation systems. The availability of methods to measure enzyme catalysis for native and engineered enzymes from this pathway remains a bottleneck because a simple quantitative enzyme assay for numerous enzymes doesn't exist. Here we present two variations of a fluorescence assay that is readily extendable to high-throughput screening and is appropriate for thiol consuming and generating enzymes including the *Escherichia* coli enzymes malonyl-coenzyme A transacylase (FabD) and keto-acylsynthase III (FabH). We measured K_M values of 60 ± 20 µM (acetyl-CoA) and 30 ± 10 µM (malonyl-ACP) and a k_{cat} of 7.4 - 9.0 s^{-1} with FabH. Assays of FabD included a precipitation step to remove the thiol-containing substrate holo-ACP from the reaction product coenzyme-A to estimate reaction rates. Analysis of saturation kinetics revealed K_M values of 60 ± 20 µM (malonyl-CoA) and 40 ± 10 µM (holo-ACP) and a k_{cat} of 2100 - 2600 $s^{-1}$for the FabD enzyme. Our data show similar results when compared to existing radioactive and continuous coupled assays in terms of sensitivity while providing the benefit of simplicity, scalability and repeatability. Fluorescence detection also eliminates the need for radioactive substrates traditionally used to assay these enzymes.

Introduction

Fatty acid biosynthesis produces reduced hydrocarbon chains and is a target of engineering efforts to develop novel routes to biorenewable chemicals [1]. Prokaryotic fatty acid biosynthesis is well characterized and a popular target for drop-in enzyme replacements due to implementation as a one-polypeptide/one-activity system unlike eukaryotic synthases that are expressed as a single fused polypeptide and likely more challenging to engineer [2,3,4]. Biorenewable chemicals are increasingly being produced in fermentative systems (ethanol, arachidonic acid, docosahexaenoic acid, short and medium chain fatty acids and others [5,6,7] and future needs will likely be met by recombinant microbes that express engineered enzymes and secrete novel materials.

Fatty acid biosynthesis builds a carbon chain on acyl carrier protein (ACP) two carbon units at a time. Acetyl-coenzyme A (acetyl-CoA) donates the two acetate carbons to prime the chain and the first reaction with malonyl-ACP generates acetoacetyl-ACP, carbon dioxide and CoA-SH. Acetoacetyl-ACP is reduced to butyryl-ACP and extended again using malonyl-ACP as the source of material. This extension/reduction cycle continues until the chain is cleaved from the acyl carrier protein or transferred directly to a lipid molecule.

Enzymes that generate carbon-carbon bonds, including the keto-acylsynthases (KAS), and enzymes that generate primers and extender units utilized by the keto-acylsynthases are of particular interest for biorenewable production. The β-ketoacyl-ACP synthase III (FabH) catalyzes the first priming in *Escherichia coli* fatty acid biosynthesis as shown in Figure 3-1.

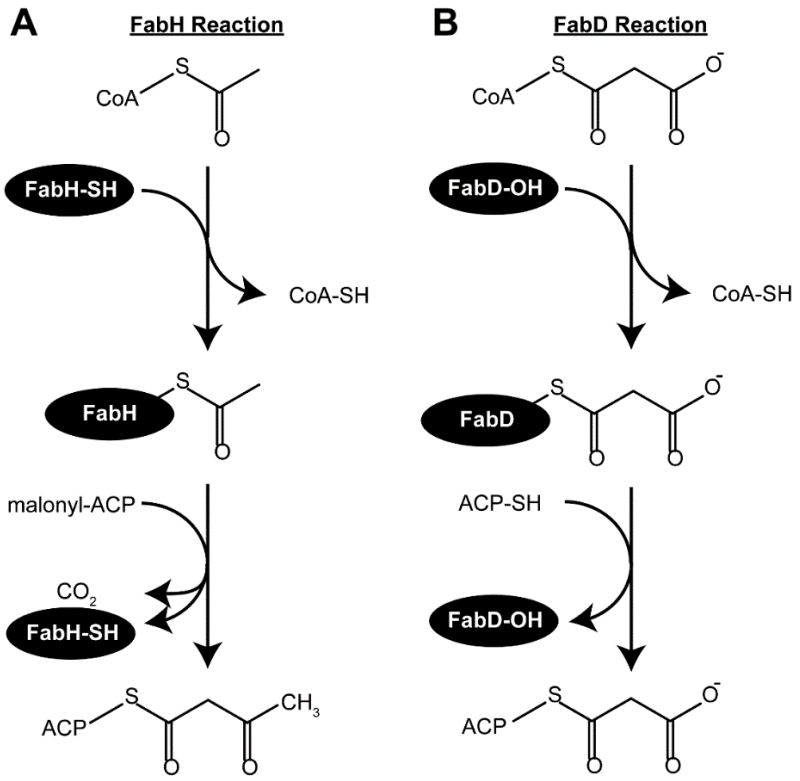

Figure 3-1. Reactions catalyzed by FabH and FabD.
A. FabH creates an acetyl-enzyme covalent intermediate at C112, releasing CoA-SH. Nucleophilic attack of the acetate by the decarboxylated malonyl-ACP forms acetoacetyl-ACP.
B. FabD catalysis begins with the generation of a covalent intermediate at S92. This releases CoA-SH and allows for holo-ACP to attack the malonate intermediate on FabD creating malonyl-ACP.

In fatty acid biosynthesis, the malonyl-CoA:ACP transacylase (FabD) generates the extender units by transferring the malonyl moiety from malonyl-CoA to holo-ACP, forming the free thiol form of CoA (CoA-SH) and malonyl-ACP as shown in Figure 3-1. The result is zero net change in free thiol concentration and is not amenable to thiol reactive enzyme assays unless the two compounds could be separated. Diversification of substrate recognition by FabD would be required to modify the extender units incorporated during chain elongation.

In vitro strategies to screen and characterize designed enzymes requires an enzyme assay that is applicable to many of the diverse fatty acid biosynthesis enzymes, including FabD and FabH, and capable of high throughput to thoroughly analyze numerous target substrates and enzyme variants. Sulfhydryl containing compounds including CoA-SH and holo-acyl carrier protein (holo-ACP) are utilized during biosynthesis and represent one common feature of many fatty acid biosynthesis enzymes that is detectable with high sensitivity in high throughput assays [11,12]. To date, the most common method of assessing enzyme activity for fatty acid biosynthesis enzymes involves radioactivity. While sensitive, these approaches are neither high throughput nor easily scalable [13,14,15,16]. Linked assays are also reported, but are neither easily adaptable to other enzymes in the pathway and [17] suffer from contaminants in the commercial enzyme preps (data not shown).

Here we describe a fluorescence-based strategy that can function with numerous enzymes in the FAS pathway including FabH and FabD at high sensitivity and is applicable to high throughput screening. Common implementations of thiol reactive reagents require a net thiol change which is problematic for detecting FabD activity through a liberated thiol as noted above [11]. We incorporated a facile step to separate CoA-SH from holo-ACP with reproducible and quantitative yields (Figure 3-2).

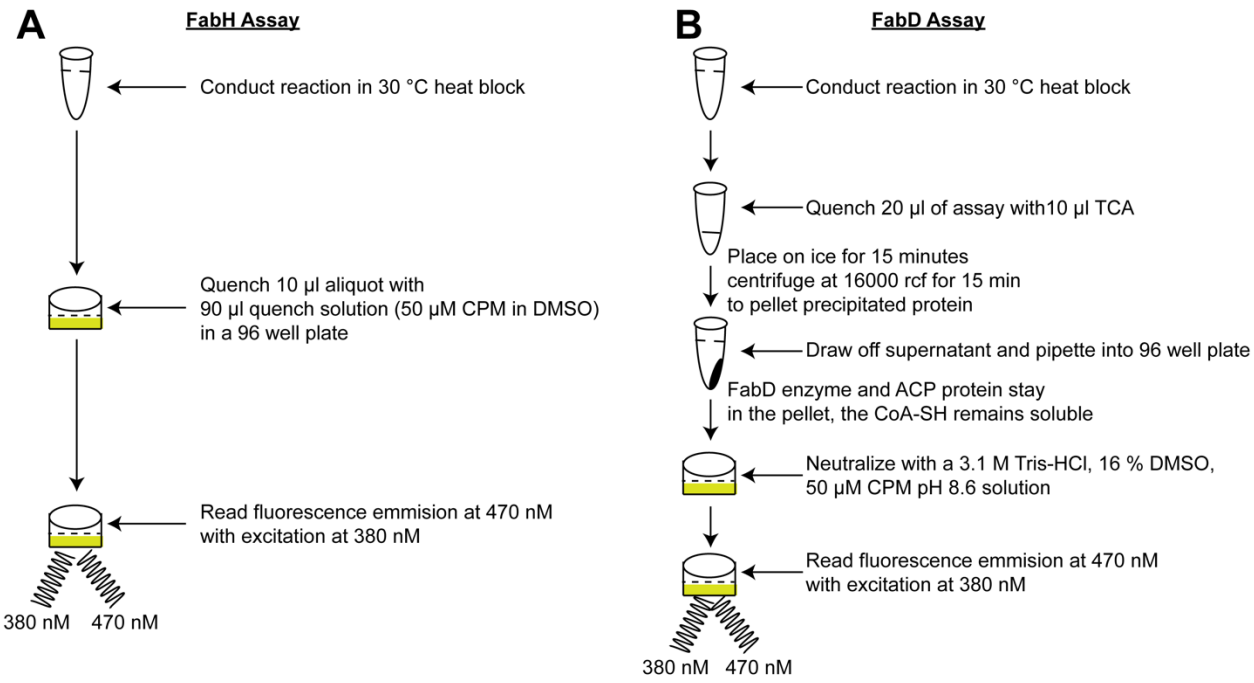

Figure 3-2. Flow diagram for the FabH and FabD assays. Both reactions utilize the reaction of CoA-SH with CPM to quantify product formation in the final step. The FabD assay differs because holo-ACP must be removed.

Free thiols, generated from the reaction cycle, are detected with 7-diethylamino-3-(4'-maleimidylphenyl)-4-methylcoumarin (CPM) [18]. This detection strategy is applicable to multiple enzymes and has proven to be reliable and sensitive [11,12].

Materials and Methods

All materials were purchased from Sigma Aldrich unless otherwise noted.

FabD Preparation. The open reading frame for the *Escherichia coli* FabD gene was cloned into pET28b using the NcoI and EcoRI sites. This cloning strategy adds only an extra glycine at the N-terminal of the enzyme and does not utilize the N or C-terminal poly-histidine tags available in the vector sequence. The

EcFabD pET28b vector was transformed into E. coli BL21* DE3 cells and a single colony was selected then grown overnight in a 5 mL Luria-Bertani (LB) culture with 50 µg/mL kanamycin. This culture was then added to 1 l LB with 50 µg/mL kanamycin and grown to mid log phase (OD_{600}~0.5) at 37 °C in a shaking incubator (Thermo Scientific MaxQ 4000). At this time fresh Isopropyl β-D-1-thiogalactopyranoside was added to a final concentration of 0.5 mM and incubated with shaking for approximately 18 hours at 18 °C. Cells were then pelleted by centrifugation and resuspended in 30 mL lysis buffer (25 mM MOPS, 1 mM EDTA, 1 mM BME, pH 7.1). The cell resuspension was lysed in an Emulsiflex C5 homogenizer (Avestin) five times at 12000 psi and the lysed cell debris pelleted at 24500 rcf in a Fisher Scientific Sorvall Legend XTR centrifuge for one hour. The clarified lysate was applied to a 110 mL Q-sepharose column (GE life sciences) and purified using two anion exchange buffers, A (lysis buffer) and B, lysis buffer supplemented with 1 M potassium chloride. The column was washed with 0.5 column volume (CV) of buffer A followed by a linear gradient from 5-50% buffer B over one column volume. The column was washed with 0.2 CV of 100% buffer B and finally 1.2 CV of 100% buffer A. Fractions were collected from the start of the gradient until the end of the run and the FabD enzyme elutes at ~30 % B.

Following anion exchange chromatography the fractions containing FabD were concentrated using a 10 kDa cutoff amicon ultracentrifugation filter unit (EMD Millipore) and applied to a Superdex S200 column (GE) equilibrated with 25 mM MOPS, 100 mM sodium chloride, 1 mM DTT, pH 7.1. Fractions

containing FabD were concentrated as above and stored in 50 % glycerol at -80 °C. FabD was quantified using the absorbance at 280 nm and an extinction coefficient of 32680 $M^{-1}cm^{-1}$.

FabH Preparation. FabH was purified using anion exchange chromatography as described previously [11]. The two buffers used were buffer A: 20 mM phosphate, 1 mM EDTA, 5 mM BME pH 7.0 and buffer B which is buffer A with 1 M potassium chloride. For FabH a linear gradient of buffer B was applied to the anion exchange column in the same manner as FabD. Following anion exchange chromatography the fractions containing FabH were pooled and applied to a blue sepharose column (GE) and a linear gradient of buffer B was used in the same way as the anion exchange step. Fractions containing FabH from the blue sepharose column were pooled and concentrated with a 10 kDa amicon filter and applied to an S200 column (GE). The S200 column was equilibrated and eluted with a buffer containing 20 mM phosphate, 50 mM KCl, 1 mM DTT, pH 7.0. Fractions containing FabH were pooled, concentrated as above and stored at 4 °C. The FabH extinction coefficient used for quantification was 25690 $M^{-1}cm^{-1}$.

Holo-ACP Preparation. Expression and purification of holo-ACP has been described previously [11]. Briefly, the acyl-carrier-protein and holo-(acyl-carrier-protein) synthase genes were cloned into a pETDUET vector (EMD-Millipore). Both proteins were expressed simultaneously following the same steps as FabD expression (above). After lysing and centrifuging the cells the clarified lysate was

applied to an 8 mL nickel column (Qiagen) and an imidazole gradient was run from 0-500 mM imidazole in buffers containing 20 mM Tris-HCl, 500 mM sodium chloride, pH 8.1. Fractions containing holo-ACP were diluted to reduce sodium chloride to 100 mM and loaded onto a 110 mL Q-Sepharose column. A linear gradient from 200-600 mM potassium chloride was applied to the column and the holo-ACP eluted around 500 mM potassium chloride. Fractions containing ACP were concentrated and exchanged into a buffer containing 25 mM MOPS, 100 mM sodium chloride, 1 mM DTT, pH 7.1 using a Superdex S75 column (GE). Fractions containing holo-ACP were concentrated using a 3 kDa amicon filter unit and stored at -80 °C in 10% glycerol. The ACP extinction coefficient used for quantification was 1490 $M^{-1}cm^{-1}$.

Malonyl-ACP Preparation. Malonyl-ACP for the FabH assays was prepared as described previously [11]. Briefly, malonyl-CoA and holo-ACP were combined at a 25:1 (mole:mole) ratio with 5 µM FabD in 5 mL of 25 mM MOPS, 100 mM sodium chloride, and 1 mM DTT, pH 7.0. After 5 hours at 0 °C the reaction was applied to a 1 mL nickel column. The column was washed 2x (5 mL each wash) with a buffer containing 20 mM Tris-HCl, 500 mM sodium chloride, pH 8.1, and eluted with 5x 1 mL aliquots of the above buffer supplemented with 250 mM imidazole. Fractions containing Malonyl-ACP were pooled concentrated and exchanged into a buffer containing 25 mM MOPS, 100 mM sodium chloride, pH 7.1, using an Amicon-Ultra 15 mL 3 kDa MWCO filter unit and stored at -80 °C following addition of glycerol to 10% v/v. The proportion of malonyl-ACP in the

total ACP pool was estimated at 40% using MALDI-TOF analysis, major contaminants include acetyl-ACP and holo-ACP (data not shown).

The FabD Assay (See Figure 3-2)**:**

Reagents:

- Wash buffer (25 mM MOPS, 100 mM sodium chloride, pH 7.1)
- Assay buffer (25 mM MOPS, 100 mM sodium chloride, 1 mg/mL BSA, pH 7.1)
- FabD Quench solution 1 (150 % w/v TCA)
- FabD Quench solution 2 (95 % w/v TCA)
- 1 mM CoA-SH
- 100 µM CoA-SH
- 3 mM holo-ACP
- 10 mM malonyl-CoA
- 1 nM FabD
- 3.75 M Tris-HCl (pH 8.6)
- 100 % DMSO
- 10 mM CPM in DMSO
- Neutralization solution (3.125 M Tris-HCl, 16.6 % DMSO, 50 µM CPM, pH 8.6)

1. Exchange FabD and holo-ACP into 25 mM MOPS, 100 mM sodium chloride, pH 7.1 buffer to reduce the concentration of DTT by about 1000 fold.

2. Conduct assays in 200 or 800 µl volumes depending on the total amount of ACP or malonyl-CoA in the assay, the higher reaction volume is needed to increase sensitivity for assays with low substrate concentrations.

3. An example 200 µl reaction is prepared with 4.7 µl 3 mM holo-ACP (70 µM final), 20 µl 1 nM FabD enzyme (100 pM), with assays being brought to final volume (196 µl) with 171.3 µl assay buffer in a 1.5 mL tube.

4. Place reactions in a 30 °C heat block to warm for 1 minute. Start assays with 4 µl of 10 mM malonyl-CoA (200 µM final).

5. Aliquots (20 µl) are taken at intervals of 10 s for 1 min. Aliquots are immediately placed into FabD quench solution 1 then incubated on ice for five minutes (for 800 µl reactions, quench 80 µl into 40 µl FabD quench solution 2 and place on ice). Quenched reactions are centrifuged at 16000 xg in a microcentrifuge at 4 °C for 15 minutes to pellet the protein.

6. Draw off the supernatant (20 µl) and pipette into a 96 well dark sided plate with clear bottom (ThermoFisher). 50 µl of the neutralization solution is added to the plates and mixed thoroughly. It is critical to use enough Tris-HCl to ensure proper buffering of the reaction solution and complete reaction with the CPM reagent. This can be verified by applying ~1 µl of neutralized reaction to pH paper.

7. Read plates in a plate reader (Tecan Safire) with an excitation wavelength of 380 nm and emission at 470 nm. Rates of product accumulation are fitted with a line over the linear portion of the assays using MS-Excel. Fits of

the Michaelis-Menten equation were performed using DynaFit (www.biokin.com/dynafit/).

8. Make a standard curve using assay buffer and CoA-SH. For the 200 µl volume assays, mix 20 µl CoA-SH solution in reaction buffer with 10 µl FabD quench solution 1, place on ice for 15 minutes, and then centrifuge at 16000 xg and 4 °C. Neutralize 20 µl of the quenched standard curve solution with 50 µl neutralization solution. This yields a final volume for fluorescence analysis of 70 µl, the same as for the assay. Concentrations of CoA-SH in the 20 µl samples are as follows: 0 µM, 2.625 µM, 5.25 µM, 10.5 µM, 26.25 µM, and 52.5 µM. This standard curve is used to calculate the concentration of CoA-SH produced in the assays.

The FabH Assay:

FabH assays were conducted similarly to FabD, but the precipitation step is not required because only one thiol is generated (CoA-SH) and none are consumed.

Reagents:

- Wash buffer (20 mM phosphate, 50 mM potassium chloride, pH 7.0)
- Assay buffer (20 mM phosphate, 50 mM potassium chloride, 1 mg/mL BSA, pH 7.0)
- FabH Quench solution (50 µM CPM in DMSO)
- 1 mM acetyl-CoA

- 2 mM malonyl-ACP
- 100 nM FabH

1. Exchange FabH into wash buffer to reduce the DTT concentration at least 1000x.

2. Perform assays at 30 °C in 100 µl volumes with 7.5 µl, 1 mM mM acetyl-CoA (75 µM), 3.5 µl, 2 mM malonyl-ACP (70 µM), and 79 µl assay buffer.

3. Start reactions with 10 µl of 100 nM FabH (10 nM). Aliquots were taken at 1, 2,4,6,8, and 10 min. At each time point 10 µl of the assay was removed from the reaction vessel then immediately quenched into 90 µl quench solution in a 96 well plate. The samples were read in a Tecan Safire plate reader with excitation wavelength of 380 nm and emission at 470 nm.

Results and Discussion

We demonstrated the measurement of FabH activity using the described method and found reproducible rate measurements with minimal noise as shown in Figure 3-3A and B. Reactions without enzyme repeatedly showed flat profiles with zero slope (data not shown).

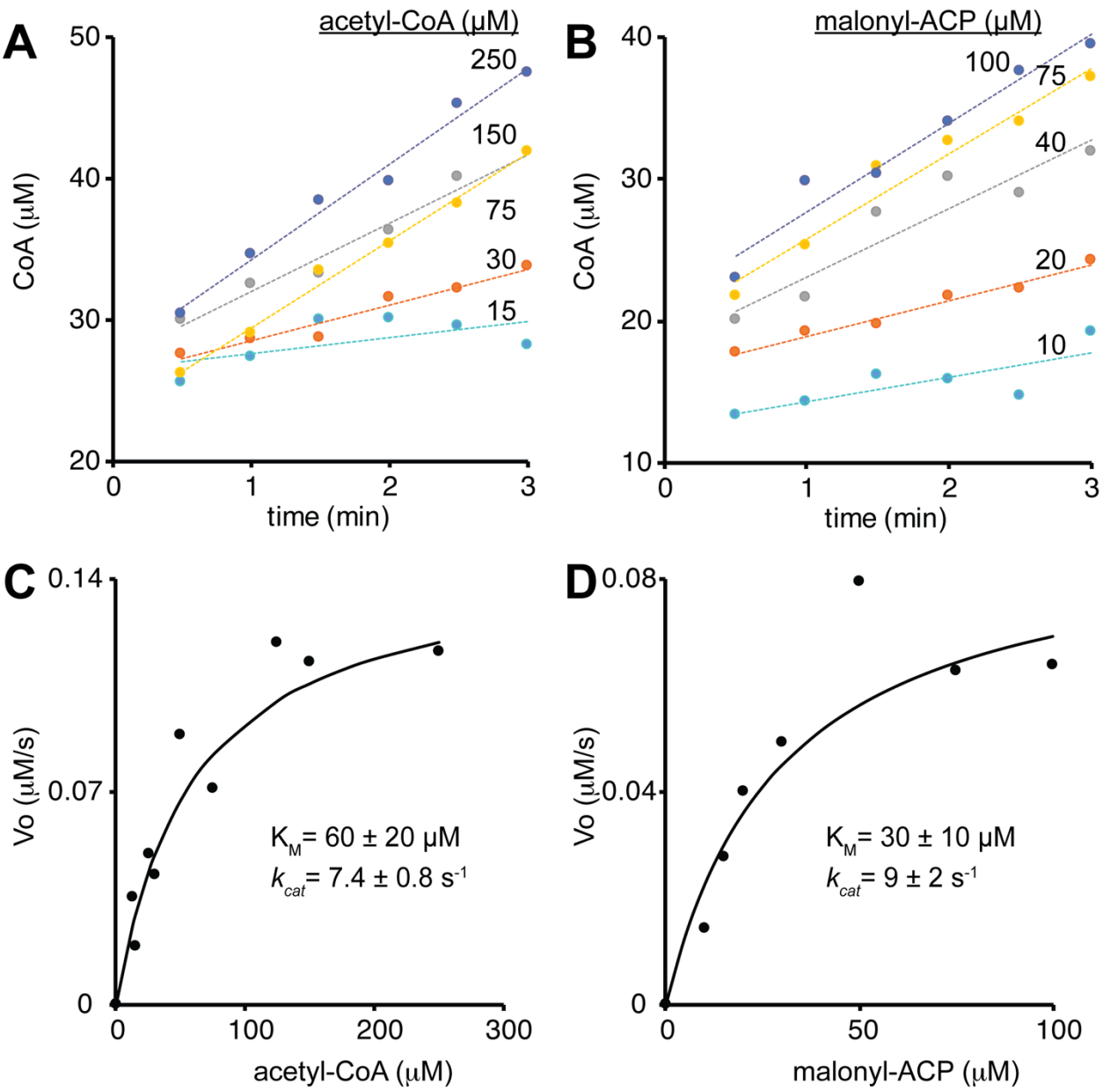

Figure 3-3. Saturation kinetics experiments for *E. coli* FabH.

A. Progress curves for FabH reactions with varying concentrations of acetyl-CoA and 80 μM malonyl-ACP. **B**. Progress curves of FabH reactions with varying concentrations of malonyl-ACP and 200 μM acetyl-CoA. **C.** A plot of reaction rates versus acetyl-CoA concentration. **D**. A plot of reaction rates versus malonyl-ACP concentration. Dashed lines represent a linear fit to product

accumulation data and solid lines represent a fit of the Michaelis-Menten equation.

Each experiment collected product accumulation data from 6 separate reactions resulting in 36 individual measurements that required one person about 45 min to complete from start to finish.

To obtain estimates of Michaelis constants (K_M) for each substrate as well as catalytic rates (k_{cat}), one substrate was held at a concentration ~4 fold higher than its K_M while the other substrate was varied. We fit the Michaelis-Menten equation to plots of the initial velocities versus the varied substrate concentration to estimate K_M (acetyl CoA 60 ± 20 μM; malonyl-ACP 30 ± 10 μM) and k_{cat} (7.4 ± 0.8 s^{-1} and 9 ± 2 s^{-1}, respectively). Data in Figure 3-3C and D show an overlay from two independent experiments collected on two different days. These data are shown in the raw form and individual experiments were not scaled for comparison which clearly demonstrates the high degree of repeatability and stability of the assay. Table 3-1 shows the resulting values measured using this method are comparable to previously measured values.

The assay of FabH activity proved sensitive due to the generation of a free thiol (in the form of CoA-SH) during the reaction cycle. Assays of FabD activity could not use the same experimental approach because though a free thiol is generated (CoA-SH) during the reaction, one is consumed (holo-ACP) resulting in no net change in measurable CPM fluorescence (Figure 3-1). We developed a method that selectively precipitated the substrate holo-ACP from the reaction

mixture, leaving the product CoA-SH in solution. This solution could then be probed for free thiol content using the CPM reagent.

Table 3-1. FabH kinetic data

Reference	Organism	Mal-ACP K_M (μM)	Acetyl-CoA K_M (μM)	$k_{cat}1$ (s^{-1})*	$k_{cat}2$ (s^{-1})**
This study	*E. coli*	30 ± 10	60 ± 20	9.0 ± 2.0	7.4 ± 0.8
Heath et al. [13]	*E. coli*	5	40	n.r.	n.r.
Qiu et al. [25]	*S. aureus*	19 ± 7	373 ± 17	261 ± 34	431 ± 113
Khandekar et al. [26]	*S. pneumoniae*	18.6 ± 1.5	40.3 ± 2.3	n.r.	n.r.

**$k_{cat}1$: measured with 75 μM malonyl-ACP and saturating acetyl-CoA*
***$k_{cat}2$: measured with 250 μM acetyl-CoA and saturating malonyl-ACP*
n.r. = data not reported

The FabD activity assay likewise proved sensitive and repeatable. Initially, multiple assays were conducted to determine optimal enzyme and substrate concentrations for saturation kinetics experiments (data not shown). Once conditions were identified, product accumulation was measured as shown in Figure 3-4 A and B.

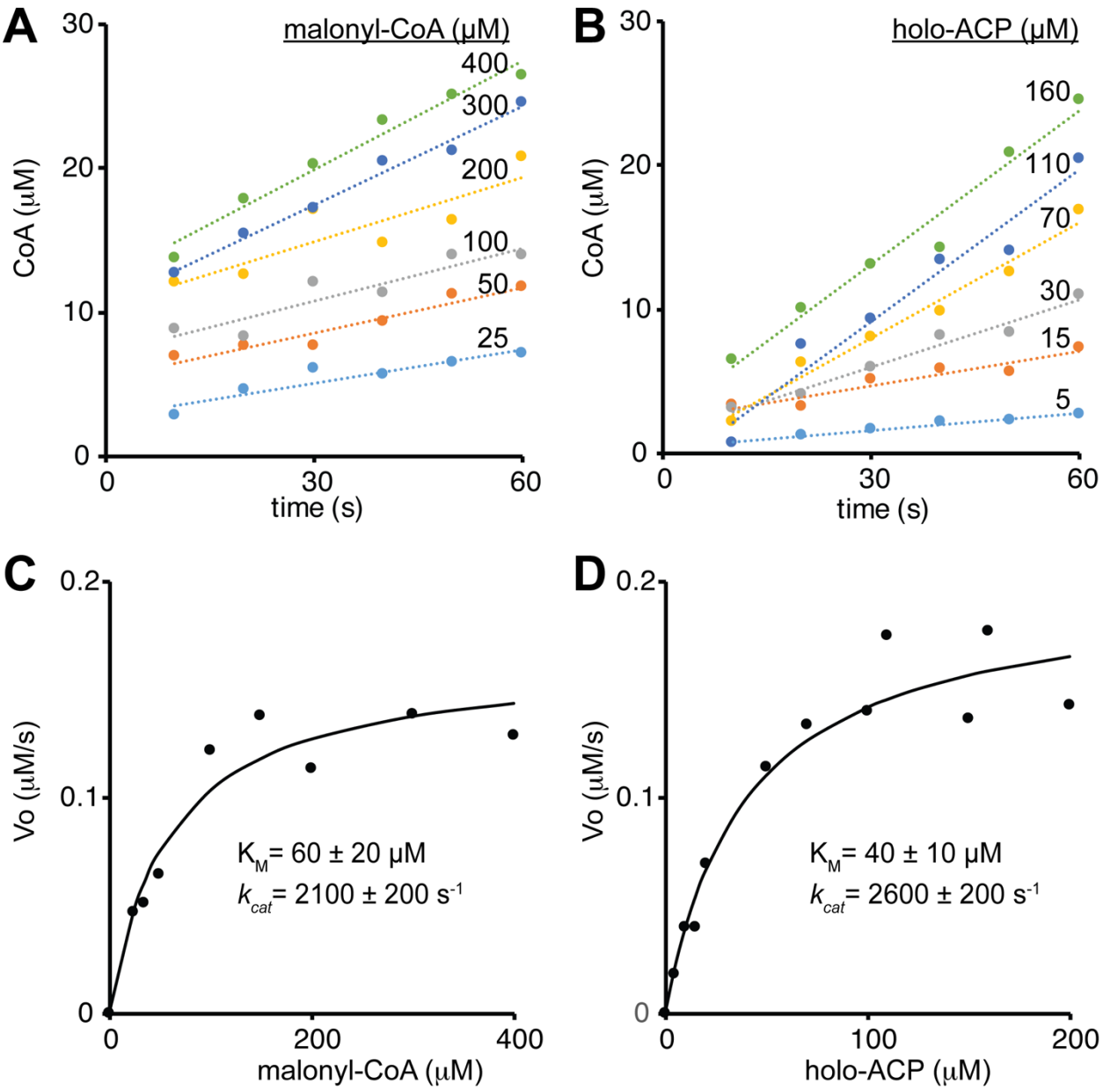

Figure 3-4. Saturation kinetics experiments for *E. coli* FabD.
A. Progress curves for FabD reactions with varying concentrations of malonyl-CoA and 125 μM holo-ACP. **B**. Progress curves of FabD reactions with varying concentrations of holo-ACP and 250 μM acetyl-CoA. **C.** A plot of reaction rates versus malonyl-CoA concentration. **D**. A plot of reaction rates versus holo-ACP concentration. Dashed lines represent a linear fit to product accumulation data and solid lines represent a fit of the Michaelis-Menten equation.

Linearity over time is evident across all substrate concentrations assayed with only minor noise present at the lower substrate concentrations. Furthermore, observed reaction rates reached saturation at high substrate concentrations and permitted K_M and k_{cat} estimation by fitting the Michaelis-Menten equation as shown in Figure 3-4C and D. Data in Figure 3-4C and D show an overlay from three independent experiments collected on three different days. Similar to that observed for FabH, these data are shown in the raw form and individual experiments were not scaled for comparison which clearly demonstrates the high degree of repeatability and stability of the assay. Based on these analyses we estimated K_M values of 40 ± 10 µM for holo-ACP and 60 ± 20 µM for malonyl-CoA. Values for k_{cat}, measured from each saturation curve, closely agreed at 2600 ± 300 s^{-1} and 2100 ± 200 s^{-1}. The comparison of the values reported herein closely agree with previously reported values shown in Table 3-2 [17,19,20,21].

Table 3-2. FabD kinetic data

Reference	Organism	Holo-ACP K_M (µM)	Malonyl-CoA K_M (µM)	$k_{cat}1$ (s^{-1})**	$k_{cat}2$ (s^{-1})***
This study	*E. coli*	40 ± 10	60 ± 20	2600 ± 300	2100 ± 200
Molnos et al. [17]	*E. coli*	19	25	n.r.	n.r.
Joshi et al. [19]	*E. coli*	54	25	n.r.	n.r.
Szfranska et al. [20]	*S. coelicolor*	73	60	450	n.r.
Kremer et al. [21]	*M. tuberculosis*	14	50*	n.r.	n.r.

** Refit of published data with non-linear least squares fitting software (reported 12.6 µM)*

*** k_{cat}1: measured with 250 µM malonyl-CoA and saturating holo-ACP*
**** k_{cat}2: measured with 125 µM holo-ACP and saturating malonyl-CoA*
n.r. = data not reported

FabD assays required care to ensure complete precipitation of holo-ACP during the quench step. Multiple TCA concentrations were tested and it should be noted that at excessive TCA concentration, holo-ACP initially precipitated but was subsequently hydrolyzed into soluble peptides that led to higher than expected CPM fluorescence. This was evident by the appearance and, within minutes, the disappearance of a white fluffy precipitate. ACP hydrolysis can be controlled by carefully tuning the TCA concentration for each different aliquot volume. For 20 µL aliquots, 10 µL 150% w/v TCA provided superior results but 80 µL aliquots required 40 µL 90% w/v TCA. It also proved important to check the final pH of the neutralized solution before fluorescence measurements. A pH greater than 8 is necessary to ensure complete and rapid reaction of the CPM with CoA-SH. It is important to note that CPM is light sensitive, and fluorescence should be measured within one hour from the time of neutralization. It should also be pointed out that the difference in background CoA-SH evidenced in both figures 3 and 4, between each A and B panel can be explained by the fact that in the two cases where the ACP substrates are held at a higher concentration, there is higher background. This is caused by the contaminating free thiol present in the ACP preparations.

This study introduces a method for safe and repeatable assays of fatty acid biosynthesis enzymes that utilize sulfhydryls. This method functions with exceptional repeatability and stability. Reliability will prove beneficial for

adaptation to high throughput screening and allow for rapid analysis of many enzymes, substrates and potentially inhibitors. Our approach utilizes commercially available reagents and functions without radioactive substrates or linking enzymes with linking substrates that can complicate analysis. Although sample handling in the assay is more involved than a continuous coupled assay, it is still straightforward and completed in a short amount of time.

Thiol quantitation using CPM lends additional benefits to the approach described here. These methods will be directly applicable to studies of other fatty acid synthesis enzymes, including the KASI and KASII enzymes, as well as polyketide synthases that liberate thiols in the form of CoA-SH and generate ACP-bound intermediates within the reaction cycle [22,23]. Furthermore, the assay method is also applicable in screens of drug molecule libraries for novel antibiotics targeting FabD, FabH or other FAS enzymes [24].

Acknowledgement:

This material is based upon work supported by the National Science Foundation under Award No. EEC-0813570, and by funds from the Roy J. Carver Department of Biochemistry, Biophysics & Molecular Biology at Iowa State University. Any opinions, findings, and conclusions or recommendations expressed in this material are those of the authors and do not necessarily reflect the views of the National Science Foundation.

Works Cited

1. Nikolau BJ, Perera MA, Brachova L, Shanks B (2008) Platform biochemicals for a biorenewable chemical industry. Plant J 54: 536-545.
2. Wakil SJ, Stoops JK, Joshi VC (1983) Fatty acid synthesis and its regulation. Annu Rev Biochem 52: 537-579.
3. Maier T, Leibundgut M, Ban N (2008) The crystal structure of a mammalian fatty acid synthase. Science 321: 1315-1322.
4. Leibundgut M, Maier T, Jenni S, Ban N (2008) The multienzyme architecture of eukaryotic fatty acid synthases. Curr Opin Struct Biol 18: 714-725.
5. Leber C, Da Silva NA (2014) Engineering of Saccharomyces cerevisiae for the synthesis of short chain fatty acids. Biotechnol Bioeng 111: 347-358.
6. Ratledge C (2004) Fatty acid biosynthesis in microorganisms being used for Single Cell Oil production. Biochimie 86: 807-815.
7. Volker AR, Gogerty DS, Bartholomay C, Hennen-Bierwagen T, Zhu H, et al. (2014) Fermentative production of short-chain fatty acids in Escherichia coli. Microbiology 160: 1513-1522.
8. Tsay JT, Oh W, Larson TJ, Jackowski S, Rock CO (1992) Isolation and characterization of the beta-ketoacyl-acyl carrier protein synthase III gene (fabH) from Escherichia coli K-12. J Biol Chem 267: 6807-6814.
9. Davies C, Heath RJ, White SW, Rock CO (2000) The 1.8 A crystal structure and active-site architecture of beta-ketoacyl-acyl carrier protein synthase III (FabH) from escherichia coli. Structure 8: 185-195.
10. Borgaro JG, Chang A, Machutta CA, Zhang X, Tonge PJ (2011) Substrate recognition by beta-ketoacyl-ACP synthases. Biochemistry 50: 10678-10686.
11. Marcella AM, Jing F, Barb AW (2015) Preparation of holo- and malonyl-[acyl-carrier-protein] in a manner suitable for analog development. Protein Expr Purif 115: 39-45.
12. Chung CC, Ohwaki K, Schneeweis JE, Stec E, Varnerin JP, et al. (2008) A fluorescence-based thiol quantification assay for ultra-high-throughput screening for inhibitors of coenzyme A production. Assay Drug Dev Technol 6: 361-374.
13. Heath RJ, Rock CO (1996) Inhibition of beta-ketoacyl-acyl carrier protein synthase III (FabH) by acyl-acyl carrier protein in Escherichia coli. J Biol Chem 271: 10996-11000.
14. Dreier J, Li Q, Khosla C (2001) Malonyl-CoA:ACP transacylase from Streptomyces coelicolor has two alternative catalytically active nucleophiles. Biochemistry 40: 12407-12411.
15. Misra A, Surolia N, Surolia A (2009) Catalysis and mechanism of malonyl transferase activity in type II fatty acid biosynthesis acyl carrier proteins. Mol Biosyst 5: 651-659.
16. Ruch FE, Vagelos PR (1973) Characterization of a malonyl-enzyme intermediate and identification of the malonyl binding site in malonyl coenzyme A-acyl carrier protein transacylase of Escherichia coli. J Biol Chem 248: 8095-8106.

17. Molnos J, Gardiner R, Dale GE, Lange R (2003) A continuous coupled enzyme assay for bacterial malonyl-CoA:acyl carrier protein transacylase (FabD). Anal Biochem 319: 171-176.
18. Sippel TO (1981) New fluorochromes for thiols: maleimide and iodoacetamide derivatives of a 3-phenylcoumarin fluorophore. J Histochem Cytochem 29: 314-316.
19. Joshi VC, Wakil SJ (1971) Studies on the mechanism of fatty acid synthesis. XXVI. Purification and properties of malonyl-coenzyme A--acyl carrier protein transacylase of Escherichia coli. Arch Biochem Biophys 143: 493-505.
20. Szafranska AE, Hitchman TS, Cox RJ, Crosby J, Simpson TJ (2002) Kinetic and mechanistic analysis of the malonyl CoA:ACP transacylase from Streptomyces coelicolor indicates a single catalytically competent serine nucleophile at the active site. Biochemistry 41: 1421-1427.
21. Kremer L, Nampoothiri KM, Lesjean S, Dover LG, Graham S, et al. (2001) Biochemical characterization of acyl carrier protein (AcpM) and malonyl-CoA:AcpM transacylase (mtFabD), two major components of Mycobacterium tuberculosis fatty acid synthase II. J Biol Chem 276: 27967-27974.
22. Newman DJ, Cragg GM (2012) Natural products as sources of new drugs over the 30 years from 1981 to 2010. J Nat Prod 75: 311-335.
23. Fischbach MA, Walsh CT (2006) Assembly-line enzymology for polyketide and nonribosomal Peptide antibiotics: logic, machinery, and mechanisms. Chem Rev 106: 3468-3496.
24. Campbell JW, Cronan JE, Jr. (2001) Bacterial fatty acid biosynthesis: targets for antibacterial drug discovery. Annu Rev Microbiol 55: 305-332.
25. Qiu X, Choudhry AE, Janson CA, Grooms M, Daines RA, et al. (2005) Crystal structure and substrate specificity of the beta-ketoacyl-acyl carrier protein synthase III (FabH) from Staphylococcus aureus. Protein Sci 14: 2087-2094.
26. Khandekar SS, Gentry DR, Van Aller GS, Warren P, Xiang H, et al. (2001) Identification, substrate specificity, and inhibition of the Streptococcus pneumoniae beta-ketoacyl-acyl carrier protein synthase III (FabH). J Biol Chem 276: 30024-30030.

CHAPTER 4: THE R117A VARIANT OF THE ESCHERICHIA COLI MALONYL-COENZYME A:HOLO-(ACYL CARRIER PROTEIN) TRANSACYLASE FABD SYNTHESIZES NOVEL ACYL-(ACYL CARRIER PROTEINS)

Aaron M. Marcella and Adam W. Barb

Roy J. Carver Department of Biochemistry, Biophysics and Molecular Biology

2437 Pammel Drive

Molecular Biology Building, rm 4210

Iowa State University, Ames, IA 50011

A manuscript prepared for the Journal of Applied Microbiology and Biotechnology

Highlights:

-An R117A variant of the FabD enzyme efficiently generates malonyl-CoA

-The variant can act on several non-cognate CoA substrates

-FabD wild type and variant kinetic constants were determined with several acyl-CoA substrates

Abstract

The commercial impact of fermentation systems producing novel and biorenewable chemicals will flourish with the expansion of enzymes engineered to synthesize new molecules. Enzymes from prokaryotic fatty acid biosynthesis naturally generate highly reduced carbon-based molecules and are therefore promising engineering targets. Though a small degree of natural variability exists in fatty acid synthesis, the molecular space accessible through enzyme engineering is fundamentally limitless. Prokaryotic fatty acid biosynthesis enzymes also build carbon chains on a functionalized acyl carrier protein (ACP) that provides solubility, stability, a scaffold for interactions with the synthetic enzymes and represents an ideal platform to shuttle metabolites. This report describes the characterization of a transacylase enzyme that produces novel ACP-based primer and extender units for fatty acid biosynthesis. Unlike the malonyl-coenzyme A(CoA):holo-ACP transacylase (FabD) from *Escherichia coli*, the R117A variant synthesized acetyl-ACP, succinyl-ACP, isobutyryl-ACP, 2-butenoyl-ACP, and β-hydroxybutyryl-ACP among others from holo-ACP and the corresponding acyl-CoAs. These reactions proceeded with specific activities from 3.7-120 nmoles min^{-1} mg^{-1}. FabD R117A maintained K_M values for holo-ACP (~40 μM) and displayed small changes in K_M for acetoacetyl-CoA (110±30 μM) and acetyl-CoA (200±70 μM) when compared to malonyl-CoA (80±30 μM). Reductions in FabD R117A k_{cat} (malonyl-CoA = 8.4±0.1 s^{-1}; acetyl-CoA = 0.05 ±0.01 s^{-1}) accounted for the disparity in efficiency with different acyl-CoA substrates. Surprisingly, both FabD and FabD R117A utilized methylmalonyl-

CoA, though with increased K_Ms of 580±100 μM and 330±90 μM, respectively. Thus, FabD R117A represents a novel catalyst that efficiently synthesizes a broad range of acyl-CoAs. The maintenance of acyl-CoA and holo-ACP binding affinities suggests FabD R117A is applicable to synthetic organisms that generate only moderate acyl-CoA and holo-ACP concentrations (10-100 μM).

Introduction

Chemicals produced from renewable sources have an opportunity to replace many petrochemicals in the near term and offer routes to novel materials and specialty chemicals [1]. Cellulosic ethanol production provides a model for the development of biorenewable resources that has proven profitable and efficient [2]. Contemporary development efforts focus on modifying existing biochemical pathways to produce valuable molecules from industrial microbe strains and are limited by the availability of expressible enzymes that harbor novel or unique activities [3,4].

Prokaryotic fatty acid synthesis provides nearly ideal targets for engineering enzymes to synthesize novel products due to organizational simplicity and efficient chemistry [5]. Prokaryotic fatty acid biosynthesis generates relatively large volumes of highly reduced carbon based molecules and operates as a dissociated multi enzyme system unlike the single polypeptide mega-enzymes utilized by eukaryotes [4,6]. These prokaryotic biosynthetic enzymes, if changed to alter substrate specificity, offer many opportunities to

develop novel products that will be applicable in recombinant microbial industrial strains.

The malonyl-coenzyme A(CoA):holo-(acyl carrier protein(ACP)) transacylase (FabD) is one target for enzyme engineering that provides multiple options with respect to where in a fatty acid chain the modification may be directed. FabD transfers the malonyl moiety from malonyl-CoA to holo-ACP to form malonyl-ACP (Fig. 1A) [7].

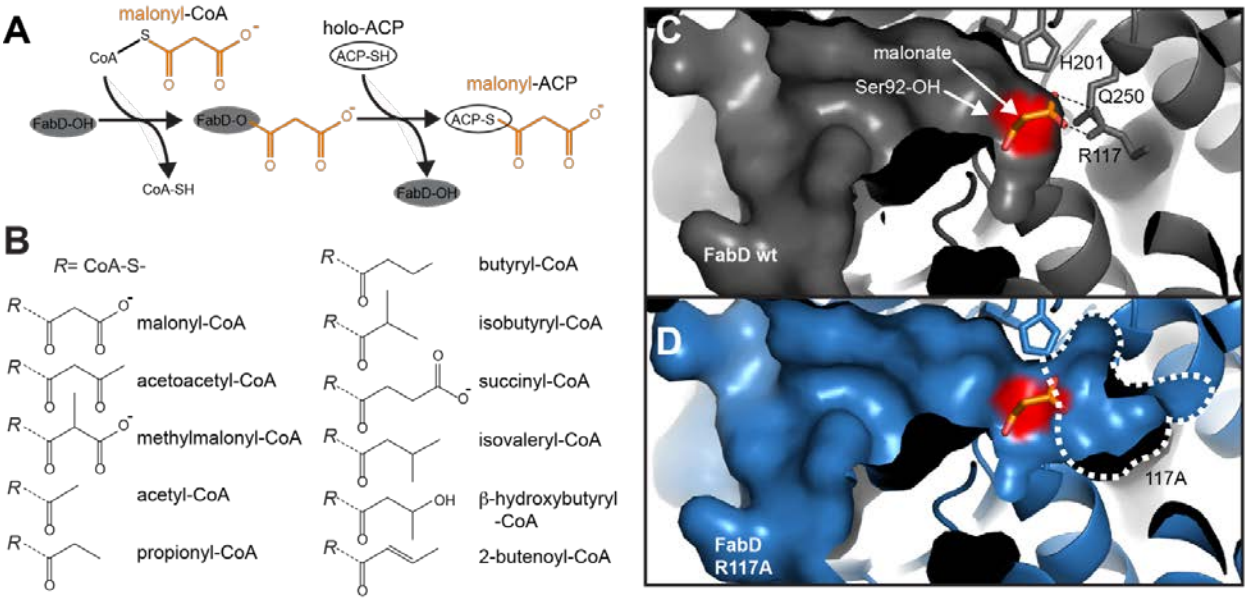

Figure 4-1. The FabD reaction and active site organization. (**A**) FabD reaction showing first the formation of a malonyl-enzyme intermediate and the subsequent transacylation of holo-ACP to malonyl-ACP. (**B**) The panel of acyl-CoA substrates tested here. Active site of the FabD wild type (**C**) and FabD R117A (**D**) enzymes. The active site pocket opened as a result of the R117A substitution is shown with a *dashed white* line in (**D**).

Malonyl-ACP donates two carbons, following decarboxylation, as an extender unit for all subsequent fatty acid chain elongation reactions in *Escherichia coli* catalyzed by the ketoacyl synthases I (KASI), KASII, and KASIII [8]. An

engineered FabD that recognized a malonyl analog with branches at the central methylene moiety could act as a chain extender unit and introduce diversity along the fatty acid chain in a designed synthesis pathway. Alternatively, FabD engineered to transfer a variety of acyl substituents (lacking the terminal carboxylate moiety) could serve to prime fatty acid synthesis with a unique motif that will form the fatty acid ω terminus.

E. coli FabD is also an excellent target for protein engineering due to its remarkable catalytic efficiency approaching the diffusion limit and the availability of high quality FabD structure models solved by x-ray crystallography [9,10]. We explored FabD amino acid variants to identify a form with broader substrate recognition than the wild-type enzyme. These efforts focused on expanding the substrate-binding pocket in the FabD active site, particularly with respect to recognition of the CoA acyl moiety. Figure 1C shows the FabD active site following a reaction with malonyl-CoA to generate a malonyl-FabD reaction intermediate [9]. The malonyl moiety forms an acyl linkage to the S92 sidechain and is stabilized at the distal carboxylate by the R117 guanidinium group [9]. Q11, Q63 and Q250 appear to stabilize the active site and H91 and H201 play important roles in catalysis [11].

Active site substitutions generally reduce FabD activity, though these have not been thoroughly explored. Substitution at R117 eliminates an important carboxylate-guanidinium interaction with malonyl-CoA (Figure 4-1C) [12,13]. H91 or H201 substitutions appear deleterious [11] and Q63 and Q11 likewise appear

essential [14]. Here we revisit the effect of these FabD amino acid substitution and thoroughly characterize the FabD R117A variant.

Materials and Methods

All materials were purchased from Sigma Aldrich unless otherwise noted.

Protein preparation: Plasmids encoding FabD variants were prepared using the pET28b:FabD plasmid [10] and the Fusion PCR protocol [15]. FabD and FabD variants were purified as described previously [10]. FabD activity assays were completed as described [10]. Holo-ACP expression, purification and MALDI-MS was performed as described [16]. His-tagged and untagged holo-ACP were assayed independently as FabD substrates; specific activities showed similar results (4100 and 3200 μmoles/min/mg, respectively). Because the untagged ACP prep contained unidentified deacetylase activity and increased noise in the assays we used the His-tagged ACP for the assays. It should also be noted that both FabD and FabD R117A proved to be highly stable, remaining active for 2 years stored at -80 °C in 25 % glycerol and maintained high levels of activity following multiple freeze thaw cycles.

ESI-MS of intact ACP, FabD and FabD R117A:

Protein (10 μL, 0.1 mg/mL in double distilled water) was applied to a C4 column and eluted from an Agilent 1260 liquid chromatography system with variable relative concentrations of Buffer A (0.1 % formic acid in water) and Buffer B (0.1 % formic acid in acetonitrile) with a constant flow rate of 0.1 mL/min: 1 mL 95% A

plus 5% B, then 0.5 mL 100% B, and final 0.5 mL 95% A plus 5% B. ESI was conducted on a Q-Exactive Hybrid Quadrupole-Orbitrap Mass Spectrometer (Thermo Scientific) with positive polarity at 35.0 eV, and a scan range of 700-4000 m/z.

ESI-MS of FabD R117A protease digests:

Trypsin: FabD R117A was diluted to a final concentration of 0.2 mg/mL in a 25 mM MOPS buffer with 100 µl final volume. This solution was boiled for 1 hour, the briefly centrifuged to collect all material at bottom of tube and then cooled on ice for 10 min. sequencing grade trypsin (Promega; 5 µg) was added and the reaction incubated for 18 h at 37 °C. The tryptic digest was applied to a C4 column eluted from the LC system. The same two buffers used for the intact mass LC-MS mentioned above were used with the following gradient. First, 540 µl of 95% A, 5% B was applied at 30 µl/min, followed by 150 µl of 65% A, 35% B at 30 µl/min. Then 300 µl 100% B at 60 µl/min was applied and 600 µl 95% A, 5% B at 60 µl/min. Finally, 30 µl of 95% A, 5% B was applied at 30 µl/min. The ESI-MS spectrum was collected with positive polarity and the initial MS step had a scan range of 350-5000 m/z. The MS/MS step was done with a scan range of 200-2000 m/z.

Pepsin: FabD R117A was diluted from its stock to a final concentration of 0.2 mg/mL in a 12.5 mM MOPS buffer with 100 µl final volume. This solution was boiled for 15 min and then cooled on ice for 10 min. Concentrated HCl (0.5 µl)

was added to the solution and an acidic pH was verified using litmus paper. Pepsin (Promega, 0.5 µg) in a 40 mM HCl solution was added and the reaction incubated for 18 hours. The reaction was stopped by boiling for 10 min. The pepsinized sample was subjected to the same LC-MS/MS as the trypsinized sample described above.

Results

Initial analyses – The *E. coli* FabD active site is specifically designed to bind malonyl-CoA and provides no obvious unoccupied cavities to accommodate larger CoA-bound substituents (Figure 4-1C; [9]). R117 forms an ionic interaction with the malonate carboxylate in the active site, and will open a large new cavity in the the FabD substrate-binding pocket if substituted with Ala (Figure 4-1D). We prepared FabD and FabDR117A to test the substrate binding potential following R117A substitution. Expression and purification of FabD and FabD R117A resulted in near homogeneous preparations at 35 mg/L and 17 mg/L, respectively, following anion exchange and gel filtration chromatography as judged by SDS-PAGE analysis (Figure 4-2). FabD, FabD R117A and the holo-ACP substrate were analyzed using ESI-MS to verify molecular mass and purity (Figure S1). FabD and holo-ACP displayed masses within 3 Da of the expected values, but the deconvoluted mass of FabD R117A was 29 ±3 Da less than expected. ESI-MS/MS of tryptic and peptic FabD R117A digests identified peptides corresponding to 95.5% of the protein sequence and matched expected masses to within 0.01 Da (Figure S2). This result indicates the 29 Da deviation,

which was found on all detectable FabD R117A protein, was limited to the 4.5% of the protein sequence not identified in the ESI-MS/MS analysis. It is important to note that the 95.5% coverage includes all of the active site residues and a mass shift of 29 ±3 Da could be explained by an unidentified N-terminal modification alone or in combination with Q deamidation (-14 Da). ESI-MS/MS analysis identified all but one Q residue.

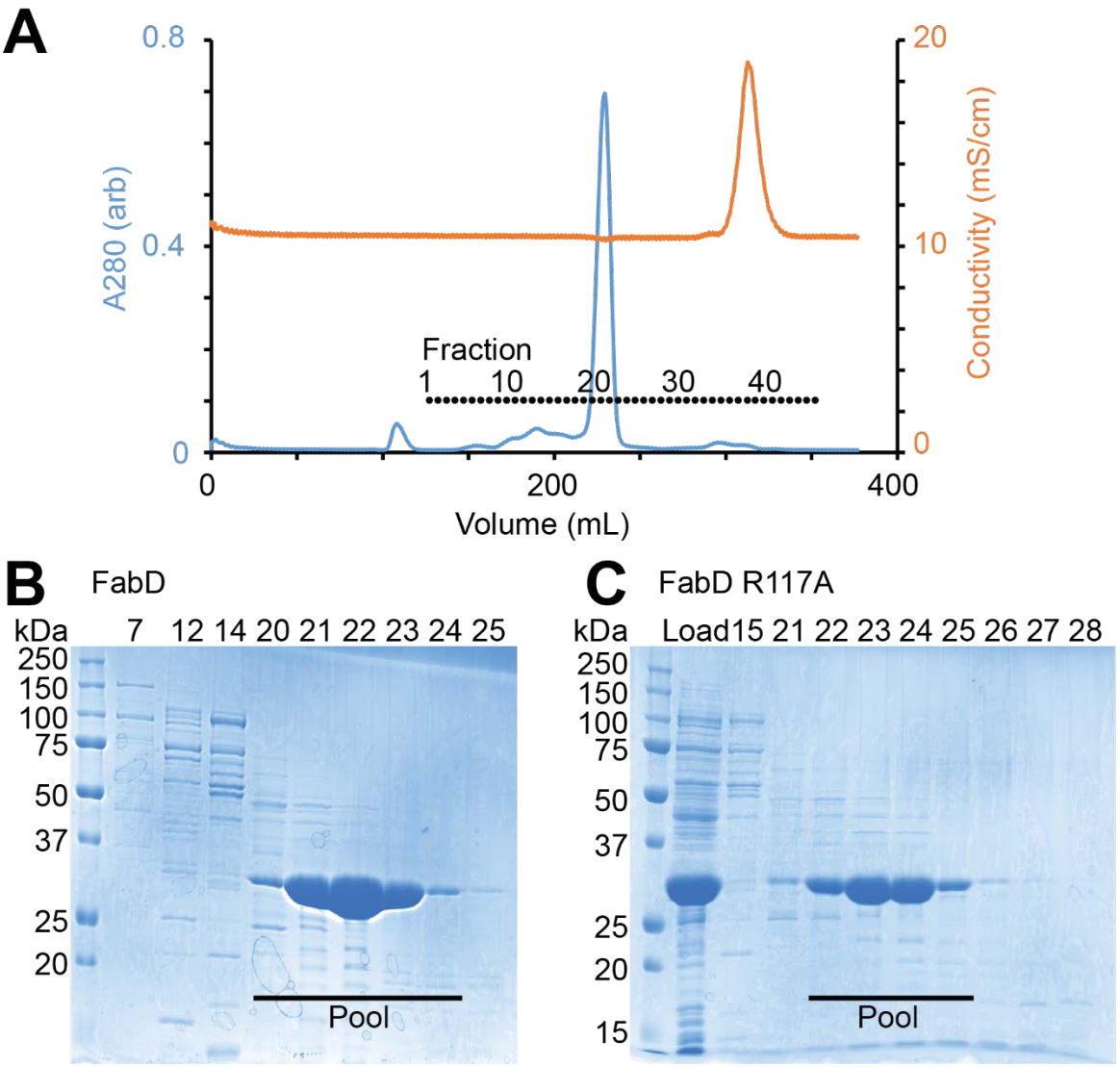

Figure 4-2. Purification of FabD and FabD R117A. (**A**) The FabD elution profile from a Superdex 200 size exclusion column shows a single symmetric peak. (**B**)

SDS-PAGE analysis of fractions from (**A**). (**C**) SDS-PAGE gel of FabD R117A purification using the S200 column.

Specific activities of FabD and FabD R117A - FabD and FabD R117A activity was quantified using a non-continuous fluorescence based assay with 250 μM acyl-CoA and 75 μM holo-ACP [10]. The assay strategy uses a thiol reactive fluorescent probe to measure CoA-SH production [17] and is applicable to FabD assays with any stable acyl-CoA. This assay technique includes a step to precipitate holo-ACP (a free thiol with a concentration in this assay equal to the starting holo-ACP concentration minus the concentration of CoA-SH) from the CoA-SH containing reaction using trichloroacetic acid before neutralizing and adding the thiol-reactive reagent. Both FabD and FabD R117A showed linear accumulations of CoA-SH over time in the presence of holo-ACP and malonyl-CoA during the time limit of the assay (Figure S3). Measurement of these initial velocities proved highly repeatable. The specific activity of FabD (4100 μmoles min^{-1} mg^{-1}) was comparable with a published value of 1800 μmoles min^{-1} mg^{-1} [18] and R117A displayed a lower, though still considerable, activity (13 μmoles min^{-1} mg^{-1}) with holo-ACP and malonyl-CoA substrates (Table 4-1). The activity of FabD and FabD R117A towards a panel of acyl-CoAs showed significant differences between the two enzymes. This panel contained acyl groups with many features of interest including odd chain length, branching, and ω or ω-1 functionalization (Figure 4-1B). These substrates potentially provide a biorenewable path to branched or alternatively functionalized compounds. The

fluorescence assay provided the specific activity towards each substrate, with the exception of succinyl-CoA.

Table 4-1. Specific activity of FabD and FabD R117A with various CoA substrates (200 μM) and 75 μM holo-ACP.

CoA Substrate	FabD Spec. Activity (μmoles/ min/mg)	FabD R117A Spec. Activity (μmoles/ min/mg)
malonyl-CoA	4100	13
acetoacetyl-CoA	0.0016	0.060
methylmalonyl-CoA	270	3.2
acetyl-CoA	n.a.	0.12
propionyl-CoA	n.a.	0.052
succinyl-CoA	n.a.	0.016
butyryl-CoA	n.a.	0.011
2-butenoyl-CoA	n.a.	0.0054
β-hydroxybutyryl-CoA	n.a.	0.0050
isobutyryl-CoA	n.a.	0.0037
isovaleryl-CoA	n.a.	0.0010

n.a.: no activity detected

Succinyl-CoA is labile at the neutral pH used for the assays [19]. As a result, MALDI-TOF MS spectra of aliquots removed early in the reaction provided data points for the specific activity measurement.

It was surprising that both FabD and FabD R117A utilized methylmalonyl-CoA, a substrate not commonly found in *E. coli* (Table 4-1). FabD R117A converted acetoacetyl-CoA with a specific activity that was four times greater

than FabD. Only FabD R117A could utilize acetyl-, propionyl-, butyryl-, isobutyryl-, succinyl-, isovaleryl-, β-hydroxybutyryl, and 2-butenoyl-CoA (Table 4-1). Conversion of holo-ACP to acyl-ACP using these acyl-CoAs was verified using MALDI-MS to eliminate the possibility of CoA-SH generation resulting from acyl-CoA hydrolysis catalyzed by FabD R117A during the assay (Figure 4-3 and Table S1).

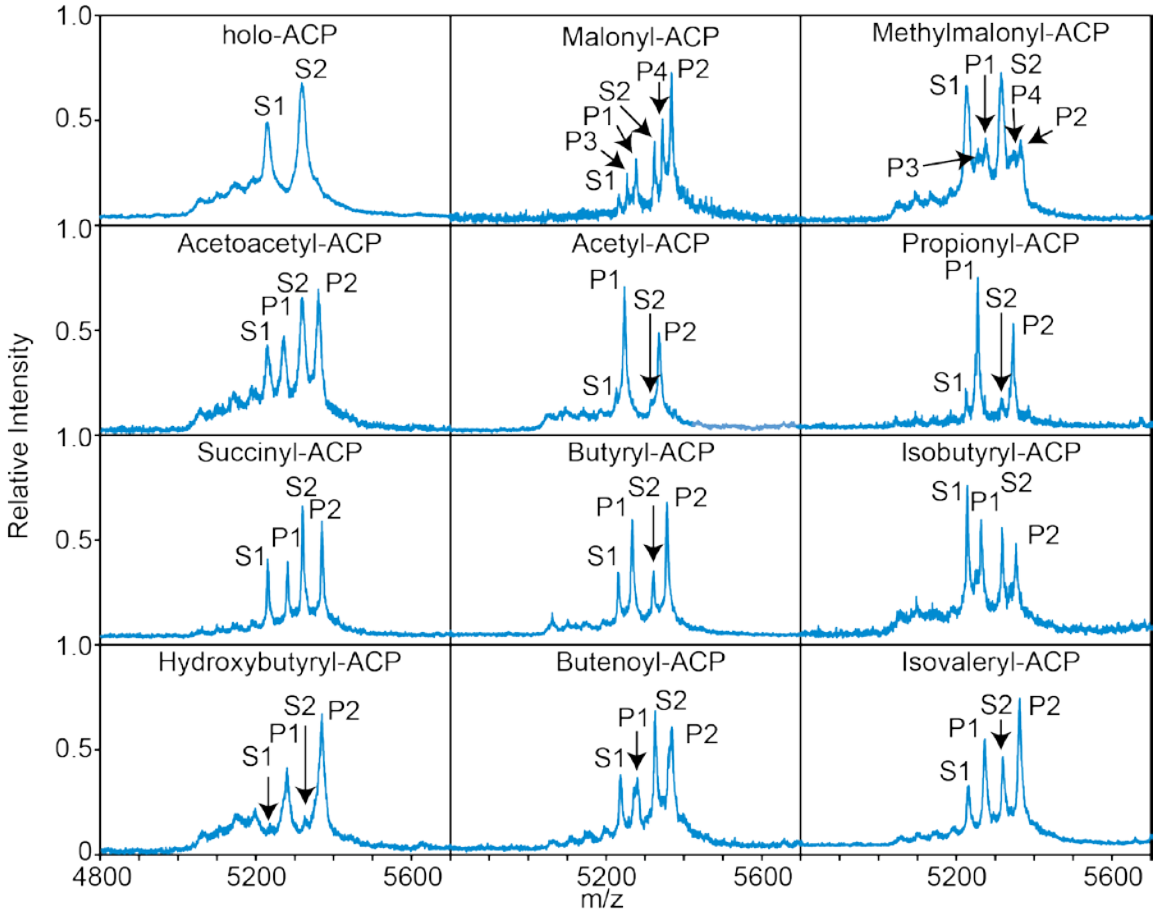

Figure 4-3. Representative MALDI-TOF MS analysis of doubly-charged holo-ACP and acyl-ACPs. S1 refers to holo-ACP; S2 is holo-ACP with a gluconylation at the N-terminal His6 tag [16]; P1 and P2 refer to the unmodified and gluconylated products, respectively, indicated in the title of each panel. P3 and P4 are the result of decarboxylation of P1 and P2 for malonyl-ACP and

methylmalonyl-ACP. Expected and observed masses for each peak are shown in Table S1.

MALDI-MS allows for screening many acyl-ACP products quickly with minimal sample requirement while providing the resolution necessary to separate peaks corresponding to the reaction product and substrate. It is surprising FabD R117A showed significant activity towards acetyl-CoA, an inhibitor of *E. coli* FabD [20]. FabD R117A utilized acyl-CoAs with shorter apolar acyl moieties more readily than longer and branched apolar acyl moieties (acetyl > propionyl > butyryl > isobutyryl > isovaleryl). FabD R117A tolerated polar acyl moieties surprisingly well with significant activity towards acetoacetyl-CoA and succinyl-CoA.

K_M and k_{cat} comparisons - Specific activity measurements provide a convenient metric to compare a wide range of substrates, but do not offer detailed information regarding relative substrate affinity that could be informative when designing new catalysts based on the FabD R117A scaffold. The FabD and FabD R117A enzymes were assayed with malonyl-CoA and holo-ACP. Initial velocities, determined from the linear portion of reaction progress curves, approached an asymptote at high substrate concentrations (Fig 4-4).

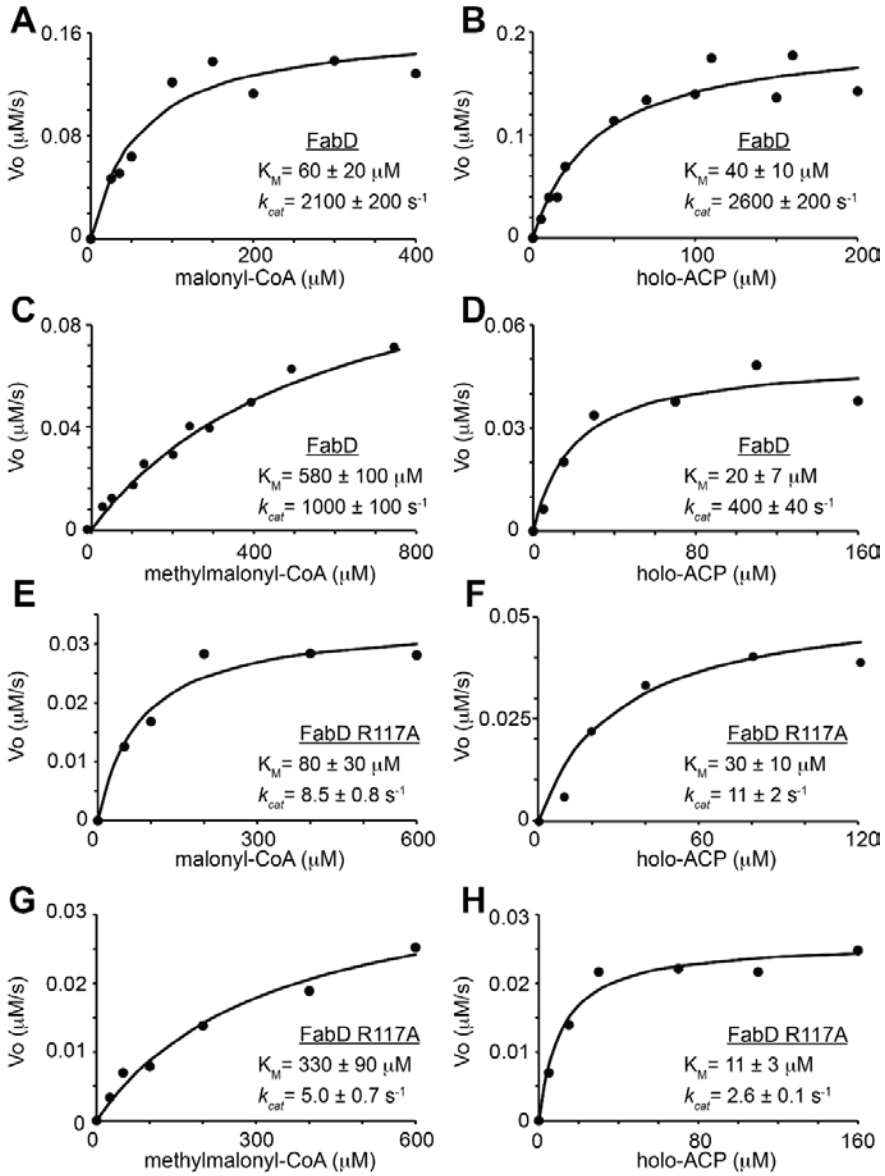

Fig 4-4. Plots of FabD and R117A saturation kinetics. Initial velocity v. substrate plots for FabD with varied malonyl-CoA (**A**; 125 μM holo-ACP) and varied holo-ACP (**B**; 250 μM malonyl-CoA) and plots of FabD activity with methylmalonyl-CoA (**C**; 125 μM holo-ACP) and holo-ACP (**D**; 250 μM methylmalonyl-CoA). The FabD R117A variant shows similar profiles with malonyl-CoA (**E**; 125 μM holo-ACP) and holo-ACP (**F**; 250 μM malonyl-CoA) and plots of FabD R117A activity with methylmalonyl-CoA (**G**; 125 μM holo-ACP) and holo-ACP (**H**; 250 μM methylmalonyl-CoA).

Fitting these data with the Michalis-Menten equation revealed K_M and k_{cat} values (Table 4-2; Fig. 4).

Table 4-2. Kinetic parameters for FabD and FabD R117A are reported ± one standard deviation of the mean.

FabD	Spec. Activity µmoles/min/mg	Acyl-CoA K_M[1] (µM)	Holo-ACP K_M[2] (µM)	k_{cat}[1] s^{-1}	k_{cat}[2] s^{-1}
Malonyl-CoA [10]	4100	60 ± 20	40 ± 10	2100 ± 200	2600 ± 200
Methylmalonyl-CoA	270	580 ± 100	20 ± 7	1000 ± 100	400 ± 40*
Acetoacetyl-CoA	0.0016	n.d.	n.d.	n.d.	n.d.
Acetyl-CoA	n.a.	n.d.	n.d.	n.d.	n.d.
FabD R117A					
Malonyl-CoA	13	80 ± 30	30 ± 10	8.5 ± 0.8	11 ± 2
Methylmalonyl-CoA	3.2	330 ± 90	11 ± 3	5.0 ± 0.7	2.6 ± 0.1*
Acetoacetyl-CoA	0.060	110 ± 30	30 ± 20	0.041 ± 0.005	0.038 ± 0.010
Acetyl-CoA	0.12	200 ± 70	40 ± 10	0.029 ± 0.005	0.052 ± 0.006

n.d.: not determined

n.a.: no activity detected

*- measured with sub-saturating amounts of methylmalonyl-CoA (250 µM)

Next, the most active substrates for FabD and FabD R117A were selected for measurement of relative substrate affinity (estimated with K_M) and catalytic rates (k_{cat}). With respect to malonyl-CoA, the R117A substitution primarily affected k_{cat} (277-fold reduction) with no measurable effect on K_M for either malonyl-CoA or holo-ACP (Table 4-2 and Fig 4-4). The methylmalonyl-CoA K_M was higher for both FabD (10-fold) and FabD R117A (4-fold) with smaller effects on k_{cat} (2.6-fold and <2-fold, respectively).

FabD R117A recognized acetoacetyl-CoA and acetyl-CoA with a moderate increase in CoA K_M (1.4- and 2.5-fold, respectively), no measureable effect on holo-ACP K_M, but much greater reductions in k_{cat} (200-300 fold). It is easy to understand how altering the substrate composition can alter binding affinity as estimated by K_M, but it is important to note that K_M is not a strict

measure of substrate affinity and substrate binding energy can contribute to catalytic rate [21]. FabD utilized acetoacetyl-CoA poorly and didn't recognize acetyl-CoA, as a result of the low activity it was not feasible to measure K_M and k_{cat} values and compare with FabD R117A.

FabD-catalyzed decarboxylation of malonyl-ACP – A reaction containing *E. coli* FabD, malonyl-CoA and holo-ACP generated a roughly 50:50 mixture of acetyl-ACP and malonyl-ACP (Fig 4-5), likely from malonyl decarboxylation during the catalytic cycle.

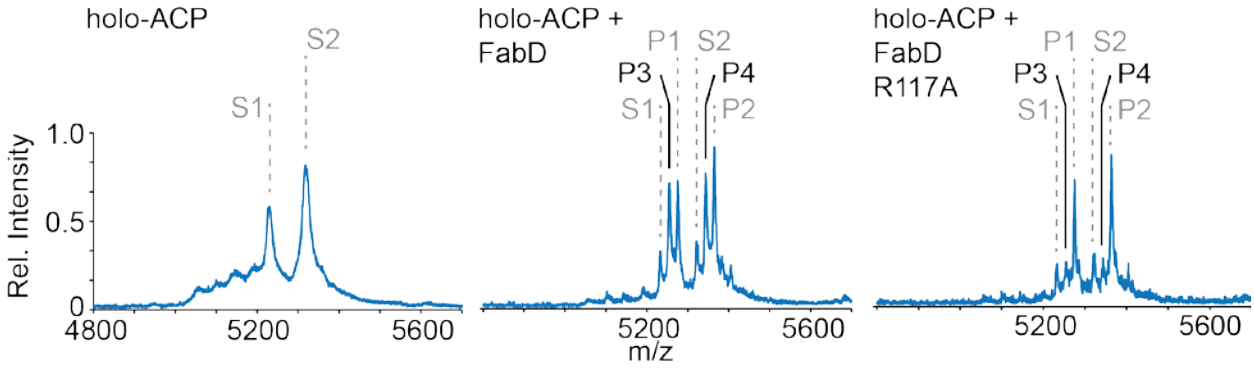

Fig 4-5. Malonyl decarboxylation during FabD catalysis. FabD and FabD R117A-catalyzed malonyl transfer leads to decarboxylation at early reaction timepoints using malonyl-CoA as the donor substrate. Only FabD R117A, however, appears to slowly recycle acetyl-ACP in a CoA-SH dependent manner, liberating holo-ACP for another malonyltransferase reaction. S1 refers to holo-ACP; S2 is holo-ACP gluconylated at the N-terminal His6 tag; P1 and P2 are malonyl-ACP and gluconylated malonyl-ACP, respectively. P3 and P4 are the result of decarboxylation of P1 and P2.

This unanticipated reaction previously stood as an impediment to preparing malonyl-ACP in vitro with high levels of purity for FabH, FabB and FabF assays until we determined that following long incubations a contaminant in the ACP preparation efficiently removed the acetyl moiety from ACP in the presence of

CoA-SH [16]. Indeed, if high levels of acetyl-ACP are formed from malonyl decarboxylation during FabD catalysis, *E. coli* must have mechanism to catabolize acetyl-ACP. Two independent groups identified an acetyl-CoA:holo-ACP transferase activity and performed a basic characterization of the enzyme, but it was never cloned [22,23]. This contaminating acetyltransferase activity allowed our laboratory to prepare malonyl-ACP to high purity and could be removed from holo-ACP preparations using a Superdex75 column (data not shown).

Preparations of malonyl-ACP formed using FabD R117A, following a longer incubation period, show dramatically lower levels of contaminating acetyl-ACP compared to malonyl-ACP (Fig 5). We previously showed FabD R117A utilizes acetyl-CoA to produce acetyl-ACP (Table 4-2 and Figure 4-3), and FabD R117A must also recycle acetyl-ACP formed in a reaction containing malonyl-CoA and holo-ACP. These reactions utilized holo-ACP purified from a Superdex75 column that removed contaminating native acetyltransferase activity. The FabD R117A-catalyzed acetyltransferase activity occurs slower than the malonyltransferase activity and also must occur when CoA-SH becomes available as an acetyl acceptor following the malonyl transfer reaction.

Our laboratory now uses FabD R117A when preparing malonyl-ACP because of the acetyltransferase activity and because FabD R117A preparations still contain a high degree of malonyltransferase activity.

Discussion

FabD R117A transferred a wide variety of acyl substituents from CoA to holo-ACP. Introducing a large range of new activities into an enzyme and organism that did not previously produce these products shows the clear effect of the R117A substitution, and eliminates the possibility of residual FabD activity contributing to the observed signal [24]. Removing the R117 sidechain enhanced the breadth of FabD substrate recognition, likely by opening a new pocket in the enzyme active site that accepts hydrophobic and polar CoA acyl groups (Figure 4-1D).

The acyl moieties tested here contain added chemical functionality and will lead to novel downstream products, some of which are shown in Figure 4-6. The resulting acyl-ACPs represent novel potential extender and primer substrates for fatty acid biosynthesis that have the potential to introduce a high degree of functionalization, resulting in branched chains, odd-numbered chains and fatty acid-like molecules with a negative charge, an alkene, hydroxyl or carboxyl groups (Figure 4-1C and 6). The use of an ACP scaffold to achieve designed chemical synthesis in vivo potentially provides access to additional fatty acid biosynthesis enzymes, though further optimization of these enzyme targets may be required.

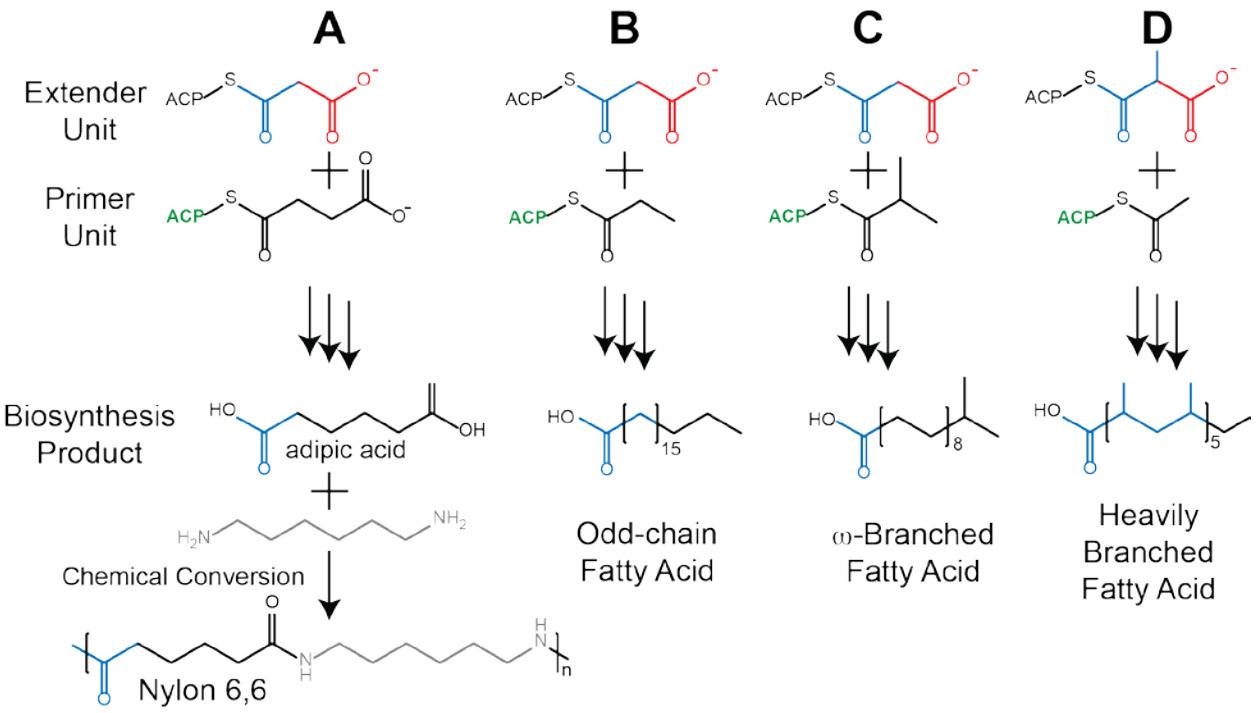

Figure 4-6. Potential strategies for developing new molecules using the novel ACPs generated by FabD R117A. FabD R117A generates unique ACP molecules with “primer units” in columns **A-C** or a unique “extender unit” in column **D** that potentially can be condensed, reduced, elongated and hydrolyzed to produce novel biorenewable chemicals including plastics and lipids.

Although the *E.coli* FabH enzyme is not reported to act on branched chain CoA substrates, *Streptomyces glaucescens* FabH will, lending support to the idea of feeding modified substrates to downstream enzymes [25]. It may be necessary to pursue further engineering of other enzymes in the pathway to accept the novel acyl-ACPs reported here.

One exciting FabD R117A catalytic product is succinyl-ACP (Figure 4-3). The CoA substrate for this reaction, succinyl-CoA is an abundant intermediate in the *E. coli* citric acid cycle (~200 μM in vivo) [26]. Following succinate transfer to holo-ACP, succinyl-ACP is available for conversion to adipyl-ACP following

condensation with malonyl-ACP and one round of FabG-FabA-FabI catalyzed reductions to remove the 3-ketone (Figure 4-6) [5]. Adipyl-ACP hydrolysis leads to adipic acid, an important diacid target of biorenewable chemical production that represents a drop-in biorenewable replacement for nylon 6,6 polymerization [27].

Branched chain fatty acids can be formed either by using a modified ACP extender or primer substrate. Isobutyryl-ACP acting as the primer substrate would produce an ω-branched fatty acid. Using methylmalonyl-ACP as an extender unit will result in methyl branches at every two carbons along the growing fatty acid chain yielding a highly substituted fatty acid. The donor substrate methylmalonyl-CoA is formed from succinyl-CoA by methylmalonyl-CoA mutase, an *E. coli* enzyme [28]. Branched chain and substituted fatty acids may be beneficial to the materials industry, providing biorenewable sources for novel lubricants, oils and other materials.

The FabD R117A substitution introduced substrate recognition plasticity into the FabD scaffold. A cursory examination of Table 4-1 might suggest the modest activity levels of FabD R117A will limit the potential application when compared to FabD, an enzyme with very high specific activity. However, FabD R117A displays significant specific activity comparable to the ‘average’ enzyme [29]. The shape of the FabD R117A substrate-binding pocket is likely not perfectly complimentary to each acyl substituent, unlike FabD and malonyl-CoA, and as a result FabD R117A activity is likely preserved by the contribution of binding energy from the CoA nucleotide-protein interaction which appeared

unaffected by R117 substitution. Though it is unknown where ACP binds, ACP-FabD interactions were also preserved given the similarity of holo-ACP K_Ms (Table 4-2). Further proof of FabD R117A activity comes from near-complete conversion of holo-ACP to acyl-ACP using each of these acyl-CoAs and mild reaction conditions (Fig 4-3). As a result of this minor impairment, it is possible an engineered microbe would need to express a higher level of FabD R117A when compared to intrinsic FabD to achieve suitable product concentrations. Increased expression is appropriate because the K_M values are only minimally perturbed, and represent reasonable goal concentrations for introducing non-cognate acyl-CoA biosynthesis [30,31].

Promiscuous enzyme paralogs with broad substrate recognition profiles represent branch points in enzyme evolution ([32] among others) and FabD R117A is expected to represent a similar branch point as a designed enzyme. It should be possible to engineer specific enzyme forms based on FabD R117A that will react with higher rates, greater affinities, and higher specificity towards each acyl-CoA. Such future designs would overcome rate-related limitations to industrial implementation with respect to the FabD R117A parent design. Broad specificity may not be negative characteristic, if the engineered microbe synthesizes a limited range of potential acyl-CoA substrates. Biosynthetic routes to many of the acyl-CoAs investigated here are described (many come from the citric acid cycle and amino acid biosynthesis/degradation) and would serve as a starting point to strain engineering.

Supplemental Information for Chapter 4

Supplemental Table 4-1. This table is related to Figure 4-3. Comparison of expected doubly-charged ACP masses (Da) and masses observed by MALDI-TOF MS. S1 refers to holo-ACP; S2 is holo-ACP with a gluconylation at the N-terminal His6 tag; P1 and P2 are the respective products. P3 and P4 are the result of decarboxylation of P1 and P2 for malonyl-ACP and mathylmalonyl-ACP.

	S1 obs	S1 exp	Δ	S2 obs	S2 exp	Δ	P1 obs	P1 exp	Δ	P2 obs	P2 exp	Δ
Holo-ACP	5237.2	5231.6	5.6	5327.6	5320.2	7.4	-	-	-	-	-	-
Malonyl-ACP	5235.4	5231.6	3.8	5324.2	5320.2	4.0	5279.4	5274.6	3.8	5368.5	5363.2	3.8
Methylmalonyl-ACP	5232.2	5231.6	0.6	5321.4	5320.2	1.2	5281.2	5281.6	0.6	5371.2	5368.7	0.6
Acetoacetyl-ACP	5235.9	5231.6	4.3	5325.6	5320.2	5.4	5277.4	5273.6	4.3	5367.7	5362.2	4.3
Acetyl-ACP	5230.7	5231.6	0.9	5320.0	5320.2	0.2	5251.4	5252.6	0.9	5340.6	5341.2	0.9
Propionyl-ACP	5227.6	5231.6	4.0	5317.6	5320.2	2.6	5258.3	5259.6	4.0	5347.2	5348.2	4.0
Succinyl-ACP	5236.0	5231.6	4.4	5325.8	5320.2	5.6	5287.3	5281.6	4.4	5375.7	5370.2	4.4
Butyryl-ACP	5231.9	5231.6	0.3	5321.5	5320.2	1.3	5267.3	5266.6	0.3	5356.9	5355.2	0.3
Isobutyryl-ACP	5228.6	5231.6	3.0	5318.3	5320.2	1.9	5264.3	5267.1	3.0	5353.7	5355.7	3.0
Hydroxybutyryl-ACP	-	5231.6	-	5322.2	5320.2	2.0	5277.4	5274.6	2.8	5365.7	5363.2	2.5
Butenoyl-ACP	5233.0	5231.6	1.4	5322.4	5320.2	2.2	5267.1	5265.6	1.4	5357.3	5354.2	1.4
Isovaleryl-ACP	5231.4	5231.6	0.2	5320.2	5320.2	0.0	5273.6	5273.6	0.2	5362.9	5362.2	0.2

	P3 obs	P3 exp	Δ	P4 obs	P4 exp	Δ
Malonyl-ACP	5255.4	5252.6	2.8	5346.8	5341.2	5.6
Methylmalonyl-ACP	5260.6	5259.6	1.0	-	5348.2	-

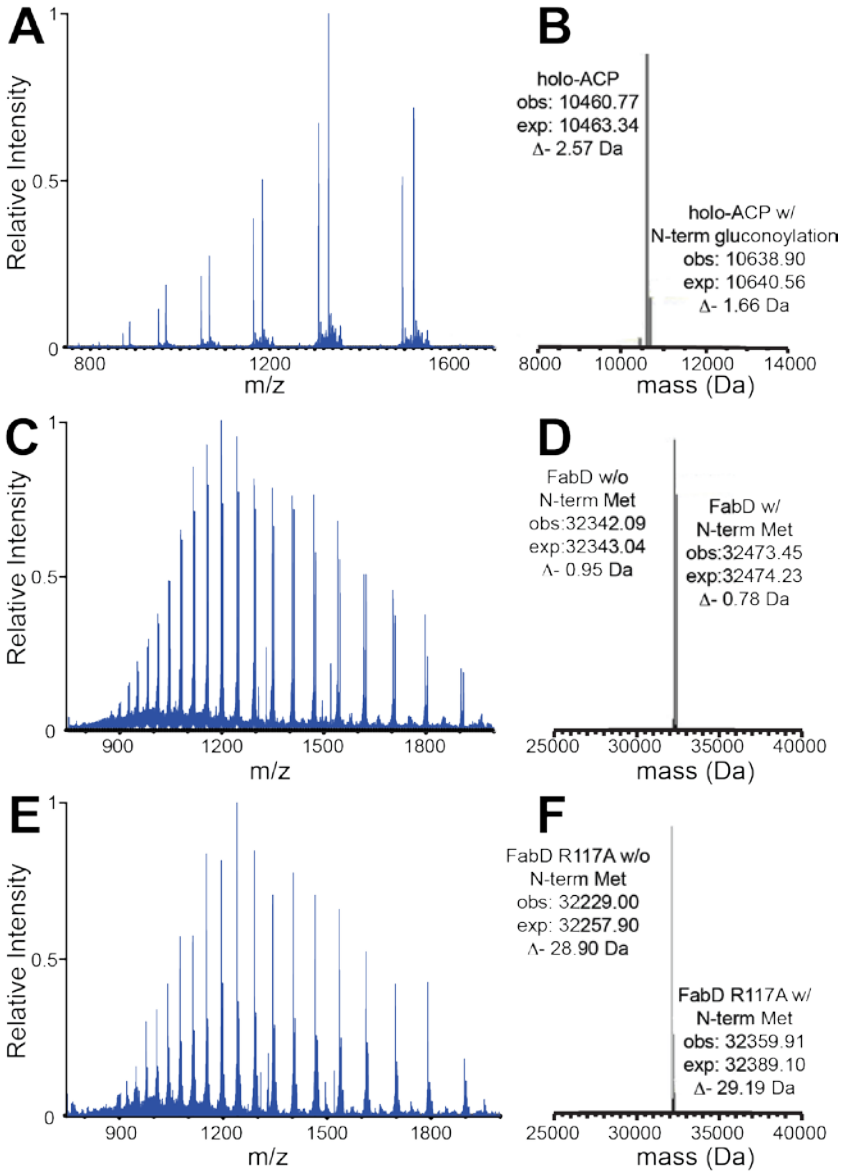

Figure S4-1. This figure is related to Figure 4-2. ESI-MS of holo-ACP, FabD and FabD R117A. Raw MS spectra of the manifold of charged states for holo-ACP (**A**), FabD (**C**), and FabD R117A (**E**). Devoncoluted MS of holo-ACP (**B**), FabD (**D**), and FabD R117A (**F**). Holo-ACP (**B**) has two major forms that were previously characterized, one without an N-terminal methionine and one with gluconoylation of the N-terminal 6x histidine tag [33].

Figure S4-2. This figure is related to Figure 4-2. Peptide coverage of FabD R117A from tryptic (*blue* lines) and peptic (*red* lines) digests analyzed by ESI-MS/MS. This analysis revealed positive identification of peptides corresponding to 95.5% of the protein. The R117A site is shown as a *bold green* “A” in the third line of text.

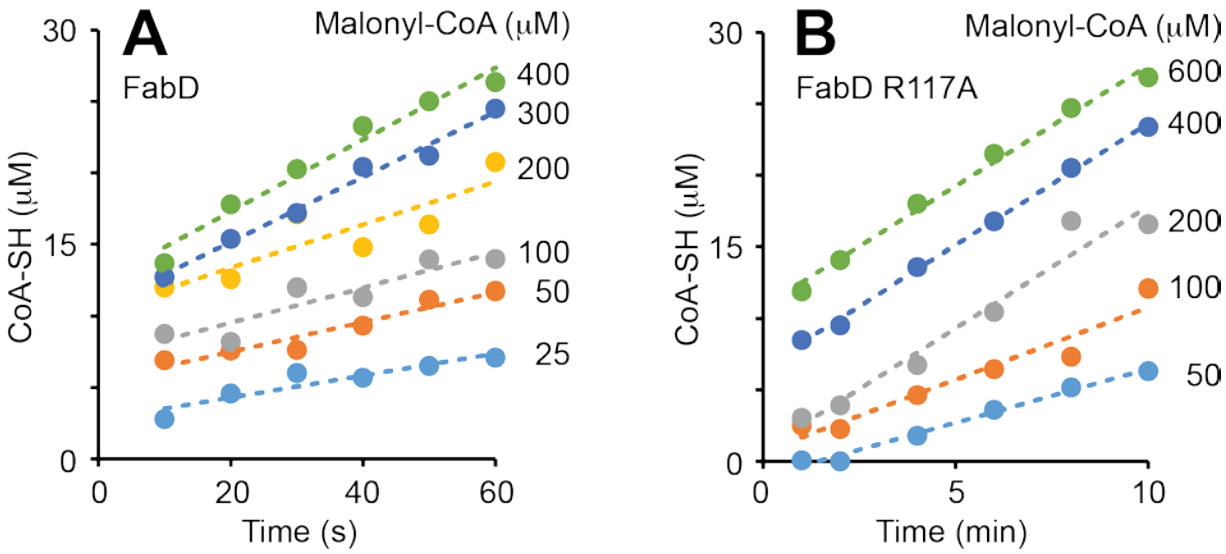

Figure S4-3. This figure is related to Fig 4-4 and Table 4-1. Reaction progress curves for representative enzyme-catalyzed assays. Initial velocity measurements were collected using FabD (**A**) and FabD R117A (**B**).

Acknowledgement

We would like to thank Joel Nott of the Protein Facility (Iowa State University) for assistance with the ESI-MS and ESI-MS/MS. This material is based upon work supported by the National Science Foundation under Award No. EEC-0813570, and by funds from the Roy J. Carver Department of Biochemistry, Biophysics & Molecular Biology at Iowa State University. Any opinions, findings, and conclusions or recommendations expressed in this material are those of the authors and do not necessarily reflect the views of the National Science Foundation.

Works Cited

1. Schell C, Riley C, Petersen GR (2008) Pathways for development of a biorenewables industry. Bioresour Technol 99: 5160-5164.
2. Kumar R, Tabatabaei M, Keikhosro K, Horvath IS (2016) Recent updates on lignocellulosic biomass derived ethanol - A review. Biofuel Research Journal 9: 347-356.
3. Nikolau BJ, Perera MA, Brachova L, Shanks B (2008) Platform biochemicals for a biorenewable chemical industry. Plant J 54: 536-545.
4. Gronenberg LS, Marcheschi RJ, Liao JC (2013) Next generation biofuel engineering in prokaryotes. Curr Opin Chem Biol 17: 462-471.
5. Janssen HJ, Steinbuchel A (2014) Fatty acid synthesis in Escherichia coli and its applications towards the production of fatty acid based biofuels. Biotechnol Biofuels 7: 7.
6. Leibundgut M, Maier T, Jenni S, Ban N (2008) The multienzyme architecture of eukaryotic fatty acid synthases. Curr Opin Struct Biol 18: 714-725.
7. Serre L, Verbree EC, Dauter Z, Stuitje AR, Derewenda ZS (1995) The Escherichia coli malonyl-CoA:acyl carrier protein transacylase at 1.5-A resolution. Crystal structure of a fatty acid synthase component. J Biol Chem 270: 12961-12964.
8. White SW, Zheng J, Zhang YM, Rock (2005) The structural biology of type II fatty acid biosynthesis. Annu Rev Biochem 74: 791-831.
9. Oefner C, Schulz H, D'Arcy A, Dale GE (2006) Mapping the active site of Escherichia coli malonyl-CoA-acyl carrier protein transacylase (FabD) by protein crystallography. Acta Crystallogr D Biol Crystallogr 62: 613-618.
10. Marcella AM, Barb AW (2016) A rapid fluorometric assay for the S-malonyltransacylase FabD and other sulfhydryl utilizing enzymes. J Biol Methods 3: 1-7.
11. Li Z, Huang Y, Ge J, Fan H, Zhou X, et al. (2007) The crystal structure of MCAT from Mycobacterium tuberculosis reveals three new catalytic models. J Mol Biol 371: 1075-1083.
12. Hong SK, Kim KH, Park JK, Jeong KW, Kim Y, et al. (2010) New design platform for malonyl-CoA-acyl carrier protein transacylase. FEBS Lett 584: 1240-1244.
13. Kremer L, Nampoothiri KM, Lesjean S, Dover LG, Graham S, et al. (2001) Biochemical characterization of acyl carrier protein (AcpM) and malonyl-CoA:AcpM transacylase (mtFabD), two major components of Mycobacterium tuberculosis fatty acid synthase II. J Biol Chem 276: 27967-27974.
14. Misra A, Surolia N, Surolia A (2009) Catalysis and mechanism of malonyl transferase activity in type II fatty acid biosynthesis acyl carrier proteins. Mol Biosyst 5: 651-659.

15. Ho SN, Hunt HD, Horton RM, Pullen JK, Pease LR (1989) Site-directed mutagenesis by overlap extension using the polymerase chain reaction. Gene 77: 51-59.
16. Marcella AM, Jing F, Barb AW (2015) Preparation of holo- and malonyl-[acyl-carrier-protein] in a manner suitable for analog development. Protein Expr Purif 115: 39-45.
17. Sippel TO (1981) New fluorochromes for thiols: maleimide and iodoacetamide derivatives of a 3-phenylcoumarin fluorophore. J Histochem Cytochem 29: 314-316.
18. Ruch FE, Vagelos PR (1973) The isolation and general properties of Escherichia coli malonyl coenzyme A-acyl carrier protein transacylase. J Biol Chem 248: 8086-8094.
19. Lambeth DO, Muhonen WW (1993) The direct assay of kinases and acyl-CoA synthetases by HPLC: application to nucleoside diphosphate kinase and succinyl-CoA synthetase. Anal Biochem 209: 192-198.
20. Joshi VC, Wakil SJ (1971) Studies on the mechanism of fatty acid synthesis. XXVI. Purification and properties of malonyl-coenzyme A--acyl carrier protein transacylase of Escherichia coli. Arch Biochem Biophys 143: 493-505.
21. Baumann WK, Bizzozero SA, Dutler H (1970) Specificity of alpha-chymotrypsin. Dipeptide substrates. FEBS Lett 8: 257-260.
22. Lowe PN, Rhodes S (1988) Purification and characterization of [acyl-carrier-protein] acetyltransferase from Escherichia coli. Biochem J 250: 789-796.
23. Williamson IP, Wakil SJ (1966) Studies on the mechanism of fatty acid synthesis. XVII. Preparation and general properties of acetyl coenzyme A and malonyl coenzyme A-acyl carrier protein transacylases. J Biol Chem 241: 2326-2332.
24. Schreier B, Stumpp C, Wiesner S, Hocker B (2009) Computational design of ligand binding is not a solved problem. Proc Natl Acad Sci U S A 106: 18491-18496.
25. Han L, Lobo S, Reynolds KA (1998) Characterization of beta-ketoacyl-acyl carrier protein synthase III from Streptomyces glaucescens and its role in initiation of fatty acid biosynthesis. J Bacteriol 180: 4481-4486.
26. Misra A, Sharma SK, Surolia N, Surolia A (2007) Self-acylation properties of type II fatty acid biosynthesis acyl carrier protein. Chem Biol 14: 775-783.
27. Vardon DR, Rorrer NA, Salvachua D, Settle AE, Johnson CW, et al. (2016) cis,cis-Muconic acid: separation and catalysis to bio-adipic acid for nylon-6,6 polymerization. Green Chemistry 18: 3397-3413.
28. Froese DS, Dobson CM, White AP, Wu X, Padovani D, et al. (2009) Sleeping beauty mutase (sbm) is expressed and interacts with ygfd in Escherichia coli. Microbiol Res 164: 1-8.
29. Bar-Even A, Noor E, Savir Y, Liebermeister W, Davidi D, et al. (2011) The moderately efficient enzyme: evolutionary and physicochemical trends shaping enzyme parameters. Biochemistry 50: 4402-4410.

30. Bennett BD, Kimball EH, Gao M, Osterhout R, Van Dien SJ, et al. (2009) Absolute metabolite concentrations and implied enzyme active site occupancy in Escherichia coli. Nat Chem Biol 5: 593-599.
31. Takamura Y, Nomura G (1988) Changes in the intracellular concentration of acetyl-CoA and malonyl-CoA in relation to the carbon and energy metabolism of Escherichia coli K12. J Gen Microbiol 134: 2249-2253.
32. Merski M, Shoichet BK (2012) Engineering a model protein cavity to catalyze the Kemp elimination. Proc Natl Acad Sci U S A 109: 16179-16183.
33. Geoghegan KF, Dixon HB, Rosner PJ, Hoth LR, Lanzetti AJ, et al. (1999) Spontaneous alpha-N-6-phosphogluconoylation of a "His tag" in Escherichia coli: the cause of extra mass of 258 or 178 Da in fusion proteins. Anal Biochem 267: 169-184.

CHAPTER 5. STRUCTURE, HIGH AFFINITY AND NEGATIVE COOPERATIVITY OF THE ESCHERICIA COLI HOLO-(ACYL CARRIER PROTEIN):HOLO-(ACYL CARRIER PROTEIN) SYNTHASE COMPLEX

Aaron M. Marcella and Adam W. Barb
Roy J. Carver Department of Biochemistry, Biophysics and Molecular Biology
2437 Pammel Drive
Molecular Biology Building, rm 4210
Iowa State University, Ames, IA 50011

Manuscript prepared for submission to the Journal of Molecular Biology

Highlights:
Structure of the Eschericia Coli holo-ACP synthase enzyme determined
Structure of the E. Coli holo-ACP synthase in complex with holo-ACP was determined
Binding energies determined for the formation of a product complex
NMR was used to validate the X-ray crystallography structures

Abstract:

The *Escherichia coli* holo-(acyl carrier protein) synthase (ACPS) catalyzes the coenzyme A-dependent activation of apo-ACPP to generate holo-(acyl carrier protein) (holo-ACPP) in an early step of fatty acid biosynthesis. ACPS is sufficiently different from the human fatty acid synthase to justify the development of novel ACPS-targeting antibiotics. Here we present two models of *E. coli* ACPS in apo- and product-bound forms solved by X-ray crystallography to 1.85 Å and 3.85 Å, respectively. Trimeric ACPS binds three holo-ACPP molecules to form a 3:3 hexamer with strong affinity and negative cooperativity. The first equivalent of holo-ACPP bound with a K_D = 50 nM, followed by the binding of two more equivalents of holo-ACPP with K_D = 1 μM. Solution NMR spectroscopy experiments validated the ACPS binding interface on holo-ACPP using chemical shift perturbations and the relative orientation of holo-ACPP to ACPS by fitting residual dipolar couplings. The structure, strong affinity and negative cooperativity of ACPS for holo-ACPP suggests a previously undescribed role of ACPS residues 65-94 in the regulation of fatty acid biosynthesis.

Introduction:

Fatty acid biosynthesis is essential for all organisms to form membranes, signaling and energy storage molecules [1] [2,3,4]. Cell membranes are comprised of fatty acids packaged into various glycerophospholipids that contain two fatty acyl tails and one polar head group. The membrane creates a semi-permeable barrier that helps cells maintain a balance of pH, charge, water, and

small molecules to survive [5,6]. The separation is not only important to protect from degradation and maintaining the interior components of the cell, but also for energy generation. Membranes provide the necessary separation of two compartments (cytosol and intermembrane space) in prokaryotes which in turn allows the proton motive force to generate ATP molecules by ATP synthase [7,8]. In eukaryotes, membranes also function as dividers for the various organelles and providing diffusion barriers within the cytoplasm [9].

Prokaryotic fatty acid biosynthesis is distinct and offers targets for antibiotic development [10,11,12]. Eukaryotes use a single polypeptide encoding all fatty acid biosynthesis activities unlike the multi enzyme system employed by prokaryotes and plants [11,12,13]. Thus, understanding the structure and function of the enzymes involved will greatly aid further studies into the mechanisms of fatty acid biosynthesis and potential inhibition.

Fatty acid biosynthesis in *Escherichia coli* is initiated by the transfer of the phosphopantetheine moiety from coenzyme A (CoA) to the Serine 36 hydroxyl on the acyl-carrier-protein (ACPP) generating holo-ACPP catalyzed by the holo-ACPP synthase (ACPS) (Figure 5-1) [14,15,16].

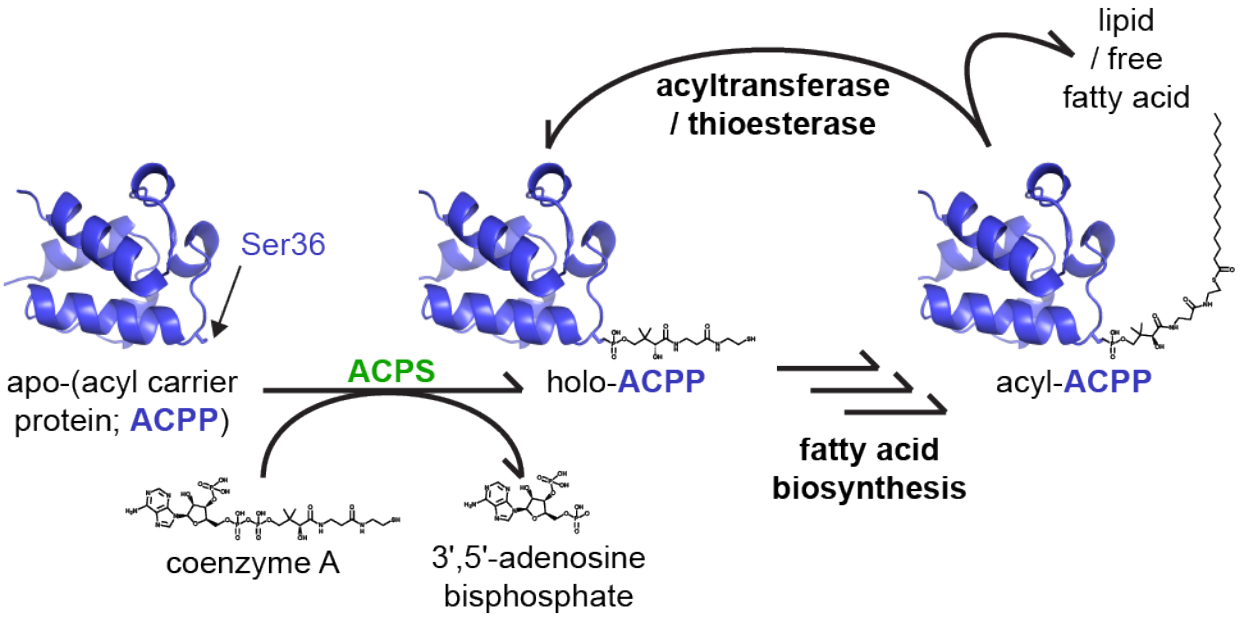

Figure 5-1. Holo-ACP synthase (ACPS) transfers the phosphopantetheine moiety from coenzyme A to Ser36 of apo-(acyl carrier protein; ACPP) to form holo-ACPP in an initial reaction of fatty acid biosynthesis.

There are several crystal structures of the enzyme from various gram positive bacteria, but only one from a gram negative bacterium [17]. ACPS forms a trimer with an aspartate and glutamate coordinating the catalytic magnesium ion in the active site. The magnesium ion activates a nearby water to perform a hydrolysis reaction on the phosphodiester bond of CoA leaving behind the phosphopantetheine moiety [14]. The final step is transferring phosphopantetheine to ACPP-Ser36, forming a phosphodiester bond. This reaction serve to activate holo-ACPP to serve as a scaffold for the growing fatty acid chain in the fatty acid biosynthesis pathway. A structure of ACPS in complex with holo-ACPP from *Bacillus subtilis* shows a 3:3 binding stoichiometry [14]. However, it is less clear how gram negative ACPS proteins are organized and

holo-ACPP binding is achieved. Multiple reports indicate the primary *E. coli* ACPS oligomer in solution was a homodimer [18,19,20].

Previous enzymatic studies on the ACPS enzyme showed what was interpreted as substrate inhibition by ACPP [18,20]. Initial kinetic characterization of the *E. coli* enzyme revealed what appeared to be substrate inhibition by ACPP above concentrations of 2 μM and set an upper bound on the K_M of 1 μM [20]. Later work confirmed this observation and reported a similar K_M for ACPP of 1.3 μM and displaying clear inhibition at higher concentrations of ACPP [18]. This substrate inhibition is interesting as it supports our observation of product inhibition by holo-ACPP with a K_D similar to the reported K_Ms of 1 μM.

We previously observed a homogenous complex formed by holo-ACPP and ACPS eluted at ~100 kDa from a gel filtration column, a mass much greater than the mass of either protein (9 and 14 kDa, respectively [21]. To determine the oligomeric stoichiometry, structural organization and functional characteristic of holo-ACPP binding by ACPS, we determine the investigated apo ACPS and ACPS in complex with holo-ACPP using a combination of X-ray crystallography, solution NMR spectroscopy and isothermal titration calorimetry.

Materials and Methods:

All materials were purchased from Sigma Aldrich unless otherwise noted.

Expression and Purification of ACPS: N-terminal 6xHis-tagged ACPP and untagged ACPS were expressed described previously [21]. The 6xHis-holo-ACPP:ACPS complex was purified on a 5 mL Ni-NTA column (Qiagen) that was

equilibrated with 3 column volumes (cv) buffer A (25 mM Tris-HCl, 500 mM sodium chloride, pH 8.5), then the 6xHis-holo-ACPP:ACPS complex was eluted with a linear gradient of 0-50% buffer B (Buffer A supplemented with 1 M imidazole) over 5 cv followed by a final 100 % buffer B elution for 1 cv and re-equilibrated with 3 cv of buffer A. Fractions containing 6xHis-holo-ACPP and ACPS were diluted >4-fold with 25 mM Tris-HCl, pH 8.5 and loaded onto a 120 mL Q-Sepharose column (GE Life Sciences). The Q column was washed with 0.5 cv of buffer C (25 mM MOPS, 1 mM EDTA, 2 mM β-mercaptoethanol, pH 7.1) following protein loading followed by a linear gradient from 20-60% buffer D (C plus 1 M potassium chloride) over 2 cv, then a 0.2 cv wash with 100% buffer D and then re-equilibrated with 1.2 cv buffer C. Fractions containing ACPS were concentrated using a 3 kDa cutoff Amicon ultra centrifugation filter unit (EMD Millipore) and loaded onto a Superdex 75 column (GE Life Sciences) equilibrated and eluted with 25 mM MOPS, 100 mM sodium chloride, 1 mM dithiothreitol, 10 mM magnesium chloride pH 7.1. Fractions containing ACPS were concentrated using a 3kDa cutoff filter unit and stored at 4 °C for less than 72 h.

Expression and Purification of holo-ACPP: The open reading frame encoding ACPP was cloned in a manner that excluded the translation of an N-term 6xHis tag, but added a single glycine as the second residue, into a pET DUET vector that already contained ACPS. Holo-ACPP was expressed as described above, and purified using the Q-sepharose and Superdex 75 chromatography steps described above. Purified holo-ACPP was diluted to 25% glycerol and stored at a concentration of ~2 mM at -80°C. Prior to NMR, X-ray crystallography or ITC

experiments, holo-ACPP was desalted into a buffer containing 25 mM MOPS, 100 mM sodium chloride, 10 mM magnesium chloride, 1 mM dithiothreitol pH 7.1 using a 5 mL G25 resin column. MALDI-TOF-MS analysis of holo-ACPP was described [21].

Crystallization of holo-ACP Synthase: Purified holo-ACPP and ACPS were mixed at a 1.1:1 molar ratio, loaded onto a Superdex 200 column (GE Life Sciences) and complex eluted with a buffer containing 25 mM MOPS, 100 mM sodium chloride, 1 mM dithiothreitol, 10 mM magnesium chloride, pH 7.1. Complex was concentrated to 8.5 mg/mL with a 3 kDa cutoff filter unit and diffraction quality plate crystals containing only holo-ACP synthase were obtained in 100 mM HEPES, pH 7.5 and 1.8-2.2 M sodium formate or 100 mM HEPES, pH 7.5 and 1.8-2.2 M sodium nitrate using the hanging drop method. Crystals were cryoprotected using 10% ethylene glycol diluted in mother liquor and crystals were flash frozen in liquid nitrogen. Data was collected on the 23-ID-B beamline at Argonne National Laboratory's Advanced Photon Source (APS) with a MAR300 detector. Data was indexed, merged, and scaled using HKL-2000 [22]. Molecular replacement was completed using PHENIX Phaser-MR with a *Bacillus subtilis* ACPS search model (PDB-1F7T). After initial molecular replacement and limited refinement using Phenix.Refine [23], refinement was finalized using Refmac5 [24,25]. Statistics for data collection and refinement are shown in Table 5-2. Structure figures were prepared using PyMol (Schrödinger, Inc). Structure coordinates and electron density files were deposited in the PDB as 5VBX.

Crystallization of holo-ACPP:ACPS complex: Purified holo-ACPP and ACPS were mixed at a 1.1:1 molar ratio and then loaded onto a Superdex 200 column. Complex was eluted with a buffer containing 25 mM MOPS, 100 mM sodium chloride, 1 mM dithiothreitol, 10 mM magnesium chloride pH 7.1 (Fig S5-1) and concentrated to 9 mg/mL using a 3 kDa cutoff filter unit. Diffraction quality rod crystals were obtained in 16-48 hours in the following conditions: 100 mM Bis-Tris propane, pH 7.0, (18-22% PEG 6k or 18-22% PEG 10k) and 100 mM sodium cacodylate, pH 6.5, (18-22% PEG 6k or 18-22% PEG 10k) using the hanging drop method mixing 1 µl protein with 1 µl mother liquor. Crystals were cryoprotected in either 10% 2,3, butanediol diluted in mother liquor or 100% Paratone-N and flash frozen with liquid nitrogen. Data was collected on the 23-ID-D beamline at APS with a Pilatus3 6M detector. Data was indexed, merged and scaled using HKL-2000. Three datasets were collected from two different rod crystals (two datasets from one crystal and one dataset from a separate crystal). The two datasets from the first crystal were collected with 2 second exposure times and 1 degree/frame (60 and 45 frames for each dataset). The final dataset was collected using a 0.5 second exposure time and 0.5 degrees/frame (162 frames). Following indexing and integration of each individual dataset in HKL-2000, data was scaled without merging the originally indexed reflections. These datasets were then merged and scaled together using the Aimless program in CCP4i. Iterative molecular replacement was performed using PHENIX Phaser-MR and the *E. coli* ACPS protein model determined in this manuscript. ACP molecules (1ACP) [26] were fit into the density using molecular replacement after

four ACPS trimers were placed in the asymmetric unit. After five ACP molecules were identified, the remaining unplaced ACPP monomers and ACPS trimer were fit using the previously identified sites as a guide. Final refinement was performed using Refmac5. Structure coordinates and electron density files were deposited in the PDB as 5VCB.

Labeled ACP preparation: [^{15}N]-holo-ACPP was expressed and purified as described above using M9 medium supplemented with [^{15}N]-ammonium chloride. [^{15}N,^{2}H]-holo-ACPP was prepared by growing an overnight 5 mL culture of the untagged ACPP construct in Luria-Bertani medium; this culture was added to 1 liter of ^{15}N labeled M9 medium in H_2O and grown to an OD_{600} of 0.44. At this point, the cells were pelleted with centrifugation in autoclaved bottles and resuspended in 1 L M9 medium supplemented with [^{15}N]-ammonium chloride and prepared with 99.5% $^{2}H_2O$. This culture was grown to OD_{600} = 0.8, then protein expression was induced with 0.5 mM IPTG and the culture was incubated with orbital shaking for 18 h at 18 °C. Holo-ACPP was purified as previously described. MALDI-TOF-MS spectra following purification showed ~85% [^{2}H, ^{15}N] labeling (data not shown). For backbone assignments of holo-ACPP, a 0.5 L culture of [^{15}N,^{13}C]- M9 medium was used for expression containing 0.5 g [^{15}N]-ammonium chloride and 1 g [$^{13}C_U$]-glucose (Cambridge Isotopes).

Backbone Resonance Assignment: All NMR experiments were performed on a 16.4T instrument equipped with a Bruker Avance II console and a 5 mm cryoprobe at 30 °C. The NMR sample for the assignments contained 300 μL of 1.2 mM [^{13}C,^{15}N]-holo-ACPP, 25 mM MOPS, 100 mM sodium chloride, 1 mM

dithiothreitol, 10 mM magnesium chloride, 1 mM DSS, and 5% $^{2}H_2O$, pH 7.1. CBCANH and CBCACONH experiments were collected with 16 scans/FID, 50 total points in the ^{15}N dimension and 100 total ^{13}C points. The HNCO experiment was collected with 4 scans/FID, 50 total points in the ^{15}N dimension and 100 total points for ^{13}C. Data were processed using TopSpin, NMRPipe [27] and 3D processing scripts and then analyzed in NMRViewJ (One Moon Scientific). Backbone assignments were deposited in the BMRB (i.d.-27061).

NMR Titrations: The change of crosspeak locations during a titration was monitored with a 2d ^{1}H-^{15}N HSQC-TROSY pulse sequence and with a sample containing 100 μM [^{2}H,^{15}N]-holo-ACPP, 25 mM MOPS, 100 mM sodium chloride, 1 mM dithiothreitol, 10 mM magnesium chloride, 1 mM DSS, 5% $^{2}H_2O$, pH 7.1. The total protein concentration in the NMR tube was quantified at each point by measuring A_{280} (ε^{ACPP}= 1490 M^{-1} cm^{-1}; ε^{ACPS}= 17990 M^{-1} cm^{-1}). The titration included the following concentrations: 0, 21.7, 39.8, 55.9, 77.7, 89.2, 101.2, 142.1 μM ACPS and 100, 92.2, 85.8, 80.3, 75.4, 71.1, 62.0, 52.3 μM holo-ACPP, respectively.

RDC Measurements: [^{2}H,^{15}N]-holo-ACPP and ACPS were mixed in a 1.1:1 molar ratio and purified over the Superdex 200 column in the same manner as described above. Complex was concentrated using a 3 kDa cutoff filter unit. The NMR sample contained 335 μM each of holo-ACPP and ACPS monomer, 1 mM DSS, 10% $^{2}H_2O$ in the following buffer: 25 mM MOPS, 100 mM sodium chloride, 1 mM dithiothreitol, 10 mM magnesium chloride, pH 7.1. An aligned sample was obtained by adding Pf1 phage (Asla Biotech) to a final concentration of 12.2

mg/mL (each monomer was reduced to 260 μM). $(^1J_{N\text{-}HN})^{iso}$ and $(^1J_{N\text{-}HN}+D)^{align}$ measurements were obtained using a *J*-modulated HSQC-TROSY pulse sequence [28] set to collect 64 scans/FID and total 128 points. Spectra were collected with a recycle delay of 3 s and *J* evolution period of 0.5, 2, 4, 5.4, 7, 9 or 10.8 ms. $(^1J_{N\text{-}HN})^{iso}$ and $(^1J_{N\text{-}HN}+^1D)^{align}$ values were determined by fitting decaying cosine functions in NMRViewJ. RDCs were calculated from $(^1J_{N\text{-}HN}+D)^{align}$ - $(^1J_{N\text{-}HN})^{iso}$ and fitted using PALES [29] and REDCAT [30]. From 47 holo-ACPP cross peaks visible in a ^1H-^{15}N HSQC-TROSY spectrum, 30 provided high quality $^1J_{HN\text{-}N}$-modulation data. Of these, 7 were removed due to locations in loop regions or as a result of poor fits to the model (18,22,33,45,56,64,69) (Figure 5-6B). The 23 RDCs used are for residues 4,7,8,10,12,14,16,19,23-25,27-28,50-52,68,70-75. Residues 4-19 belong to a helix, 23-25 and 27-28 are on a loop region, 50-52 are at the base of a helix, and 68-75 belong to the c-terminal helix.

ITC Titrations: ACPS or holo-ACPP exchanged into a buffer containing 25 mM MOPS, 100 mM sodium chloride, 1 mM dithiothreitol, 10 mM magnesium chloride, pH 7.1 using a Superdex 75 or G25 column, respectively. ACPS (220 μl of 86.3 μM) was placed in the sample cell of the MicroCal ITC200 (GE Life Sciences). Holo-ACPP (40 μl of 980 μM) was injected with 28 total injections (1x0.2 μl, 4x0.5 μl, 14x1 μl, 5x2 μl, and 4x3 μl) with a cell temperature of 25 °C, reference power=1, initial delay of 60 s, and stirring speed of 1000 rpm. There was a 120 s delay between the 0.2, 0.5, and 1 μl injections and 180 s delay

between the 2 and 3 µl injections. Isotherms were analyzed using the CHASM ITC data analysis program [31,32].

Results

Holo-ACPP binding by ACPS-

Holo-ACPP bound ACPS with surprisingly high affinity (Figure 5-2 and S2).

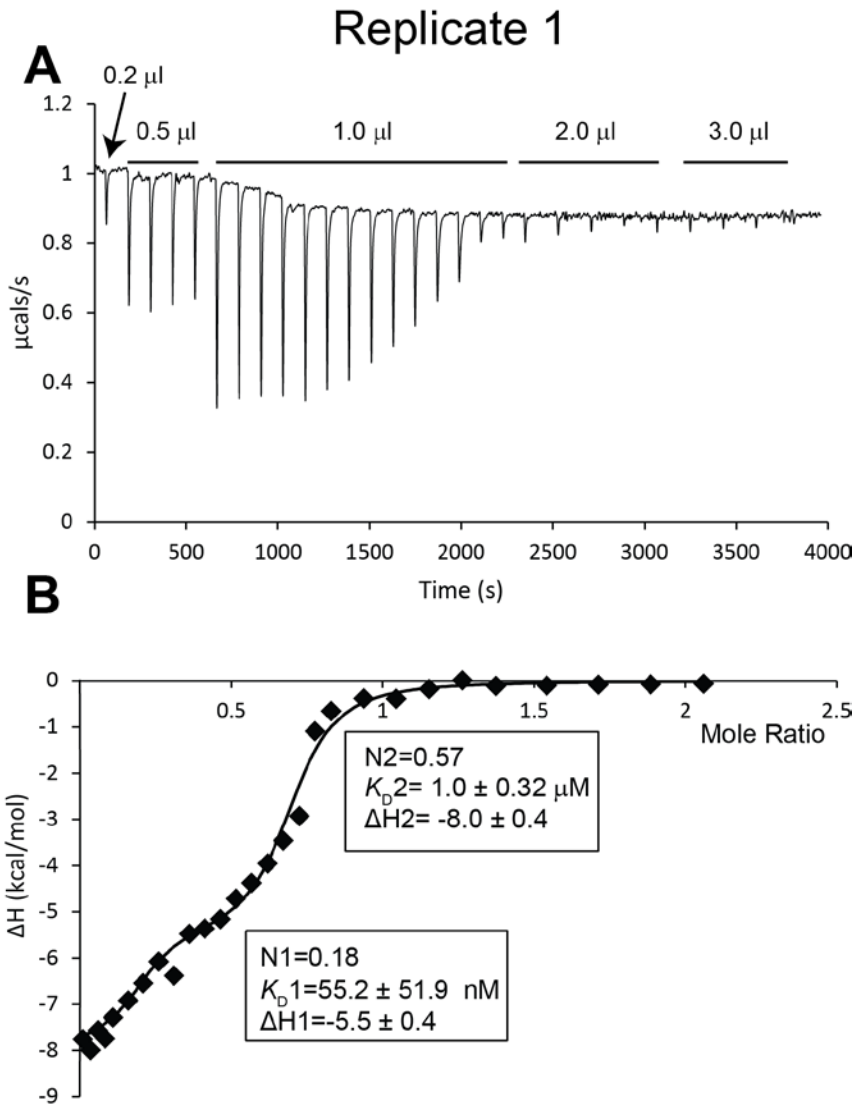

Figure 5-2. Holo-ACPP binding by ACPS reveals negative cooperativity. A. Heat change upon each injection (volume indicated) observed during a titration

as monitored by isothermal titration calorimetry. **B.** The binding isotherm derived from integrating peaks in (**A**) demonstrates two independent binding events. An independent experiment is shown in Figure S5-2.

If we assume 3:3 stoichiometry in the complex, the ratio of *N* values from ITC (relative to 1 ACPS trimer) of 0.18 and 0.57 indicate two independent binding events with an approximate binding stoichiometry of 2:1. One holo-ACPP binds with a K_D = 55 nM followed by the final two holo-ACPPs which bind with an indistinguishable K_D = 1 μM (Table 5-1).

Table 5-1.

Run #1		**Run #2**	
Event #1		**Event #1**	
N	0.18	N	0.14
K_D	55.2 ± 51.9 nM	K_D	45.5 ± 95.0 nM
ΔG	-41.4 ± 38.9 kJ mol^{-1}	ΔG	-41.9 ± 87.6 kJ mol^{-1}
ΔH	-23.0 ± 1.7 kJ mol^{-1}	ΔH	-25.9 ± 1.7 kJ mol^{-1}
ΔS	61.7 ± 58.1 J mol^{-1} K^{-1}	ΔS	53.5 ± 111.9 J mol^{-1} K^{-1}
Event #2		**Event #2**	
N	0.57	N	0.53
K_D	1.0 ± 0.3 μM	K_D	1.25 ± 0.5 μM
ΔG	-34.2 ± 10.9 kJ mol^{-1}	ΔG	-33.7 ± 13.5 kJ mol^{-1}
ΔH	-33.5 ± 1.7 kJ mol^{-1}	ΔH	-33.9 ± 5.4 kJ mol^{-1}
ΔS	2.5 ± 0.8 J mol^{-1} K^{-1}	ΔS	-0.7 ± 0.3 J mol^{-1} K^{-1}

These data are consistent with negative cooperativity: binding one holo-ACPP molecule to the ACPS trimer reduces affinity by ~20-fold for the next two holo-ACPP molecules. The two binding events are marked by a free energy difference of 7.4 kJ/mol (-41.4 kJ/mol and -34 kJ/mol for each event) and also a significant

difference in entropy (61.7 J mol^{-1} K^{-1} and 2.5 J mol^{-1} K^{-1} for the first and second events). Positive entropy coupled with a –ΔG and –ΔH are consistent with a model of stabilizing hydrogen bonds and an unfavorable conformational change. These data suggest there is both high affinity and negative cooperativity in product binding.

X-ray crystallography of ACPS-

Crystallization of the holo-ACPP:ACPS complex yielded both rod and plate crystal forms. The plate crystals diffracted to 1.6 Å. Molecular replacement with a *Bacillus subtilis* ACPS model (pdb=1F7T;[14]) revealed initial phases and the presence of only one ACPS enzyme in the asymmetric unit, a finding confirmed with MALDI-TOF-MS analysis of the plate crystals (data not shown). It is likely the high salt concentration in the crystallization condition (~2.0 M sodium formate/nitrate) separated the holo-ACPP:ACPS complex.

Diffraction data from the plate crystals were of high completeness and quality to 1.85 Å and used to solve a model of unliganded *E. coli* ACPS (Table 5-2). ACPS forms a trimer with a central nine-strand beta-barrel (3 per monomer) observed in other ACPS crystal structures (Figure 5-3A) [14,15,17]. Electron density at the active site residues and catalytic magnesium ion is shown in Fig 5-3C. There are differences in secondary structure position and orientation between *E. coli*, *Bacillus subtilis* and *Neisseria meningitidis* structures (Fig S5-5). The main helix from residues 46-64 shifts 6.5 Å from the *N. meningitidis* to the *E. coli*/*B. subtilis* structures.

Table 5-2.

Data collection	**ACPS**	**holo-ACPP:ACPS complex**
Space group	*C*2	$P4_3$
Cell dimensions		
a, b, c (Å)	100.376, 69.522, 59.894	251.424, 251.424, 58.939
α, β, γ (°)	90, 109.55, 90	90, 90, 90
Resolution (Å)	29.6-1.604	49.31-3.85
No. Datasets	1	3
R_{merge}	0.1458 (2.368)*	0.254 (1.968)
I/δI	7.85 (0.28)	4.6 (0.7)
$CC_{1/2}$	0.995 (0.0801)	0.989 (0.085)
Completeness (%)	98.0 (82.0)	93.7 (71.6)
Redundancy	3.8 (2.1)	5.6 (3.7)
Unique Reflections	32448 (2704)	31881 (3464)
Refinement		
Resolution	29.6-1.85	49.19-3.85
R_{work}/R_{free}	0.209/0.211	0.307/0.313
No. atoms	3200	23714
Protein	2956	23633
Ligand/ion	44	81
Water	200	n.a.
B-factors	35.44	82.59
Protein ($Å^2$)	34.99	n.a.
Ligand/ion ($Å^2$)	44.93	n.a.
R.m.s deviations		
Bond lengths (Å)	0.021	0.019
Bond angles (°)	2.170	1.680
PDB i.d.	5VBX	5VCB

*values in parentheses refer to the outer shell

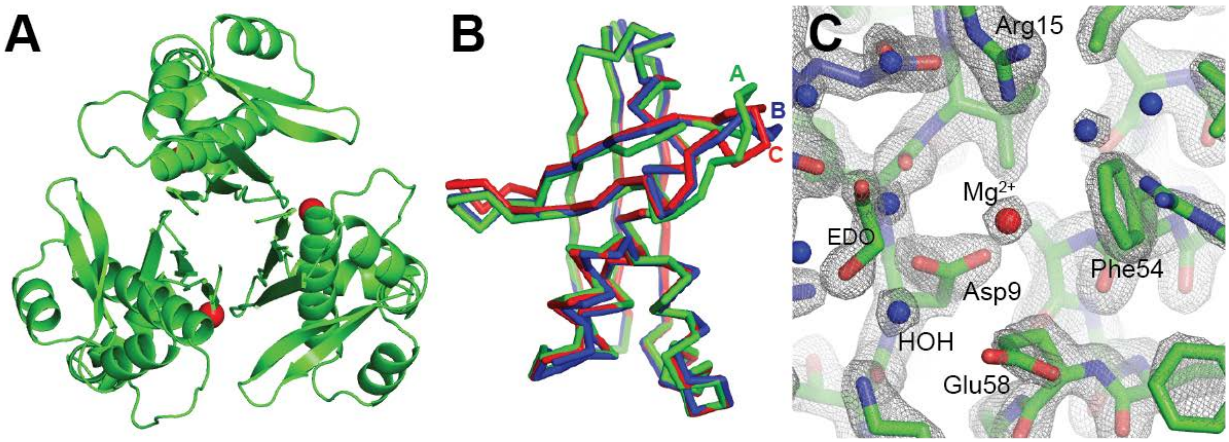

Figure 5-3. The structure of *E. coli* ACPS solved to 1.85 Å. A. The ACPS backbone (*green* ribbons) as viewed down the 3-fold symmetry axis, Mg^{2+} ions at the active site are shown as *red* spheres. **B.** An overlay of chain A (*green*), B (*blue*) and C (*red*) highlight conformational heterogeneity that is largely limited to residues 65-94. **C.** Electron density (scaled to 1.5 σ) showing the ACPS active site with Asp9, Glu58 and the coordinated magnesium ion. Waters are shown as *blue* spheres (EDO = ethylene glycol).

There is also a difference of 5 Å on the helix from residues 12-24. These are significant deviations in secondary structure position within structures that have very close agreement of the central 9 antiparallel beta strands. In general there are significant differences in orientation of the 3 helix bundle from residues 13-43. The ACPS structure is well defined with the exception of residues 64-69 that form a loop and different conformations in the ACPS trimer (Fig 5-3B). These residues also showed high isotropic B values (>90). It is not surprising that this loop is mobile as it sits at the ACPP binding interface and likely reorients to accommodate binding.

X-ray crystallography of the holo-ACPP:ACPS complex-

MALDI-TOF-MS indicated the presence of both holo-ACPP and ACPS in the rod-shaped crystals that diffracted to 3.5 Å and had a much larger asymmetric unit

(Table 5-2). Analysis of the diffraction data with a Pearson correlation coefficient (CC1/2) and a student's t-test ($p<0.01$) indicated near complete and reliable data to 3.85 Å [33,34,35]. Molecular replacement with the *Bacillus subtilis* holo-ACPP:ACPS complex was unsuccessful, and not surprising given the low resolution data and lack of sequence identity (38 %). We utilized an iterative method to sequentially build the asymmetric unit with *E. coli* ACPS structure determined above. After determining the location of four ACPS trimers, five holo-ACPP monomers were fitted. The remaining seven ACPP molecules were fit using rigid body placement and the previously fit ACPs as a guide. Only at this stage was clear density for the final holo-ACPP:ACPS hexamer visible revealing an asymmetric unit that contained 15 holo-ACPP and 15 ACPS monomers arranged into five hexamers (Figure 5-4A). Electron density maps showed very clear secondary structure elements and some side chain definition (Figure 5-4B). Electron density near Ser36 on several ACPP molecules could not be accounted for by polypeptide atoms and was modeled with atoms of the phosphopantetheine moiety (Figure 5-4C). This model is similar to a model of the holo-ACPP:ACPS complex from *B. subtilis* though some differences are evident, including the placement of ACPP molecules that are closer to the ACPS in the *E. coli* complex (Figure 5-4D).

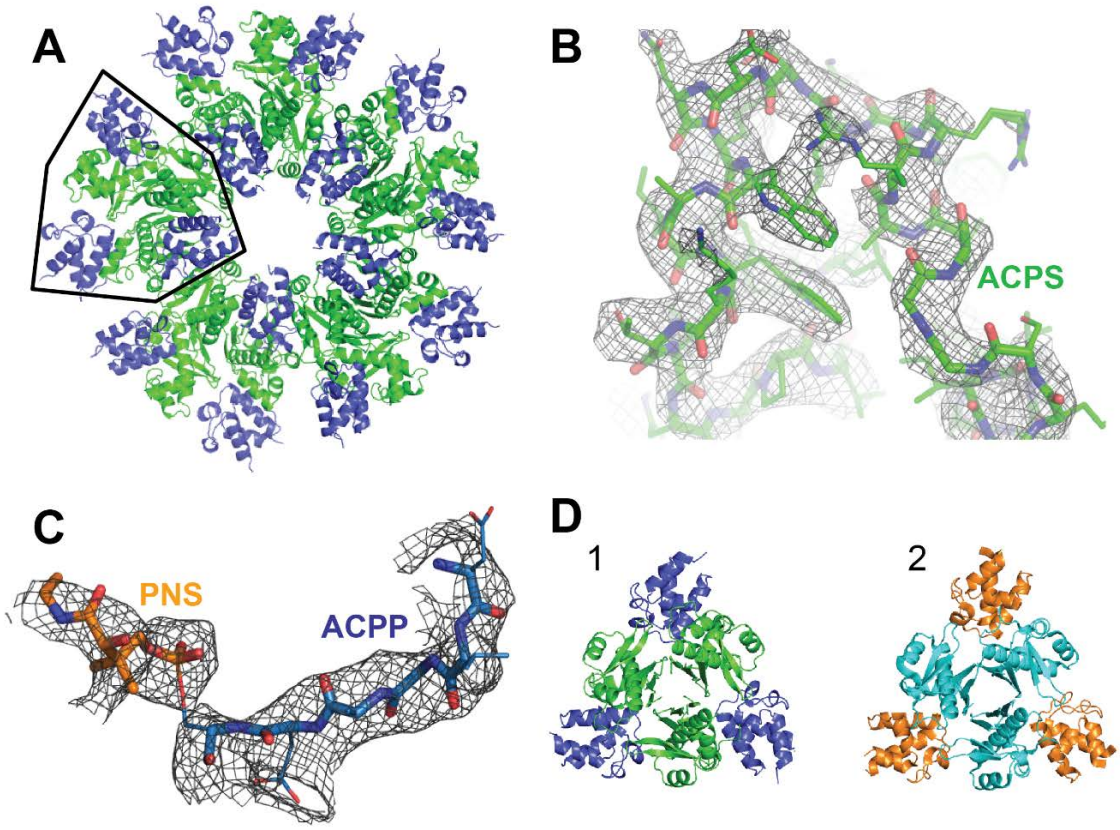

Figure 5-4. Structure of the *E. coli* holo-ACPP/ACPS complex solved to 3.85 Å. A. The asymmetric unit contained 5 hexameric holo-ACPP/ACPS complexes. One hexamer is highlighted with a black outline. **B.** Electron density (scaled to 1.25 σ) shows the clear resolution of ACPS polypeptide features in *green* and **C.** partial resolution of the pendant phosphopantetheine (PNS, *orange* stick model). Electron density corresponding to sidechain atoms was observed but sidechain models are not shown in this image. A comparison of the *E. coli* holo-ACPP/ACPS complex (**D1**) is similar to a structure of the catalytically inactive apo-ACPP/ACPS complex from *Bacillus subtilis* (**D2.,** PDB-1F80), though the *E. coli* holo-ACPP ligands are closer to the center of the complex than the apo-ACP from *B. subtilis*.

Identifying the ACPS binding interface of holo-ACPP-

Analysis of the holo-ACPP:ACPS complex by solution NMR spectroscopy provided an independent analysis of the binding interface. Though ACPP is often used for NMR experiments [26][36,37,38], assignments of backbone heavy atoms are necessary to characterize binding interfaces and molecular orientation but are not available in the BioMagResBank (www.bmrb.wisc.edu) for holo-ACPP. We assigned 100% of the HN, 98.7% N, 98.7% CA, 98.6% CB and 97.5% of CO resonances using standard triple-resonance experiments (Figure S5-4).

Chemical shift perturbations of holo-ACPP upon ACPS titration identified a binding interface. Of 47 amide crosspeaks unambiguously identified in ^{1}H-^{15}N HSQC-TROSY spectra, those with large chemical shift perturbations clustered on one facet of ACPP, near Ser36, that was comparable to the interface observed by X-ray crystallography (Figure 5-5A-C). Multiple peaks disappeared during the titration, including many peaks at the core of the interface that correspond to atoms from the loop and helix around Ser36 (residues 30-47).

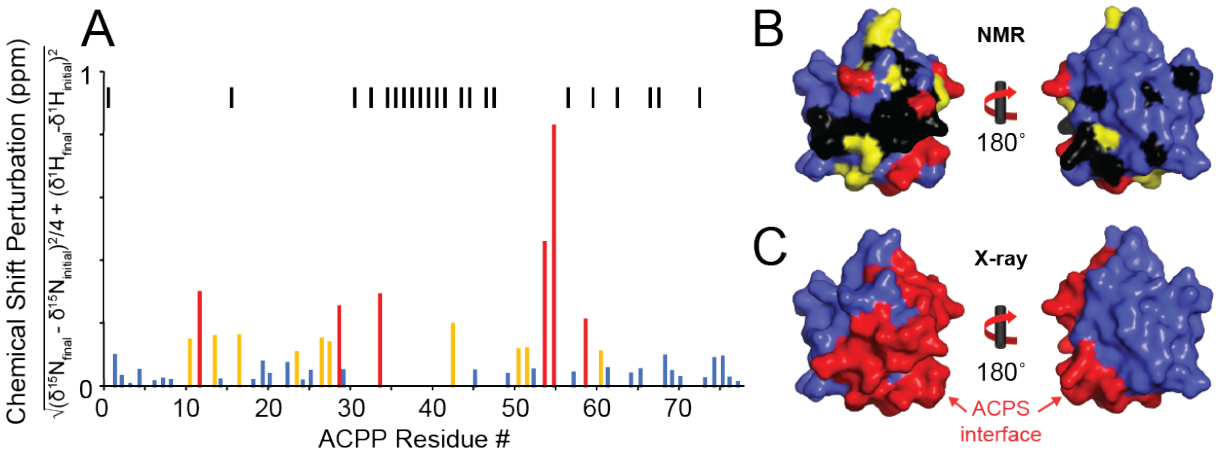

Figure 5-5. The holo-ACPP/ACPS interfaces identified by solution NMR spectroscopy and X-ray crystallography are compatible. A. Chemical shift perturbations of backbone holo-ACPP residues were measured following a titration with ACPS. Amide crosspeaks with significant (*red* lines: 0.2-1.0 ppm), moderate (*yellow*, 0.10-0.19 ppm), minimal (blue, <0.1 ppm) perturbation or crosspeaks broadened beyond the point of detection (vertical *black* line) are indicated and mapped onto a model of ACPP (**B.**). **C.** The holo-ACPP/ACPS interface residues identified through X-ray crystallography are shown as a *red* surface on ACPP.

NMR measurement of holo-ACPP orientation in the complex-

Symmetric oligomers with three or more subunits provide additional opportunities to characterize relative binding orientation by measuring residual dipolar couplings (RDCs) with a solution NMR spectroscopy approach [39,40]. It is known from RDCs of $n \geq 3$ homo-oligomer that 1) the principle alignment tensor axis must be coincident with the molecular rotational symmetry axis, and 2) the alignment tensor will be axially symmetric (*Rhombicity* ~0) [40,41]. RDCs are expected to provide the orientation of holo-ACPP with respect to the ACPS molecular symmetry axis (the *z* axis), but this measurement does not report whether holo-ACPP is oriented along the + or - *z* axis (differing by a 180 degree rotation around the *x* or *y* axes), or what rotation each holo-ACPP experiences relative to ACPS (all rotations around the *z* axis are indistinguishable), respective to 1) and 2) above. The incorporation of additional RDCs collected with a unique alignment condition does not provide additional information.

HSQC-TROSY-based experiments measured the $^{1}J_{HN\text{-}N}$-modulation of amide nitrogen nuclei using the [^{2}H,^{15}N]-holo-ACPP:[unlabeled]ACPS complex in the presence (anisotropic) or absence (isotropic) of Pf1 phage [28,42].

Subtracting coupling values obtained without phage ($^1J_{HN-N}$) from measurements with phage ($^1J_{HN-N}+^1D$) provided RDC measurements. We fitted values from 23 residues found in multiple ACPP helices to the X- ray model of the holo-ACPP:ACPP hexamer with a high quality of fit (Q = 0.17; Fig 5-6B) [43,44]. The analysis also revealed an axially symmetric alignment tensor (*Rhombicity* = 0.03) that was aligned with the *z*-axis when using models of the hexamer oriented with the molecular symmetry axis parallel to the *z* axis (Figure 5-6A)[44].

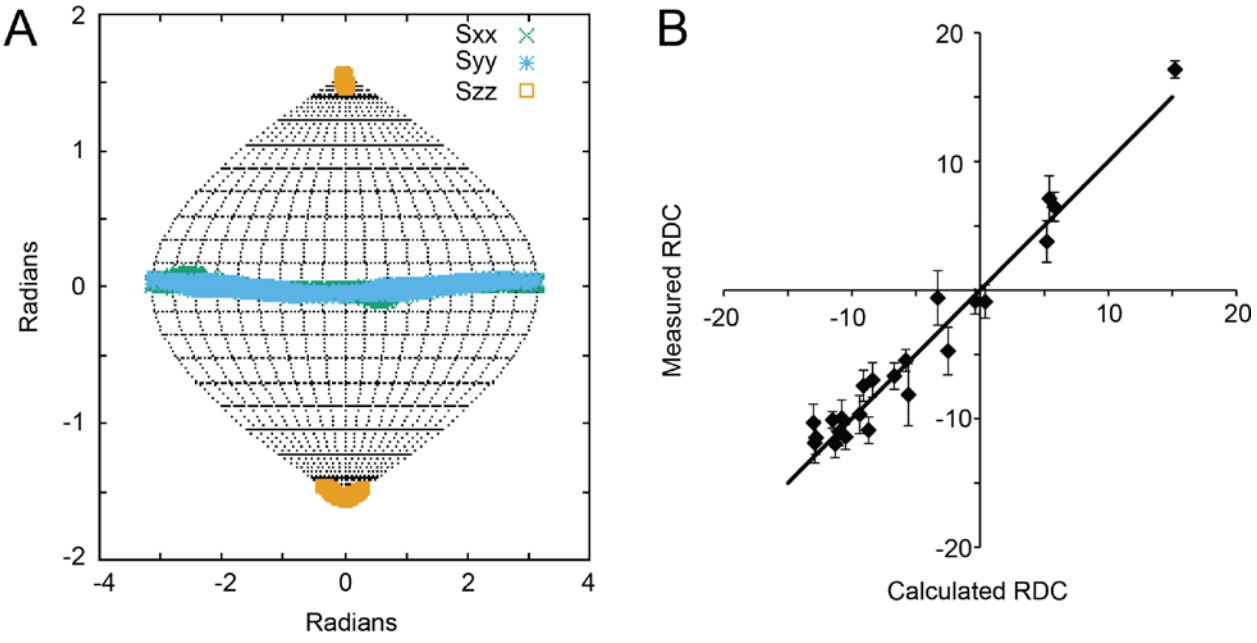

Figure 5-6. The orientation of holo-ACPP relative to ACPS measured by residual dipolar couplings is indistinguishable from the orientation observed by X-ray crystallography. A. Sauson-Flamsteed plot shows the best-fit alignment tensors and indicates axial symmetry of the ACPP protein in complex with ACPS. RDCs were fitted to the ACPP model from the holo-ACPP:ACPS complex determined by X-ray crystallography after the rotational symmetry axis of the heterohexamer was rotated to be parallel to the z-axis. **B.** A plot comparing the measured RDCs with RDCs calculated following the best fit of the alignment tensors. (Bars represent the sum of fitted *J* and *J+D* errors for each RDC).

As expected, orientation of holo-ACPP along either the + or - *z* axis along with all possible rotations around *z* yielded the same quality of RDC fit. This degeneracy was resolved by analyzing how each possible holo-ACPP orientation matched the interface identified by NMR and if Ser36 was brought within close proximity of the ACPS catalytic residues leaving only one likely orientation that was indistinguishable from the orientation observed by X-ray crystallography. In conclusion, the solution NMR data and X-ray crystallography model unambiguously define the holo-ACPP:ACPS interface and relative orientation.

Discussion

We characterized the *E. coli* ACPS in apo and holo-ACPP-bound forms using multiple techniques. A model of the apo ACPS solved by X-ray crystallography showed many similarities in secondary structure to previously solved models [14,17,45] though some differences were noted. We also determined the structure of the holo-ACPP:ACPS complex with ACPS and validated the model using solution NMR spectroscopy. These data clearly identify the ACPP/ACPS interface and relative orientations in the 3:3 oligomer.

This solution and solid state characterization of ACPS clearly indicate a trimeric stoichiometry and ability to bind three holo-ACPP products. It is not clear why previous efforts identified ACPS dimer forms in solution [18,19,20]. We found no evidence of smaller ACPS oligomers in gel filtration chromatography experiments, though it is possible that ACPS at lower concentrations forms monomers or homodimers (data not shown).

It is surprising that ACPS has such strong affinity for product, but previous studies claiming the observation of substrate inhibition could have been misinterpreted product inhibition [18,20]. Our binding data clearly shows negative cooperativity with a second binding event having a K_D of 1 μM, the same value reported previously for ACPP K_M. Product inhibition would seem more mechanistically likely as ACPP should not bind ACPS until after CoA binding as reported (however, the crystal structure of this ACPS-ACPP complex was catalytically dead) [14]. The strong binding of holo-ACPP to ACPS is facilitated by strong charge-charge interactions given the disparate calculated isoelectric points (4.0 and 9.3, respectively). There are several aspartates and glutamates on holo-ACPP and contribute to the interface, being located near arginines and lysines on ACPS. The loop from residues 64-74 and turn from 82-85 on the apo-ACPS show the most conformational heterogeneity and in the case of the loop, high B factors and low side chain occupancy (Figure 5-3B and Figure 5-7). These two regions are located at the binding site of holo-ACPP likely deform to accommodate ACP binding. Loop orientations as well as secondary structure motifs of ACPS that differ in the apo and complex structures support this observation. ACPS residues 65-94 make an intimate connection with holo-ACPP to form a contiguous “belt” around the enzyme. This belt is poised to serve as a conduit to transmit the status of single holo-ACPP binding to the other two holo-ACPP binding sites and may mediate the observed negative cooperativity with respect to holo-ACPP binding. This type of negative feedback inhibition may act as a checkpoint in fatty acid biosynthesis.

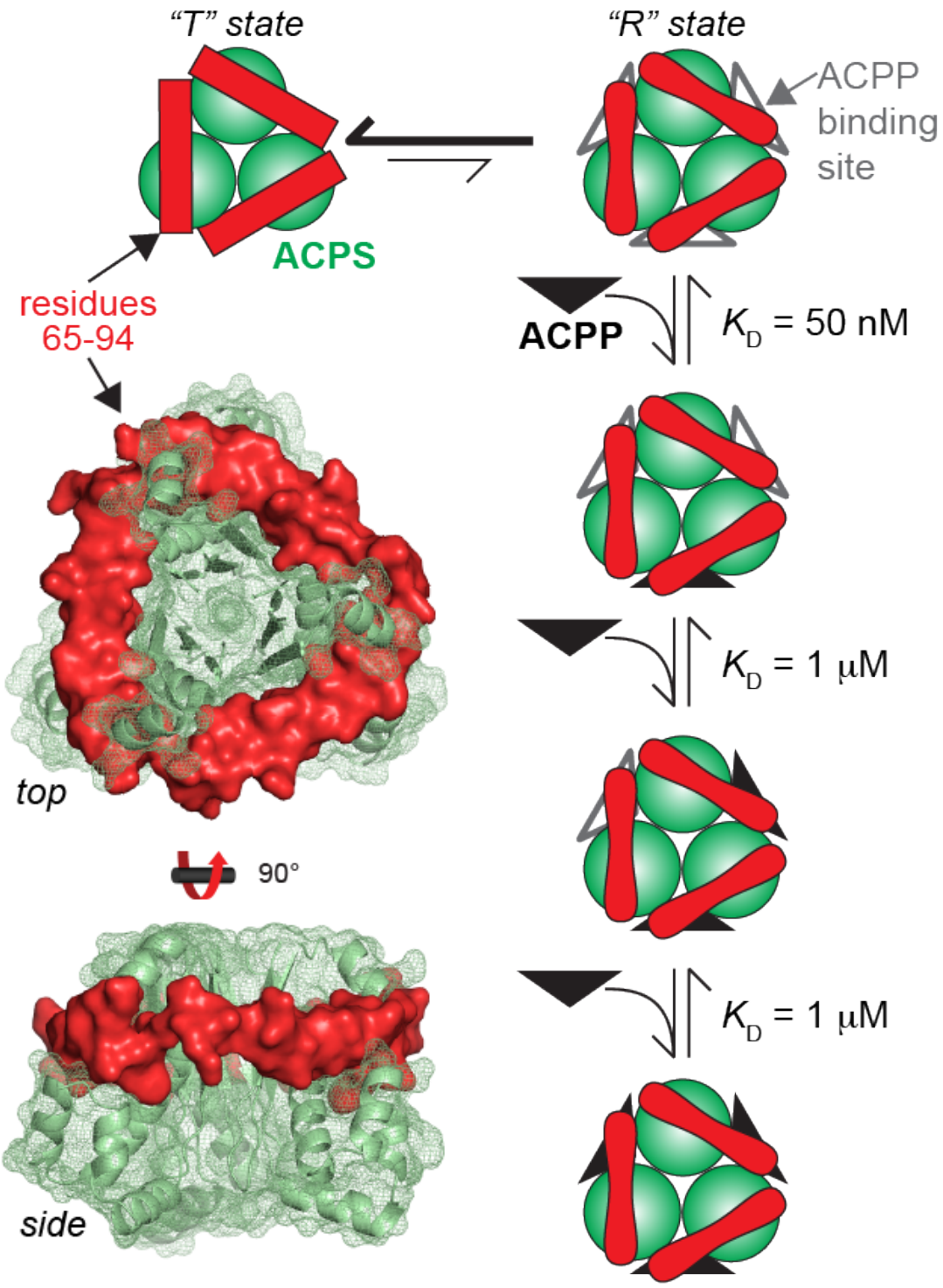

Figure 5-7. Allosteric binding model representing negative cooperativity in holo-ACPP binding by ACPS. Holo-ACP synthase is shown in *green* with a "belt" of residues (65-94) in *red*.

Cellular coenzyme A levels are tightly controlled and regulated in multiple manners [46,47,48,49]. Inhibiting ACPS activity would prevent unnecessary coenzyme A degradation and holo-ACPP production.

There are significant differences between the ACPS enzyme from humans and *E. coli*. The most notable difference is the human ACPS is a single polypeptide that folds into an intramolecular dimer [15]. A 10 amino acid expansion from the human enzyme is present in the region of residues 82-85 on the *E. coli* enzyme which is part of the belt proposed to impart negative cooperativity. This is important as the loop expansion in the human enzyme takes up the space where a third ACPS molecule would bind ensuring the intramolecular dimer and not a trimer is the active unit. The loop from 62-73 on the *E. coli* enzyme that interacts with ACPP deviates by ~5-15 Å when compared to the human enzyme. Residues from 81-85 on the *E. coli* enzyme involved in ACP binding are very different from those in the human enzyme, NDELG vs RTAKGKP. There are also two potential salt bridges formed between Asp38 and Glu41 on holo-ACPP and Arg15 and Arg22 on ACPS in the *E. coli* enzyme that are not present in the human enzyme. These key differences could allow for the generation of highly specific inhibitors of the *E. coli* enzyme that would not have any effect on the human enzyme.

Acknowledgment

We thank D. Bruce Fulton of the Iowa State University Biomolecular NMR Facility for assistance running the backbone resonance assignment experiments. This material is based upon work supported by the National Science Foundation under Award No. EEC-0813570, a grant for synchrotron time at the Argonne National Laboratory Advanced Photon Source by the Department of Energy (GUP-48455), and by funds from the Roy J. Carver Department of Biochemistry, Biophysics & Molecular Biology at Iowa State University. Any opinions, findings, and conclusions or recommendations expressed in this material are those of the authors and do not necessarily reflect the views of the National Science Foundation or the Department of Energy.

Supplement for:

Structure, high affinity and negative cooperativity of the *Escherichia coli* holo-(acyl carrier protein):holo-(acyl carrier protein) synthase complex

Aaron M. Marcella and Adam W. Barb
Roy J. Carver Department of Biochemistry, Biophysics and Molecular Biology
2437 Pammel Drive
Molecular Biology Building, rm 4210
Iowa State University, Ames, IA 50011

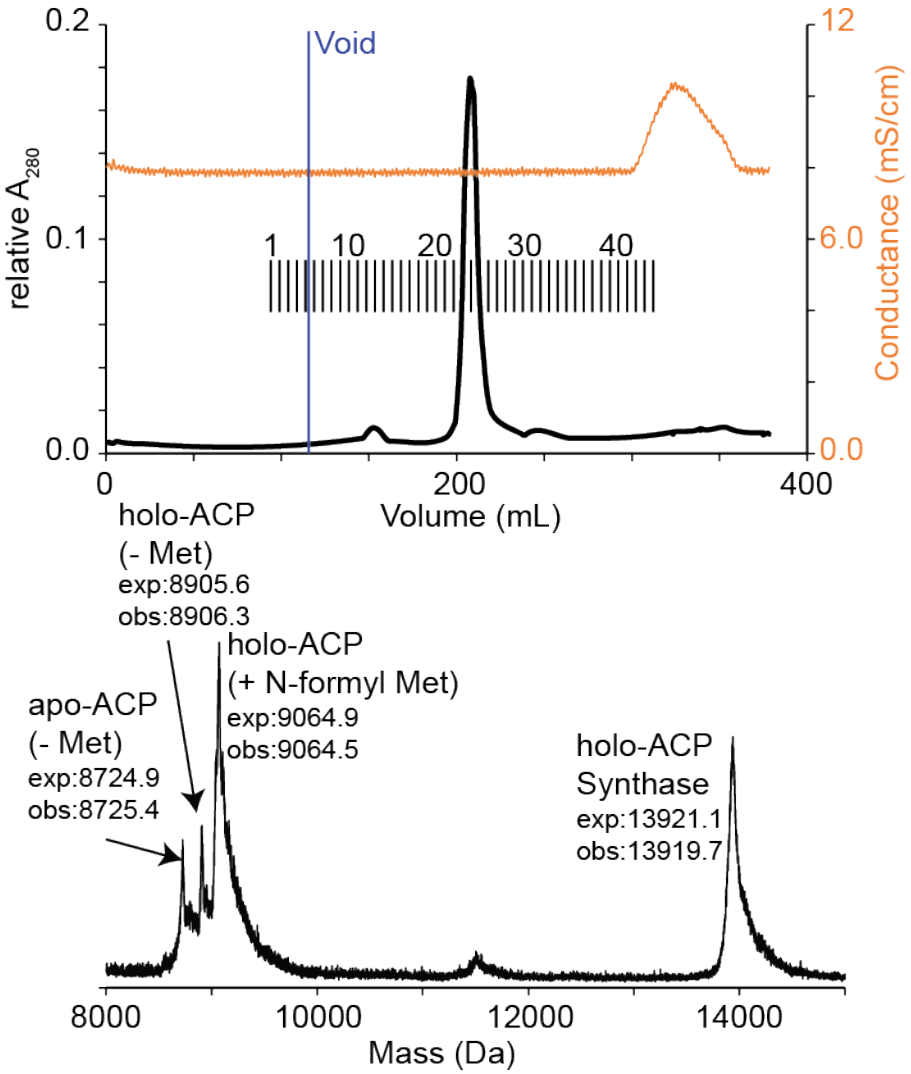

Figure S5-1. Gel filtration and MALDI-TOF-MS of the ACPP:ACPS complex. **A.** The ACPP:ACPS complex elutes from a Superdex 200 column in a single peak. Fractions are marked with vertical lines; the void column of the column, measured with blue dextran, is indicated with a solid *blue* vertical line. **B.** Analysis of the ACPP:ACPS complex by MALDI-TOF-MS reveals both a high proportion of holo-ACP.

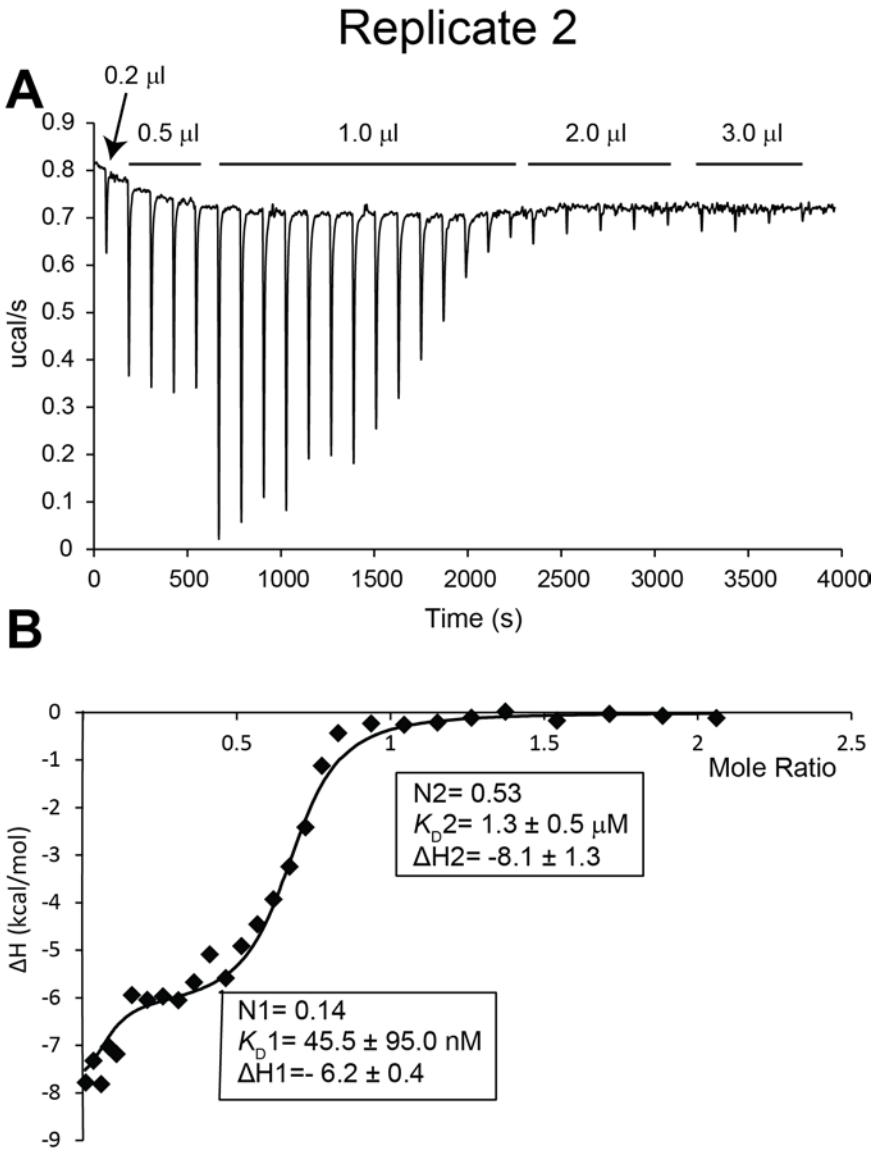

Figure S5-2. ITC replicate 2.

A direct replicate of the experiment shown in Figure 5-2 with all parameters in close agreement.

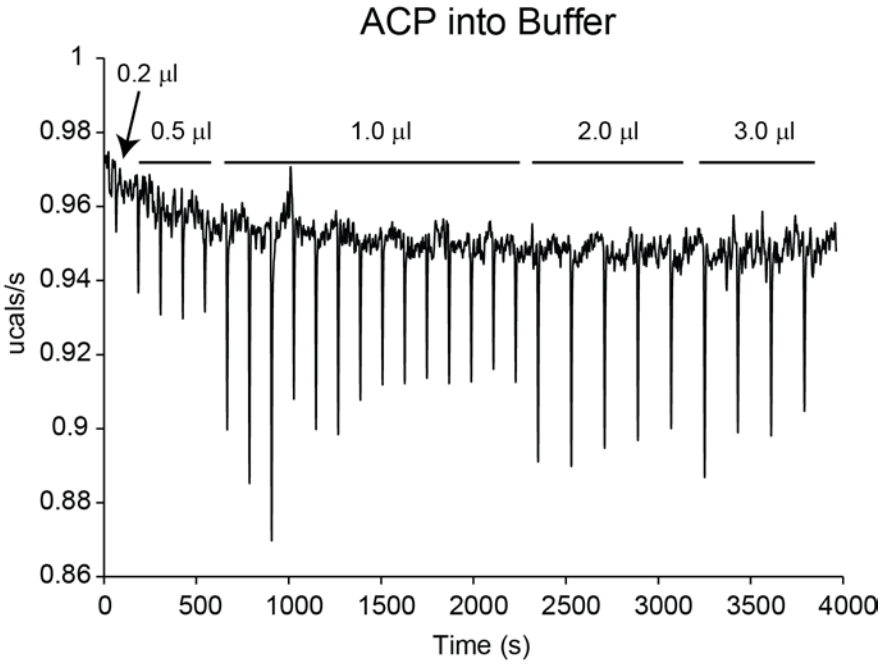

Figure S5-3. Blank Titration

Blank titration of holo-ACP into buffer, very low responses were observed.

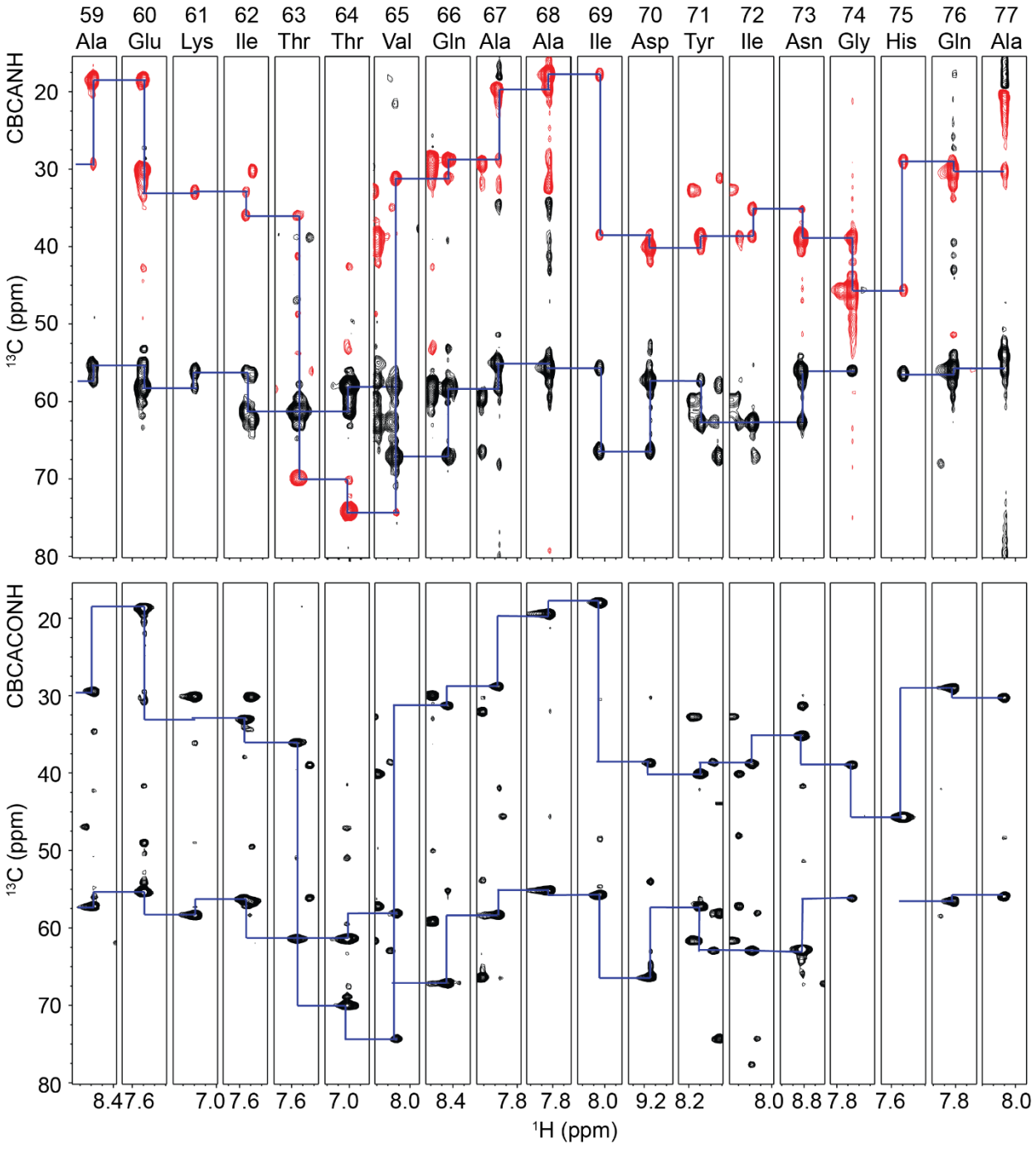

Figure S5-4. Assignment Strips for holo-ACP

2D strips from triple resonance assignments for C-terminus residues 59-77 of holo-ACP.

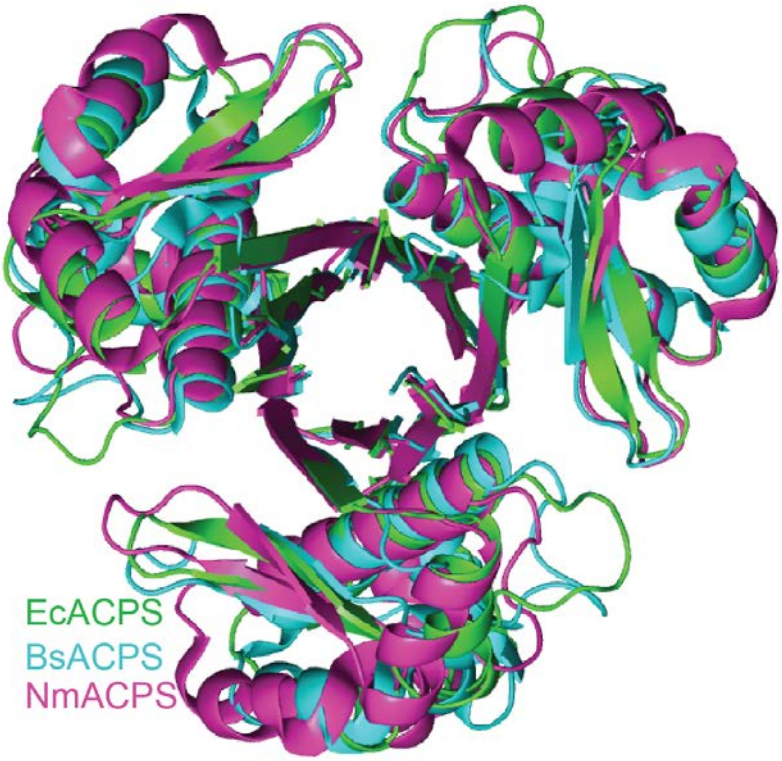

Figure S5-5.

Alignments of the ACPS crystal structures from *E. coli*, *B. subtilis* and *N. meningitidis*. Shows the differences in secondary structure orientations present within the same overall fold of the enzyme.

Works Cited

1. Leibundgut M, Maier T, Jenni S, Ban N (2008) The multienzyme architecture of eukaryotic fatty acid synthases. Curr Opin Struct Biol 18: 714-725.
2. Alvarez HM, Steinbuchel A (2002) Triacylglycerols in prokaryotic microorganisms. Appl Microbiol Biotechnol 60: 367-376.
3. van Meer G, Voelker DR, Feigenson GW (2008) Membrane lipids: where they are and how they behave. Nat Rev Mol Cell Biol 9: 112-124.
4. Raetz CR, Whitfield C (2002) Lipopolysaccharide endotoxins. Annu Rev Biochem 71: 635-700.
5. Aoi W, Marunaka Y (2014) Importance of pH homeostasis in metabolic health and diseases: crucial role of membrane proton transport. Biomed Res Int 2014: 598986.
6. Elmoazzen HY, Elliott JA, McGann LE (2009) Osmotic transport across cell membranes in nondilute solutions: a new nondilute solute transport equation. Biophys J 96: 2559-2571.
7. Cingolani G, Duncan TM (2011) Structure of the ATP synthase catalytic complex (F(1)) from Escherichia coli in an autoinhibited conformation. Nat Struct Mol Biol 18: 701-707.
8. Junge W, Nelson N (2015) ATP synthase. Annu Rev Biochem 84: 631-657.
9. Heald R, Cohen-Fix O (2014) Morphology and function of membrane-bound organelles. Curr Opin Cell Biol 26: 79-86.
10. Campbell JW, Cronan JE, Jr. (2001) Bacterial fatty acid biosynthesis: targets for antibacterial drug discovery. Annu Rev Microbiol 55: 305-332.
11. White SW, Zheng J, Zhang YM, Rock (2005) The structural biology of type II fatty acid biosynthesis. Annu Rev Biochem 74: 791-831.
12. Wakil SJ, Stoops JK, Joshi VC (1983) Fatty acid synthesis and its regulation. Annu Rev Biochem 52: 537-579.
13. Maier T, Leibundgut M, Ban N (2008) The crystal structure of a mammalian fatty acid synthase. Science 321: 1315-1322.
14. Parris KD, Lin L, Tam A, Mathew R, Hixon J, et al. (2000) Crystal structures of substrate binding to Bacillus subtilis holo-(acyl carrier protein) synthase reveal a novel trimeric arrangement of molecules resulting in three active sites. Structure 8: 883-895.
15. Bunkoczi G, Pasta S, Joshi A, Wu X, Kavanagh KL, et al. (2007) Mechanism and substrate recognition of human holo ACP synthase. Chem Biol 14: 1243-1253.
16. Gehring AM, Lambalot RH, Vogel KW, Drueckhammer DG, Walsh CT (1997) Ability of Streptomyces spp. acyl carrier proteins and coenzyme A analogs to serve as substrates in vitro for E. coli holo-ACP synthase. Chem Biol 4: 17-24.
17. Halavaty AS, Kim Y, Minasov G, Shuvalova L, Dubrovska I, et al. (2012) Structural characterization and comparison of three acyl-carrier-protein

synthases from pathogenic bacteria. Acta Crystallogr D Biol Crystallogr 68: 1359-1370.
18. McAllister KA, Peery RB, Zhao G (2006) Acyl carrier protein synthases from gram-negative, gram-positive, and atypical bacterial species: Biochemical and structural properties and physiological implications. J Bacteriol 188: 4737-4748.
19. Reuter K, Mofid MR, Marahiel MA, Ficner R (1999) Crystal structure of the surfactin synthetase-activating enzyme sfp: a prototype of the 4'-phosphopantetheinyl transferase superfamily. EMBO J 18: 6823-6831.
20. Lambalot RH, Walsh CT (1995) Cloning, overproduction, and characterization of the Escherichia coli holo-acyl carrier protein synthase. J Biol Chem 270: 24658-24661.
21. Marcella AM, Jing F, Barb AW (2015) Preparation of holo- and malonyl-[acyl-carrier-protein] in a manner suitable for analog development. Protein Expr Purif 115: 39-45.
22. Otwinowski Z, Minor W (1997) Processing of X-ray diffraction data collected in oscillation mode. Methods Enzymol 276: 307-326.
23. McCoy AJ, Grosse-Kunstleve RW, Adams PD, Winn MD, Storoni LC, et al. (2007) Phaser crystallographic software. J Appl Crystallogr 40: 658-674.
24. Winn MD, Ballard CC, Cowtan KD, Dodson EJ, Emsley P, et al. (2011) Overview of the CCP4 suite and current developments. Acta Crystallogr D Biol Crystallogr 67: 235-242.
25. Murshudov GN, Vagin AA, Dodson EJ (1997) Refinement of macromolecular structures by the maximum-likelihood method. Acta Crystallogr D Biol Crystallogr 53: 240-255.
26. Kim Y, Prestegard JH (1990) Refinement of the NMR structures for acyl carrier protein with scalar coupling data. Proteins 8: 377-385.
27. Delaglio F, Grzesiek S, Vuister GW, Zhu G, Pfeifer J, et al. (1995) NMRPipe: a multidimensional spectral processing system based on UNIX pipes. J Biomol NMR 6: 277-293.
28. Liu Y, Prestegard JH (2009) Measurement of one and two bond N-C couplings in large proteins by TROSY-based J-modulation experiments. J Magn Reson 200: 109-118.
29. Zweckstetter M (2008) NMR: prediction of molecular alignment from structure using the PALES software. Nat Protoc 3: 679-690.
30. Valafar H, Prestegard JH (2004) REDCAT: a residual dipolar coupling analysis tool. J Magn Reson 167: 228-241.
31. Freyer MW, Buscaglia R, Cashman D, Hyslop S, Wilson WD, et al. (2007) Binding of netropsin to several DNA constructs: evidence for at least two different 1:1 complexes formed from an -AATT-containing ds-DNA construct and a single minor groove binding ligand. Biophys Chem 126: 186-196.
32. Freyer MW, Buscaglia R, Nguyen B, Wilson WD, Lewis EA (2006) Binding of netropsin and 4,6-diamidino-2-phenylindole to an A2T2 DNA hairpin: a comparison of biophysical techniques. Anal Biochem 355: 259-266.

33. Evans PR, Murshudov GN (2013) How good are my data and what is the resolution? Acta Crystallogr D Biol Crystallogr 69: 1204-1214.
34. Diederichs K, Karplus PA (2013) Better models by discarding data? Acta Crystallogr D Biol Crystallogr 69: 1215-1222.
35. Karplus PA, Diederichs K (2012) Linking crystallographic model and data quality. Science 336: 1030-1033.
36. Kim Y, Kovrigin EL, Eletr Z (2006) NMR studies of Escherichia coli acyl carrier protein: dynamic and structural differences of the apo- and holo-forms. Biochem Biophys Res Commun 341: 776-783.
37. Oswood MC, Kim Y, Ohlrogge JB, Prestegard JH (1997) Structural homology of spinach acyl carrier protein and Escherichia coli acyl carrier protein based on NMR data. Proteins 27: 131-143.
38. Gally HU, Spencer AK, Armitage IM, Prestegard JH, Cronan JE, Jr. (1978) Acyl carrier protein from Escherichia coli: characterization by proton and fluorine-19 nuclear magnetic resonance and evidence for restricted mobility of the fatty acid chain in tetradecanoyl-acyl-carrier protein. Biochemistry 17: 5377-5382.
39. Prestegard JH, Bougault CM, Kishore AI (2004) Residual dipolar couplings in structure determination of biomolecules. Chem Rev 104: 3519-3540.
40. Jain NU, Wyckoff TJ, Raetz CR, Prestegard JH (2004) Rapid analysis of large protein-protein complexes using NMR-derived orientational constraints: the 95 kDa complex of LpxA with acyl carrier protein. J Mol Biol 343: 1379-1389.
41. Al-Hashimi HM, Bolon PJ, Prestegard JH (2000) Molecular symmetry as an aid to geometry determination in ligand protein complexes. J Magn Reson 142: 153-158.
42. Hansen MR, Mueller L, Pardi A (1998) Tunable alignment of macromolecules by filamentous phage yields dipolar coupling interactions. Nat Struct Biol 5: 1065-1074.
43. Cornilescu G, Marquardt JL, Ottiger M, Bax A (1998) Validation of Protein Structure from Anisotropic Carbonyl Chemical Shifts in a Dilute Liquid Crystalline Phase. J Am Chem Soc 120: 6836-6837.
44. Chen K, Tjandra N (2011) The Use of Residual Dipolar Coupling in Studying Proteins by NMR. Top Curr Chem 326: 47-68.
45. Gokulan K, Aggarwal A, Shipman L, Besra GS, Sacchettini JC (2011) Mycobacterium tuberculosis acyl carrier protein synthase adopts two different pH-dependent structural conformations. Acta Crystallogr D Biol Crystallogr 67: 657-669.
46. Rock CO, Calder RB, Karim MA, Jackowski S (2000) Pantothenate kinase regulation of the intracellular concentration of coenzyme A. J Biol Chem 275: 1377-1383.
47. Vallari DS, Jackowski S, Rock CO (1987) Regulation of pantothenate kinase by coenzyme A and its thioesters. J Biol Chem 262: 2468-2471.
48. Jackowski S, Rock CO (1981) Regulation of coenzyme A biosynthesis. J Bacteriol 148: 926-932.

49. Shi L, Tu BP (2015) Acetyl-CoA and the regulation of metabolism: mechanisms and consequences. Curr Opin Cell Biol 33: 125-131.